Identification of mechanisms defining resistance and susceptibility of *Camellia* plants to necrotrophic petal blight disease

A thesis presented in partial fulfilment of

the requirements for the degree of

Doctor of Philosophy

in

Plant Biology

at Massey University, Manawatū,

New Zealand

Nikolai Kondratev

2019

Abstract

Species in the genus *Camellia*, which includes the tea crops, oil-producers and valuable ornamental plants, have economic and cultural significance for many countries. The fungus *Ciborinia camelliae* causes petal blight disease of *Camellia* plants, which has a short initial asymptomatic phase and results in rapid necrosis and fall of blooms. *Ciborinia camelliae* is a necrotrophic pathogen of the family Sclerotiniaceae, which also includes two broad-host range necrotrophic pathogens, *Botrytis cinerea* and *Sclerotinia sclerotiorum*. Previously it was shown that some *Camellia* plants, such as *Camellia lutchuensis*, are naturally resistant to petal blight. In order to find molecular mechanisms underpinning this resistance, a genome-wide analysis of gene expression in *C. lutchuensis* petals was conducted. The analysis revealed a fast modulation of host transcriptional activity in response to *C. camelliae* ascospores. Interaction network analysis of fungus-responsive genes showed that petal blight resistance includes increased expression of important plant defence pathways, such as *WRKY33-MPK3*, phenylpropanoid and jasmonate biosynthesis. A much-delayed activation of the same pathways was observed in the susceptible *Camellia* cultivar, *Camellia* 'Nicky Crisp' (*Camellia japonica* x *Camellia pitardii* var. *pitardii*), suggesting that failure to activate early defence enables *C. camelliae* to invade and cause tissue necrosis. Early artificial induction of defence pathways using methyl jasmonate reduced the rate of petal blight in susceptible 'Nicky Crisp' plants, further verifying the role of a rapid defence activation in petal-blight resistance. Overall, transcriptomic and functional analysis of the *Camellia* spp.-*C. camelliae* interaction demonstrated that the same plant defence pathways contribute to both resistance and susceptibility against this necrotrophic pathogen, depending on the timing of their activation.

To further understand the molecular mechanisms of petal blight resistance, the role of the phenylpropanoid pathway, identified as a key feature in the transcriptome study above, was investigated in more detail. This pathway produces various metabolites, including phenolic acids, aldehydes, and alcohols, which have numerous physiological functions and also participate in the production of flavonoids and lignin. Resistant *C. lutchuensis* was shown to rapidly activate the expression of core phenylpropanoid genes after treatment with *C. camelliae* ascospores. LC-MS-based quantification of phenylpropanoid compounds demonstrated that within the first 6 h of the infection, resistant plants had already accumulated coumaric, ferulic and sinapic acids, while at 24 hpi, concentrations of coumaraldehyde, sinapaldehyde, and caffeyalcohol were significantly increased. Thus, I further hypothesized that the compounds produced by the phenylpropanoid pathway may have fungistatic activity. Indeed, all tested phenylpropanoids inhibited the growth of *C. camelliae* in agar plates with different efficacy. Moreover, the application of phenylpropanoid compounds, including ferulic and coumaric acids, fully prevented the formation of petal blight lesions on susceptible *Camellia* 'Nicky Crisp' petals. Taken together, it can be concluded that the phenylpropanoid pathway may contribute to the early defence against the petal blight via the rapid production of fungistatic compounds. Ultimately, these compounds could be used to develop natural antifungal sprays to protect susceptible *Camellia* flowers.

The analysis of the *C. camelliae* secretome using LC-MS/MS detection of proteins showed that the pathogen produces a large number of carbohydrate-active enzymes in liquid culture and plant petals. Injection of these proteins induced necrosis not only in susceptible *Camellia* petals but also in petals of the resistant species and leaves of non-host *Nicotiana benthamiana*. It was proposed that these enzymes can contribute to the virulence of the pathogen by inducing cell death and facilitating necrosis propagation. Thus, the early defence responses of resistant *Camellia* plants may possibly stop the development of *C.*

camelliae before it starts releasing carbohydrate-active enzymes during the necrotrophic step of the infection.

Overall, the results of this research further expand our understanding of plant-necrotroph interactions, suggesting that the timing of plant immune responses may be a crucial factor defining the outcome of the necrotrophic infection.

Acknowledgments

First of all, I would like to offer my deepest gratitude to my primary supervisor Assoc Prof Paul Dijkwel. Paul selected me for this project and attentively guided me through this process, while also allowing me to have complete freedom while carrying out the research. His professional and personal support made this journey profoundly interesting. I also want to thank my co-supervisors Prof Rosie Bradshaw and Prof Murray Cox. Their attention and support were unequivocally greater than one might assume from a pair of co-supervisors.

I am grateful for the New Zealand Camellia Society for making this project possible. Their enthusiasm and interest in science is undeniable and is exemplified through the support of this research. I would like to specifically thank Tony Barnes who was tasked with multiple organisational aspects of the project, including planning several meetings and sharing his personal experience of growing camellias. I also would like to thank the members of the International Camellia Society and the petal blight research teams from Spain and Italy for numerous productive discussions. I also wish to acknowledge Dr Matthew Denton-Giles who readily shared his experience in *Camellia* studies.

Furthermore, I would like to express my gratitude towards the Bio-Protection Research Centre and the School of Fundamental Sciences for continued financial support of this research.

I was very lucky to be a part of a lab and institute full of nice and intelligent people; many thanks to Tina, Rama, Elva, Xi, Asmat, Trevorne, Saurabh, Aakansha, Meriem. I would also like to say thanks to my colleagues from the office C5.29 – Faya, John, India, Tina and Sophie – for creating a warm and welcoming working environment. Special

thanks to my fellow *Camellia* researchers – Hannah McCarthy and Cade Fulton – who made this research even more fun. I also want to thank the members of SFS Molecular Plant Pathology lab – Simren, Lukas, Melissa, Silvia, Mercedes, Mariana, Ellie – who always welcomed me in their group meetings. Finally, I want to offer a special thank you to Dr Carl Mesarich for his valuable comments and insightful discussions.

Many of my friends supported me during my PhD studies. Vakil Takhaveev (University of Groningen, the Netherlands), Alisa Garaeva (University of Groningen, the Netherlands), and Irina Garanina (Parexel International, Moscow, Russia) – I am grateful for their willingness to always provide me with helpful advice for navigating my research and PhD student life.

Last but not least, I want to thank my family for their love and support during my study.

Table of Contents

List of Tables

List of Figures

List of Abbreviations

°C	degrees Celsius
4CL	4-coumarate-CoA ligase
ACX	acyl-CoA oxidase
ANOVA	analysis of variance
AOC	allene oxide cyclase
AOS	allene oxide synthase
Avr	avirulence
BAK1	BRASSINOSTEROID INSENSITIVE 1-ASSOCIATED KINASE 1
BcSSP	*Botrytis cinerea* small secreted protein
BIK	Botrytis-induced kinase
bp	base pairs
BSA	bovine serum albumin
C-C	coiled-coil
C3H	p-coumaroyl shikimate/quinate 3'-hydroxylase
C4H	trans-cinnamate 4-monooxygenase
CAD	cinnamyl-alcohol dehydrogenase
CAZyme	carbohydrate-active enzyme
CCR	cinnamoyl-CoA reductase
CcSSP	*Ciborinia camelliae* small secreted protein
CDPK	calcium-dependent protein kinases
CHS	naringenin-chalcone synthase
cm	centimetre
COMT	caffeate O-methyltransferase
Cq	quantification cycle
cv.	cultivar
Da	Daltons
DAMP	damage-associated molecular pattern
DNA	deoxyribonucleic acid
DNase	deoxyribonuclease
dpi	days post inoculation
EDTA	ethylenediaminetetraacetic acid
EF-1	eukaryotic elongation factor-1
ETI	effectror-triggered immunity
F5H	ferulate 5-hydroxylase
FPLC	fast protein liquid chromatography
g	gram
g	gravitations

GAPDH	glyceraldehyde 3-phosphate dehydrogenase
Gb	giga base pairs
GO	gene ontology
h	hour
hpi	hours post inoculation
HPLC	high performance liquid chromatography
HR	hypersensitive response
HST	host-specific toxin
ICMP	International Collection of Microorganisms from Plants
IP	invasion pattern
IPR	invasion pattern receptors
IS	internal standard
iTRAQ	isobaric tags for relative and absolute quantification
JA	jasmonic acid/jasmonate
kb	kilo base pairs
L	litre
LC	liquid chromatography
LOX	lipoxygenase
LRR	leucine-rich repeat
LSD	least significant difference
M	molar/mol per litre
mA	milliampere
MAMP	microbe-associated molecular pattern
MAPK	mitogen-activated protein kinase
MeJA	methyl jasmonate
min	minute
mL	millilitre
mln	million
mm	millimetre
mM	millimolar/mmol per litre
mol	mole
MPK3	mitogen-activated protein kinase 3
MS	mass spectrometry
n.s.	non-significant
NADPH	nicotinamide adenine dinucleotide phosphate
NBS	nucleotide-binding site
NCBI	National Center for Biotechnology Information, USA
NLP	necrosis and ethylene-inducing protein-like
nm	nanomolar/nmol per litre
NMR	nuclear magnetic resonance
NOX	NADPH oxidase
nr	non-redundant protein database
nt	nucleotide database

OAH1	oxaloacetate acetylhydrolase 1
OPCL	OPC-8:0 CoA ligase 1
OPR	12-oxophytodienoate reductases
PAGE	polyacrylamide gel electrophoresis
PAL	phenylalanine ammonia lyase
PAMP	pathogen-associated molecular pattern
PCA	principal component analysis
PCR	polymerase chain reaction
PDA	potato dextrose agar
PDB	potato dextrose broth
pmol	picomole
PPI	protein-protein interaction
PR	pathogenesis-related
PRR	pathogen recognition receptor
PTB1	polypyrimidine tract-binding protein 1
PTI	PAMP-triggered immunity
QC	quality control
QDR	quantitative disease resistance
qPCR	quantitative polymerase chain reaction
qRT-PCR	real-time reverse transcription polymerase chain reaction
QTL	quantitative trait locus
R gene	resistance gene
R protein	resistance protein
RIN	RNA integrity number
RIN4	RPM1-interacting 4
RN	random network
RNA	ribonucleic acid
RNA-seq	RNA sequencing
RNase	ribonuclease
ROS	reactive oxygen species
RPM1	RESISTANCE TO PSEUDOMONAS SYRINGAE PV MACULICOLA 1
RPS2	RESISTANCE TO PSEUDOMONAS SYRINGAE 2
RRF	relative response factor
rRNA	ribosomal RNA
s	second
SA	salicylic acid
SAR	systemic acquired resistance
SDS	sodium dodecyl sulphate
SOBIR1	SUPPRESSOR OF BIR1-1
spp.	species
sRNA	small RNA
SSP	small secreted protein
SsSSP	*Scelrotinia sclerotiorum* small secreted protein

TAE	Tris-acetate-EDTA
TCA	trichloroacetic acid
TIR	Toll/Interleukin-1 receptor
TOF	time-of-flight
UHPLC	ultra-high-performance liquid chromatography
UV	ultraviolet
v	volume
V	volt
var.	variety
w	weight
µL	microlitre
µm	micrometre
µM	micromolar/µmol per litre

Chapter 1. General introduction

1.1. Plant immune system

Unlike vertebrates, plants lack a sophisticated immune system. Thus, each particular cell of a plant must be able to detect and stop pathogen invasions. Molecular studies of the cellular defence events form one of the major branches of modern plant biology. Traditionally, these works describe the plant cellular immune system as two layers of defence. The first layer is activated when a plant detects a microorganism and tries to stop its penetration. If a pathogen overcomes this first defence line, plants activate next level defence mechanisms, which result in necrosis of plant tissues in the area of contact with this pathogen. These two layers of immunity are called (1) microbial- or pathogen-associated molecular pattern-triggered immunity (PTI) and (2) effector-triggered immunity (ETI) (J. D. G. Jones & Dangl, 2006). The next paragraphs of this section will describe molecular events associated with these two immunity layers, and how these processes interact and sometimes overlap.

The first layer of plant immune system, or PTI. The first line of plant defence is activated upon contact with potential pathogens. Plant cells can sense the presence of invaders via detection of invaders' molecules (Zipfel & Robatzek, 2010). This set of molecules is called microbe- or pathogen-associated molecular patterns (MAMPs or PAMPs). Additionally, plant cells detect not only the presence of pathogens but also the damage some pathogens cause in the course of the attempted penetration. In this case, host molecules, which were released due to the wounding and pathogen entry, become triggers of the immune response. This last type of triggers is called damage-associated molecular patterns (DAMPs).

The process of MAMPs/PAMPs or DAMPs detection is based on the action of molecular receptors. Specific pathogen recognition receptors (PRRs) bind PAMPs such as different bacterial or fungal cell wall components. Receptor-ligand (receptor-PAMP, or receptor-DAMP) interaction triggers downstream intracellular signalling pathways, including mitogen-activated protein kinases (MAPK), thereby inducing transcriptional reprogramming with various transcription factors, such as DNA-binding proteins with a WRKY domain. These transcription factors activate expression of other genes, which execute early (ion flux, oxidative burst), intermediate (ethylene production, stromatal closure) and late (callose deposition and salicylic acid release) processes on cellular and tissue levels, which stop the penetration of pathogens (Zipfel & Robatzek, 2010). A scheme of the described pathways and probable interpathway interactions are shown below (Figure 1-1).

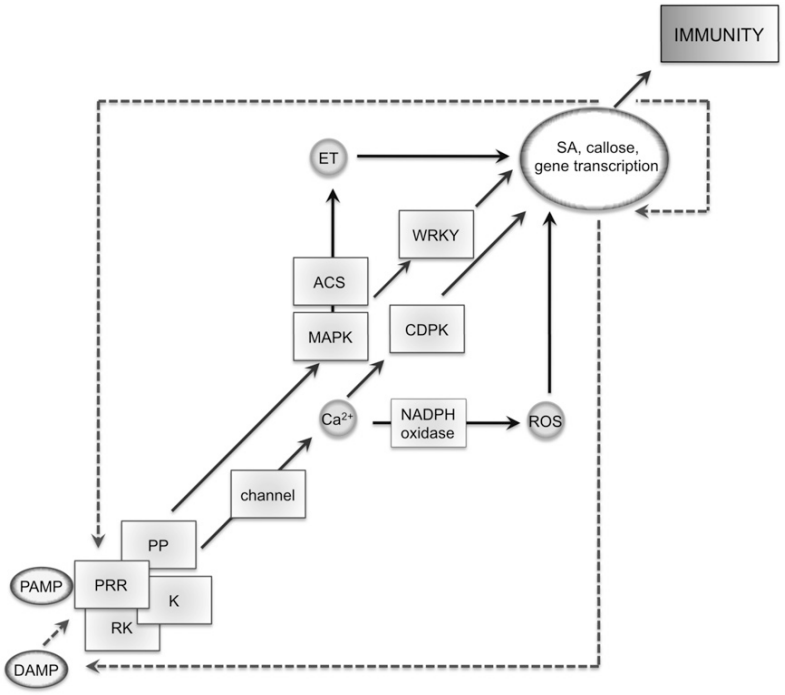

Figure 1-1 | Molecular components of PAMP-triggered immunity (PTI).
Pathogen-associated molecular patterns (PAMP), damage-associated molecular patterns (DAMP) (left bottom corner) interact with receptor complexes, which can include pathogen recognition receptor (PRR), RK (receptor kinase), cytoplasmic kinase (K) and phosphatase (PP) molecules. This interaction activates Ca^{2+} channels, inducing Ca^{2+} influx. Intracellular signalling involves mitogen-activated protein kinases (MAPK), calcium-dependent protein kinases (CDPK) and reactive oxygen species (ROS) production – pathways, which are activated upon the receptor-ligand interaction. Subsequent activation of 1-

aminocyclopropane-1-carboxylate synthase (ACS) leads to ethylene (ET) production. Also, activation of WRKY transcription factors (WRKY) induces salicylic acid (SA) production and other downstream processes, associated with the resistance. Black arrows show pathways, dashed arrows show probable interactions between upstream and downstream processes. Republished with permission of American Society of Plant Biologists from (Zipfel & Robatzek, 2010); permission conveyed through Copyright Clearance Center, Inc.

The second layer of plant immune system, or ETI. While the previous defence layer prevents infection with non-adapted microbes, some pathogens can use a special molecular machinery to circumvent PTI. For example, fungi, to inhibit basal defence, excrete specific molecules, also known as virulence factors, or effectors. Effectors are usually small proteins (< 300 amino acid) and sometimes have elevated cysteine content (Sperschneider et al., 2016). Examples of fungal effectors and their mechanisms of action are described in the next section (1.2 Necrotrophic fungi and their effectors). Nevertheless, some plant cells learned to sense the presence of these effector molecules, making plants resistant. Therefore, the second layer of plant immune system, ETI, is based on the detection of effector molecules by plant cells and subsequent activation of immune responses (Lo Presti et al., 2015).

The main outcome of ETI is localized cell death, which is supposed to stop pathogen propagation in the plant. Similar to PTI, ETI also starts with recognition of pathogens' molecules. Resistance proteins (R proteins) – products of R genes – play the role of receptors in ETI. The majority of R proteins harbours a leucine-rich repeat domain (LRR) and a nucleotide-binding site (NBS). Additionally, they can contain Toll/Interleukin-1 receptor (TIR) domains, coiled-coil (C-C) domains and domains with kinase activity (Figure 1-2) (Gururani et al., 2012).

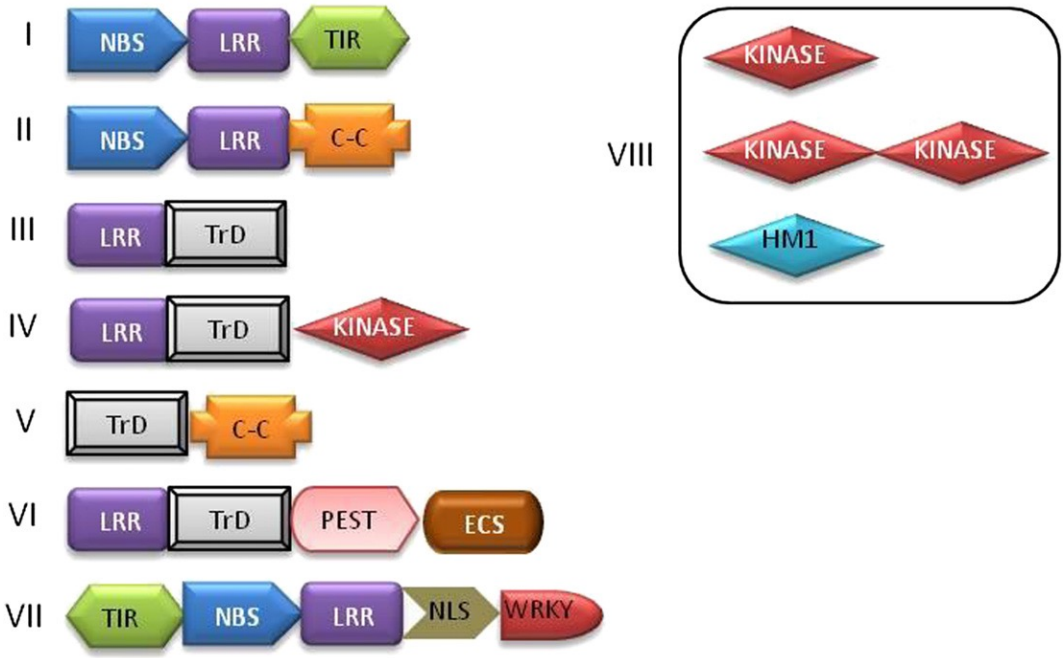

Figure 1-2 | Major classes of plant R genes.
The scheme shows observed combinations of functional domains in R proteins. NBS – nucleotide-binding site; LRR – leucine-rich repeat; TIR – Toll/Interleukin-1 receptor; C-C – coiled-coil; TrD – transmembrane domain; PEST – protein degradation domain; ECS – endocytosis cell signalling domain; NLS – nuclear localisation signal; WRKY – WRKY amino acid domain; HM1 - Helminthosporium carbonum toxin reductase enzyme. Republished with permission of Elsevier from (Gururani et al., 2012); permission conveyed through Copyright Clearance Center, Inc.

More than 50 years ago the gene-for-gene relationship model was proposed by H. H. Flor (Flor, 1971), which postulates that each pathogen's virulence (effector) gene has a corresponding plant resistance gene. Products of these two corresponding genes interact and induce downstream ETI processes in a plant. If an effector of the pathogen can be recognized by an R protein, and this interaction provokes plant immune responses, this effector is called an avirulence factor (Avr). For example, strains of *Magnaporthe grisea* producing AVR-PITA protein are not virulent for rice plants that harbour the *Pi-ta* R gene. These plant and fungal proteins interact directly (Jia, McAdams, Bryan, Hershey, & Valent, 2000). However, given the number of possible pathogens and their potential virulence factors, a single plant genome would have to contain a massive number of R genes. Indeed, genetic recombination is frequent in genomic regions that contain R genes, which results in a large variation of R proteins within a population. This process resembles somatic DNA

rearrangements in vertebrate immunoglobulin genes, which provide an organism with new antibodies (Bakker, Toomajian, Kreitman, & Bergelson, 2006; Spoel & Dong, 2012). Nevertheless, the observed variety of R genes in plants cannot explain the whole spectrum of resistance. The way to detect numerous effectors having a limited number of R genes is explained with the "guard hypothesis". It was proposed that certain R proteins could detect effector-induced changes in plant cells instead of direct effector detection. According to the model, R proteins ("guards") have corresponding plant proteins ("guardees"). These "guardees" are targets for various pathogen effectors. R proteins activate ETI if conformational or structural changes occur in "guardee" proteins. That means that one R protein can detect the whole group of effectors which interact with its "guardee" target (Dangl & Jones, 2001). For instance, the RIN4 protein of *Arabidopsis thaliana* is a target for AvrRpm1, AvrB and AvrRpt2 *Pseudomonas syringae* effectors. Its guards are RPM1 (RESISTANCE TO PSEUDOMONAS SYRINGAE PV MACULICOLA 1) and RPS2 (RESISTANCE TO PSEUDOMONAS SYRINGAE 2), R proteins belonging to the class of CC-NBS-LRR (M. G. Kim et al., 2005).

R-Avr interaction activates localized programmed cell death, also known as a hypersensitive response (HR). This type of cell death shares features with necroptosis and pyroptosis from the animal kingdom and involves the accumulation of ROS and activation of caspase-like proteolytic enzymes (Coll, Epple, & Dangl, 2011).

Interestingly, ETI shares molecular mechanisms with PTI, such as MAPK cascade signalling and WRKY transcription factors activation; ROS accumulation and Ca^{2+} influx processes are involved in both PTI and ETI, although the two processes are quantitatively different: ETI is stronger and long lasting, thus, leads to cell death, while PTI responses are not self-destructive (Cui, Tsuda, & Parker, 2015).

Invasion model as an alternative to PTI-ETI dichotomy. The accumulation of knowledge about various plant defence-responses required a creation of generalized model

of plant immunity. The Invasion Model was proposed in 2015, and it describes plant immunity as a surveillance system detecting pathogens (Cook, Mesarich, & Thomma, 2015). According to the model, immunogenic molecules, such as PAMPs, DAMPs or effectors, can be termed invasion patterns (IPs). Corresponding plant receptors, which detect the presence of invasion patterns (e.g. PRRs and R proteins), can be generally designated as invasion pattern receptors (IPRs). The interactions between IPs and IPRs execute IP-triggered responses in plants (e.g. production of ROS, localized cell death). Depending on the infection strategy of a pathogen, these responses may result in immunity to a pathogen or, in case of necrotrophic infections, facilitate the invasion. Alternatively, pathogens may produce effectors which suppress the development of IP-triggered responses and inhibit plant immunity.

Systemic immune response and immune memory in plants. Previously discussed models describe the mechanisms of plant immunity from a single plant cell perspective. Although plants do not have a circulating immune system as in vertebrates, they do produce mobile immune signals activating an immune response in the whole organism. In 1961, A. Frank Ross showed that a single local inoculation of tobacco mosaic virus protects whole plants from infection (Ross, 1961). This observation has been called systemic acquired resistance (SAR). The main difference of SAR with vertebrate adaptive immunity is that SAR has no specificity to the initial infection (Fu & Dong, 2013).

SAR is based on the activation of plant cellular defences with specific mobile signals that are released from the other cells of the same plant, or even from the other plants upon the attack of pathogens or wounding. These signals can have a hormonal and non-hormonal nature. Salicylic acid (SA), a widely studied plant hormone, is involved in SAR (Biologie, Fribourg, & Gockel, 1998). The signal transport is likely based on the methylated inactive form of SA, methyl salicylic acid. Recent studies on tobacco have shown that plants with a silenced methyl salicylate esterase gene, coding an enzyme

converting the methylated form of SA into SA, cannot develop SAR. (Park, Kaimoyo, Kumar, Mosher, & Klessig, 2007). Jasmonic acid (JA) and azelaic acid also participate in SAR hormonal signalling (Fu & Dong, 2013; Shah & Zeier, 2013). An example of a non-hormonal signalling molecule is glycerol-3-phosphate. Cooperative interaction of glycerol-3-phosphate with lipid-transfer protein DIR1 (DEFECTIVE IN INDUCED RESISTANCE 1) has been shown to be involved in the SAR system (Chanda et al., 2011).

Downstream SAR events consist of transcriptional reprogramming processes. NPR1 transcription factor, a key regulator of SAR, initiates synthesis of antimicrobial pathogenesis-related (PR) genes (Spoel & Dong, 2012). PR-proteins are classified into 17 families based on their activity. Families PR-3, PR-4, PR-8 and PR-11 possess chitinase activity, PR-2 – beta-1,3-glucanase; both groups attack pathogens' cell walls. Thaumatin-like proteins, defensins and thionines – which are named families PR-5, PR-12, PR-13, respectively – target invaders' membranes (Sels, Mathys, De Coninck, Cammue, & De Bolle, 2008).

Developing immune memory is one of the SAR outcomes. Content and activity of MAP3 and MAP6 kinases were elevated after plants' contact with immune system elicitors. This process is also regulated by the NPR1 transcription factor and might be considered as the accumulation of immune signalling components – one of the ways of plant immune memory organization (Beckers et al., 2009). Other observed plant immune memory mechanisms are epigenetic in nature. Histone modifications – H3, H4 acetylation, and H3K4 methylation – activated expression of several WRKY transcription factors involved in defence response (Jaskiewicz, Conrath, & Peterhänsel, 2011). DNA repair and homologous recombination proteins were shown to play a role in immune genes' activation, suggesting one more possible mechanism of plant immune memory establishment (Spoel & Dong, 2012).

Spatial distribution of plant immunity-associated molecular events. As discussed in previous paragraphs, plant immunity involves the detection of pathogens occurring on the cellular level, and also transmission of signals between organs of a single plant or even between different plants. Interestingly, the development of immune responses can have a rather complex temporal and spatial structure even just within a single plant organ. For example, spatial analysis of the activity of hormonal signalling pathways demonstrated that, after the infiltration with *P. syringae*, *A. thaliana* leaves form two distinctive domains around the infiltration zone (Figure 1-3). While the infiltration area undergoes programmed cell death, the surrounding cells activate the production of SA. In their turn, cells surrounding the SA-domain start the production of JA, which is likely to restrict the propagation of SA signalling and localize the necrogenic response (Betsuyaku et al., 2018).

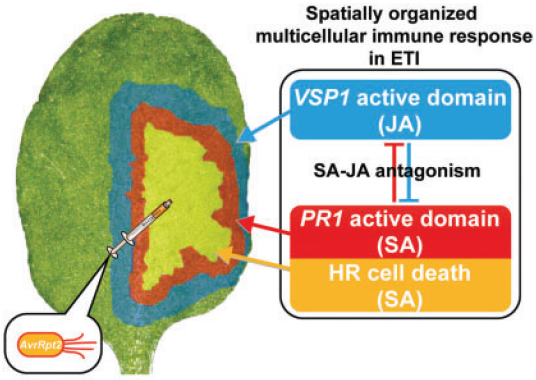

Figure 1-3 | Spatial distribution of events occurring during the ETI response of *Arabidopsis thaliana* to *Pseudomonas syringae*.
The scheme represents the pattern of response events occurring in A. thaliana *triggered by the inoculation with* P. syringae. *Central yellow area shows the region of HR cell death, middle red area corresponds to the SA-mediated responses, and blue outermost circle shows the area of JA-mediated responses. PR1 and VSP1 are marker genes whose promotors were used to detect the activation of SA and JA pathways in the study. Republished with permission of Oxford University Press from (Betsuyaku et al., 2018); permission conveyed through Copyright Clearance Center, Inc.*

1.2. Necrotrophic fungi and their effectors

Classification of fungal pathogens. Based on their infection strategies, fungal phytopathogens are classified into three groups: biotrophs, hemibiotrophs and necrotrophs. Biotrophic pathogens need living plant tissues to grow, develop and propagate. They usually form specific outgrowths on hyphae, haustoria, penetrating through the cell wall but not the host membrane (Mendgen & Hahn, 2002). Well-studied examples of biotrophic fungi are the smut fungus (*Ustilago maydis*), tomato leaf mould (*Cladosporium fulvum*), rice blast fungus (*Magnaporthe oryzae*) and powdery mildew fungus (*Blumeria graminis*) (Koeck, Hardham, & Dodds, 2011). Biotrophs can deliver effectors via haustoria, which can modulate cell processes but keep host cells alive (Chaudhari, Ahmed, Joly, & Germain, 2014). Among the well-described biotrophic effectors are *C. fulvum* Avr4 that binds chitin and protects fungal cell walls from plant chitinases (van Esse et al., 2007), and Avr2 that inhibits tomato proteases (van Esse et al., 2008).

Hemibiotrophic fungi behave like biotrophic ones on the early stages of the infection, but usually produce toxins and kill host tissues on the later stages of the infection and complete their life cycles as necrotrophs. For *Colletotrichum* genera species (e.g. maize anthracnose, *Colletotrichum graminicola*), both development stages are established (Münch et al., 2008). Determination of the biotrophic and necrotrophic stages is not trivial: to identify a hemibiotrophic lifestyle, histological observations are used in combination with transcriptomic analysis, which shows switches in gene expressions associated with changes in fungus' lifestyle. Observations of this transition on the transcriptomic level for the pine needle blight pathogen, *Dothistroma septosporum*, have shown that the necrotrophic stage is characterized by the higher expression of small secreted proteins (SSPs), some of which could be effector molecules (Bradshaw et al., 2016).

Necrotrophs comprise the third group of pathogens. Necrotrophic pathogens kill plant cells before colonization and grow on necrotized tissues. They produce a big variety

of cell-wall degrading enzymes and toxins to induce tissue necrosis (Lo Presti et al., 2015). Necrotrophic fungi are represented by host-specific (*Ciborinia camelliae*, *Stagonospora nodorum, Pyrenophora tritici-repentis*) and broad host-range pathogens (*Botrytis cinerea, Sclerotinia sclerotiorum*) (Denton-Giles, Bradshaw, & Dijkwel, 2013; X. Wang, Jiang, Liu, Liu, & Wang, 2014).

According to the Invasion Model, biotrophic and necrotrophic pathogens use opposite strategies for infection establishment and propagation. The recognition of IPs by IPRs leads to the formation of immunity against biotrophic pathogens. Necrotrophic pathogens use IPs to activate immune responses in host tissues, which facilitate the propagation of necrosis and enhances the further colonization (Cook et al., 2015).

Host-specific toxins of necrotrophs (HST). In biotrophic fungal-plant interactions, recognition of virulence factors by R proteins induces ETI and leads to the HR. Necrotrophic HSTs are also recognized by R proteins, but their recognition and triggering of HR only favour the infection propagation. HST-receptor interactions have been studied in *S. nodorum*, the wheat blotch pathogen. SnTox1 is 10.3 kDa cysteine-rich effector protein (Oliver, Friesen, Faris, & Solomon, 2012). It interacts with the *Snn1* gene product, belonging to NBS-LRR class of R genes, and induces a light-dependent necrosis reaction (Z. Liu et al., 2012). Interaction of SnTox2-SnTox5 proteins with corresponding *Snn2-Snn5* receptors have also been described (Oliver et al., 2012).

ToxA – a gene that encodes HST – was transferred from *S. nodorum* to *P. tritici-repentis* by horizontal gene transfer (Friesen et al., 2006). Once delivered into a plant cell, ToxA binds ToxABP1 (ToxA Binding Protein 1) and Tsn1 receptor, and induces light-dependent ROS accumulation and, probably, perturbation of photosystem II followed by cell death (Ciuffetti, Manning, Pandelova, Betts, & Martinez, 2010).

LOV1 (LOCUS ORCHESTRATING VICTORIN EFFECTS 1) encodes an NB-LRR protein in *A. thaliana*, which is associated with susceptibility to *Cochliobolus victoria*. This

fungus produces a toxin, victorin (Lorang, Carkaci-Salli, & Wolpert, 2004). Victorin interaction follows the previously described "guard" model. Victorin, cyclic pentapetide toxin, interacts with "guardee" – TRX-h5, a defence-associated thioredoxin (Gilbert & Wolpert, 2013). LOV1 protein detects this interaction and triggers cell death favouring the pathogen propagation.

Effector-triggered immunity in necrotrophic infection. *Leptosphaeria maculans* (blackleg disease pathogen) is a challenging necrotrophic pathogen causing losses in the canola industry (Sivasithamparam, Barbetti, & Li, 2005). Seven *Avr* genes, designated *AvrLm 1-2-3-4-6-7-9*, have been described, as well as twelve corresponding resistance genes *Rlm1-9*, *LepR1-3* encoding TIR-NB-LRR proteins (Staal, Kaliff, Bohman, & Dixelius, 2006; van de Wouw et al., 2010). To the best of my knowledge, this is the only Avr-R interaction described for necrotrophs so far (X. Wang et al., 2014).

Broad-host necrotrophic pathogens and their toxins. Two polyphagous fungi, *Botrytis cinerea* (grey mould fungus) and *Sclerotinia sclerotiorum* (white mould fungus), infect more than 200 plant species and cause massive losses in agriculture (Dean et al., 2012; Peltier et al., 2012). These fungi use multiple virulence factors, which help successfully colonize a large variety of hosts. They utilise extensive sets of cell wall degrading enzymes. Pectin methyl-esterases, endo-polygalacturonases and endo-β-1,4-xylanases have been shown to be essential for the virulence of *B. cinerea* (Choquer et al., 2007).

There is a resemblance in colonization strategies of these two fungi. Initial stages of invasion and colonization are coupled with a pH decrease. While this process is probably based on citrate and succinate production in *B. cinerea* (Billon-Grand, Rascle, Droux, Rollins, & Poussereau, 2012), oxalic acid is one of the key virulence factors of *S. sclerotiorum*. Sclerotinia strains with mutations in *oxaloacetate acetylhydrolase 1* (*OAH1*) gene had lower virulence (Liang et al., 2015). Apart from pH modulation, oxalic acid is believed to suppress plant ROS production and Ca^{2+} signalling ion fluxes into the cytosol (Cessna,

Sears, Dickman, & Low, 2000; Heller & Witt-Geiges, 2013). There are also evidences that oxalic acid can induce cell death (K. S. Kim, Min, & Dickman, 2008).

There are several examples of effectors produced by *B. cinerea* and *S. sclerotiorum*. *Botrytis cinerea* uses two Nep1-like proteins (necrosis and ethylene-inducing protein-like) – NLP1 and NLP2. Both purified proteins induced necrosis in dicotyledonous plants tested. They were shown to interact with the plasma membrane and nuclear envelope, and induce H_2O_2 accumulation in chloroplasts (Schouten, Van Baarlen, & Van Kan, 2008). A cerato-platanin family protein, BcSpl, elicits plant immunity and stimulates plant cell death (Frías, Brito, González, & González, 2014). Small secreted proteins of *S. sclerotiorum* have also been detected and partially characterized. This fungus produces Ca^{2+} binding SsCAF1 eliciting cell death (Xiao et al., 2014) and integrin-like SsITL protein suppressing plant resistance (W. Zhu et al., 2013). No R-Avr interaction has been observed in *S. sclerotiorum* and *B. cinerea* pathogenicity systems yet: possibly because the activation of R genes and ETI in their host only functions to increase colonization effectivity and infection propagation rate in plants (Mbengue et al., 2016).

Interestingly, in *B. cinerea*, a new type of plant-fungus signal transfer pathway has been studied. The fungus utilizes sRNA effectors, to silence host immunity genes. This recently described process is an example of a cross-kingdom RNA interference process. Mechanisms of the sRNA delivery are still to be clarified (Weiberg et al., 2013). *Sclerotinia sclerotiorum* micro-RNAs were sequenced for fungal development studies, but this research did not check for the presence of RNA effectors (Zhou et al., 2012).

1.3. Plant responses to necrotrophic pathogens

Most of the current models of plant immunity were described for the interaction with biotrophic or viral pathogens. In the previous section, particular exploitation of the second layer of immunity by pathogens for necrotrophic infections was described. Resistance mechanisms of plants to necrotrophic fungi seem to be complicated and sometimes even controversial (e.g. the role of ROS in resistance and virulence).

PTI. PAMPs and DAMPs activate the first layer of plant immunity via the interaction with receptor-like kinases. Several mechanisms of PTI have been studied in plant-necrotroph interactions so far. Chitin, a major component of the fungal cell wall, is considered as one of the main plant immune elicitors. *Brassica* dark leaf spot pathogen, *Alternaria brassicola*, is recognized by non-host *A. thaliana* via chitin and LysM receptor interactions, which trigger immune responses (Wan et al., 2008). *Botrytis cinerea* endopolygalacturonases induce necrotic responses in *A. thaliana* and were shown to be targets of LRR-RLP RBPG1 receptors (L. Zhang et al., 2014).

Pathogen polygalacturonase enzymes produce oligogalacturonides in the course of the attack on the host cell wall (an example of DAMP). They can be detected by specific wall-associated kinase and LRR receptor complexes (X. Wang et al., 2014).

Small peptides (peptide DAMPs), are produced in *A. thaliana* upon pathogen attack. Their interaction with PEPR receptors is shown to trigger resistance signalling pathways (Tintor et al., 2013).

BAK1 (BRASSINOSTEROID INSENSITIVE 1-ASSOCIATED KINASE 1) membrane receptor interacts with other receptors, forming receptor complexes for different D/PAMPs. It activates MAPK-signalling pathways and BIK (BOTRYTIS-INDUCED KINASE) mediated responses, which were shown to be specific for resistance to necrotrophs (Mengiste, 2012).

The recognition mechanisms described above activate typical downstream PTI events in the cell, providing resistance to necrotrophs (X. Wang et al., 2014).

ETI. As mentioned in the previous section, only resistance of *Brassica napus* to *L. maculans* follows a classic ETI mechanism. Other necrotrophs hijack the plant immune system with specific toxins such as victorin, toxA or non-specific ones, such as NLP1 (necrosis and ethylene-inducing protein-like) of *B. cinerea*. Thus, the presence of an R gene that recognises a necrotrophic effector makes plants susceptible to the necrotroph. It has been shown that *RLM3* TOL-NB (R gene) gene mutation enhanced susceptibility to necrotrophs (Staal, Kaliff, Dewaele, Persson, & Dixelius, 2008). It indicates that R genes' roles are difficult to be defined in the resistance to necrotrophs.

Oxidative burst. ROS play a significant role in a plants resistance to pathogens (Lehmann, Serrano, L'Haridon, Tjamos, & Metraux, 2015). *Botrytis cinerea* and *S. sclerotiorum*, in turn, use ROS as virulence molecules. *Sclerotinia sclerotiorum* has two *Nox* (*NADPH oxidase*) genes, which are involved in ROS generation. Silencing of *Nox1* resulted in disrupted pathogenicity; *Nox2* has been shown to be necessary for sclerotia formation (H. Kim, Chen, Kabbage, & Dickman, 2011). The importance of Nox-associated ROS production also has been studied on the necrotrophic stage of hemibiotroph, *Zymoseptoria tritici*, lifecycle (Choi, Lee, & Goodwin, 2016). ROS accumulation also occurs as a response to the particular toxins, such as SnTox1 (Z. Liu et al., 2012).

Nevertheless, in early stages of development *Botrytis* and *Sclerotinia* are susceptible to plant ROS-mediated defence. *Sclerotinia sclerotiorum* inhibits plant ROS production with oxalic acid (Williams, Kabbage, Kim, Britt, & Dickman, 2011). In tomatoes, early accumulation of H_2O_2 induces resistance to *B. cinerea* (Asselbergh et al., 2007). In summary, ROS can contribute both to resistance and susceptibility in plant-necrotroph interactions, depending on dynamics and kinetics of ROS accumulation.

Quantitative disease resistance (QDR) is an incomplete resistance to the pathogen leading to the reduction of disease rate, but not to total resistance. It was observed that the disease resistance to necrotrophs is often determined by multiple quantitative trait loci (QTLs). In the case of biotrophs, having one R gene provides full disease resistance; single QDR gene introduction into a susceptible line would result only in partial improvement in resistance (Figure 1-4) (Roux et al., 2014). Resistance to *S. sclerotiorum* and *B. cinerea* are examples of QDR (Mbengue et al., 2016).

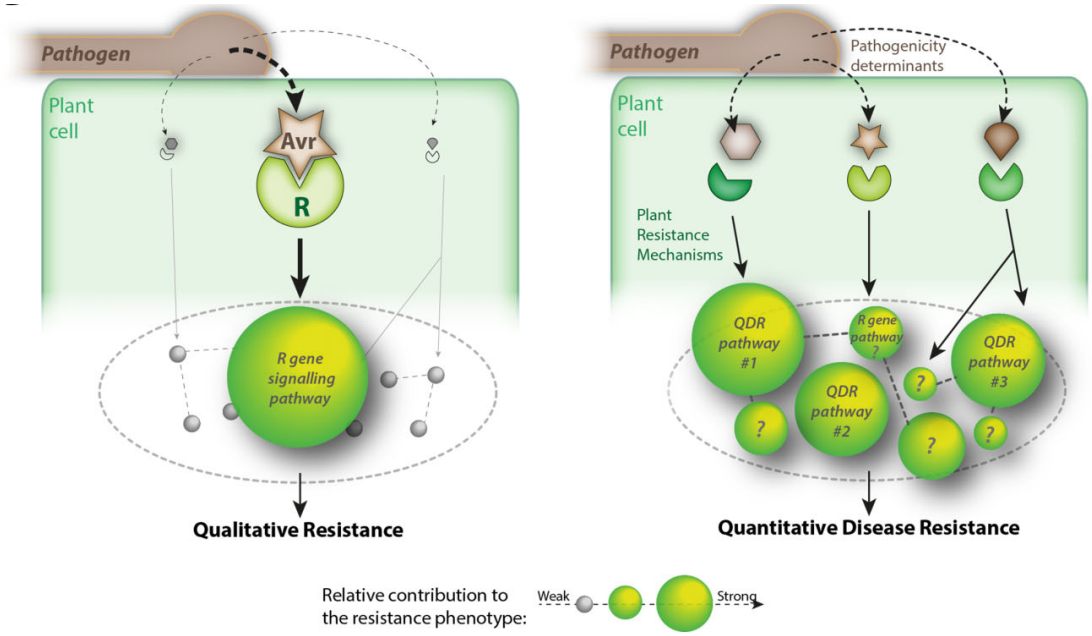

Figure 1-4 | Qualitative and quantitative forms of plant resistance.
Left: qualitative resistance is a result of one Avr effector and R gene interaction; right: quantitative disease resistance (QDR) is a combination of multiple perception and defence pathways. Republished with permission of John Wiley and Sons from (Roux et al., 2014); permission conveyed through Copyright Clearance Center, Inc.

1.4. *Ciborinia camelliae*

Ciborinia camelliae L. M. Kohn is a necrotrophic floral- and host-specific pathogen which infects many plants from the genus *Camellia* with ornamental value (Kohn & Nagasawa, 1984). It belongs to the family Sclerotiniaceae and has a close phylogenetic relationship with better-studied broad-host necrotrophs – *S. sclerotiorum* and *B. cinerea*. The disease it causes is known as camellia petal blight. It was identified in Japan in 1919 (Hara, 1919) and was transferred to the USA with plants in 1938 (Hansen & Thomas, 1940). In New Zealand, petal blight disease was first reported in 1993 (Stewart & Neilson, 1993).

Lifecycle of the pathogen. The infection starts from an airborne fungal ascospore, produced by an apothecium (fungal fruit body) (Figure 1-5). After contact with petal tissue, ascospores germinate and produce primary hyphae. After 24 hours, visible infection spots start appearing on petals (Denton-Giles et al., 2013). Whole flowers (including petals, androecium, and gynoecium) become brown, detach and fall. The sexual reproductive stage of the fungus is based on microconidia formation on decaying petals but details of the process are not described yet (van Toor, 2002). Fallen petals form black rind-coated sclerotia – a dormant stage of the fungus. In this way, the pathogen spends summer. During the cold, moist winter, possibly after vernalisation, sclerotia start the production of long white stipes; stipes form discoid structures – apothecia. Apothecia formation and maturation is likely to require natural light, and so far cannot be reproduced *in vitro* (Taylor, 2004). Apothecia produce new ascospores, which give a start to a new generation of the pathogen.

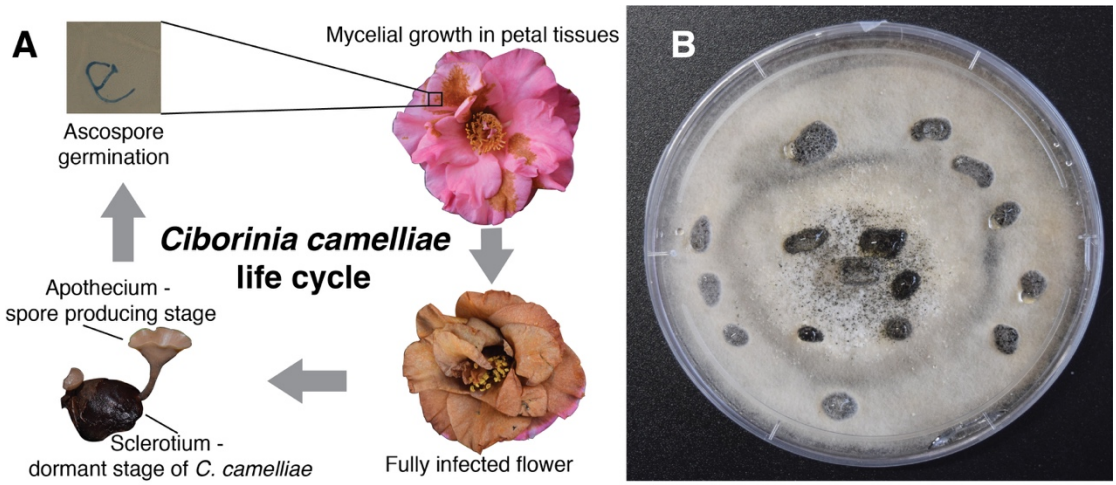

Figure 1-5 | Lifecycle of *Ciborinia camelliae*.
(A) *The lifecycle of the petal-blight parasite starts from the spore landing and germination on the surface of the petal. Fungal mycelium keeps growing inside petal tissues causing necrosis and fall of the flowers. Fallen infected blooms form sclerotia, dormant form of the parasite. In winter, fruiting bodies, apothecia, grow from sclerotia and release new spores. (B) The mycelial stage of the fungus can be cultivated in lab on Potato Dextrose Agar.*

Compatible and incompatible interaction features. There is a broad spectrum of resistance levels to *C. camelliae* in plants from the genus *Camellia*. A previous study conducted at Massey University used microscopic and macroscopic criteria to estimate levels of resistance in 40 plant species and one interspecific hybrid (Denton-Giles, 2014). *Camellia lutchuensis*, *C. yuhsienensis*, and *C. transnokoensis* were the most resistant species tested. The most susceptible plant was a hybrid of *C. japonica* and *C. pitardii* var. *pitardii*, *Camellia* 'Nicky Crisp'. Subsequent comparative studies, including the present work, have been carried out on two plants with extreme resistance levels: highly susceptible hybrid *Camellia* 'Nicky Crisp' and highly resistant species *C. lutchuensis* (Denton-Giles et al., 2013).

Histological studies characterized *Camellia* spp.-*C. camelliae* interactions on the cellular level. During the compatible interaction, ascospores germinated and formed primary hyphae at 12 hpi, and subcuticular growth started at 24 hpi. From 36 hpi secondary hyphae were formed (Figure 1-6).

In the resistance response, accumulation of H_2O_2 occurred at the sites of attempted fungal penetration. Moreover, resistant epidermis cells formed papillae, callose-based cell

wall structures, at the sites of contact with primary fungal hyphae (Figure 1-6) (Vingana-Singam, Long, & Rowland, 2000).

It was proposed that a susceptible interaction can be a result of the effector-triggered susceptibility, while the resistant one can be based on a PTI response (Denton-Giles et al., 2013).

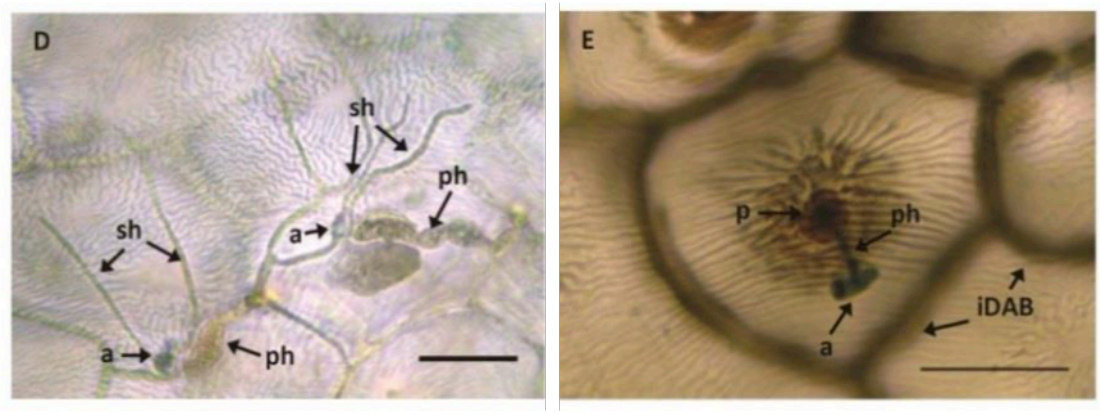

Figure 1-6 | Susceptibility and resistance response to *C. camelliae*.
Left: at 36 hours after the germinated fungus starts apoplastic growth and formation of secondary hyphae (a – ascospore, ph – primary hyphae, sh – secondary hyphae); right: fungal growth is inhibited by cell-wall associated peroxide accumulation and papillae opposition (a – ascospore, ph – primary hyphae, p – papilla). Reproduced with author's permission from (Denton-Giles, 2014).

Secretome and effectors. To identify the effector machinery of *C. camelliae*, an *in silico* secretome prediction pipeline was used (Guyon, Balagué, Roby, & Raffaele, 2014). The genome of the fungus was sequenced and used to obtain fungal protein coding genes. All predicted proteins with secretion signals were functionally annotated. 80% of proteins could be assigned to the groups: predicted proteins, carbohydrate-active enzymes (CAZymes), oxidoreductases, SSPs, and proteases. Subsequently, the comparative analysis of *B. cinerea*, *S. sclerotiorum* and *C. camelliae in silico* secretomes demonstrated that *C. camelliae* genome harbours twice as many SSPs as two other species.

Among predicted SSPs, a conserved family of cysteine-rich SSPs was found. *Ciborinia camelliae* contains 73 members (CcSSPs) of this family, while each of *B. cinerea* and *S. sclerotiorum* has only one homolog (BcSSP and SsSSP). qRT-PCR showed the activation

of CcSSPs expression during the early infection stage at 6 hpi. Ten recombinant CcSSPs, BcSSP, and SsSSP were produced in *Pichia pastoris* as secreted proteins to test their functional activity. Culture filtrates containing BcSSPs and SsSSPs, but not CcSSPs, induced necrosis in *Camellia* 'Nicky Crisp' and *C. lutchuensis* petals. It's still unclear whether CcSSPs did not induce necrosis because they are inactive homologs of BcSSP and SsSSP, or whether production and test system conditions disrupted native protein structure, inactivating them (Denton-Giles, 2014).

1.5. 'Omics' studies on plants from the genus *Camellia*

Plants of the genus *Camellia* of the family Theaceae have great economic and cultural importance having among them a cash crop (*C. sinensis*, or tea shrub), oil-producer plants (*C. oleifera)* (S. Li & Liu, 2011) and plants with ornamental value (*C. japonica, C. reticulata)* (Xin et al., 2015). The genus is one of the most challenging plant groups for taxonomy since it contains a great number of interspecific hybrids and polyploids, which also makes it difficult to sequence and assemble high-quality plant genomes and transcriptomes (Huang, Tong, Zhang, & Gao, 2013). Nevertheless, as can be seen from the growth of number of published *Camellia* sequences in GenBank (Figure 1-7), plants from the genus became subjects of numerous genomic and molecular studies.

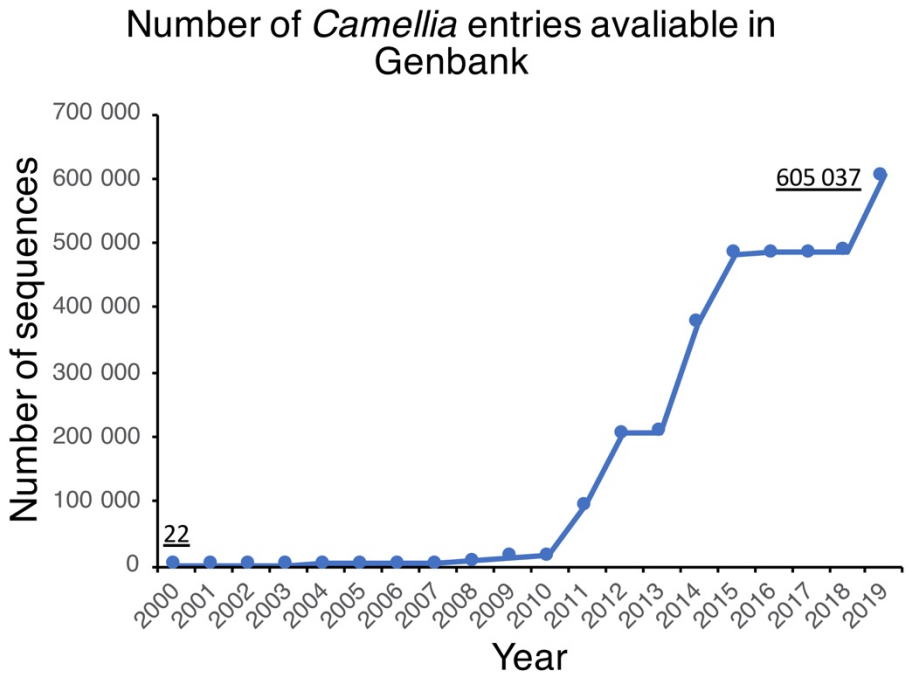

Figure 1-7 | Number of *Camellia* sequences available in GenBank between 2000 and 2019.

***Camellia* genomes.** Two assembled *Camellia* genomes were published in 2017 and 2018. Both genomes belong to the same species, *C. sinensis* (tea crop), and, indeed, reflect complex genomic organization of plants from the genus. The projects analysed two most popular tea cultivars *C. sinensis* var. *sinensis* (Wei et al., 2018) and *C. sinensis* var. *assamica* (Xia

et al., 2017). Both varieties had large 3-Gb genomes (as compared to ~ 0.13 Gb for *A. thaliana* (The Arabidopsis Genome Initiative, 2000)), with high-repeat content of about 80% (repeat-content in *A. thaliana* genome is about 20% (The Arabidopsis Genome Initiative, 2000)). It was proposed that the expansion of the tea genome happened due to the amplification of transposable elements, whose content was estimated to be 64% and 58% of total genomes for *C. sinensis* var. *sinensis* and *C. sinensis* var. *assamica*, respectively. The researchers also found that the tea genome underwent two rounds of whole-genome duplications within last 100 mln years (Wei et al., 2018). In total, 33,932 and 36,951 protein-coding genes were predicted for *C. sinensis* var. *sinensis* (Wei et al., 2018) and *C. sinensis* var. *assamica* (Xia et al., 2017), respectively (25,498 in *A. thaliana* genome (The Arabidopsis Genome Initiative, 2000)).

Transcriptome assemblies. To understand molecular mechanisms of biological processes, RNA sequencing (RNA-seq) is widely utilized nowadays, and it is the most commonly used approach to obtain genetic datasets of *Camellia* plants.

The first *Camellia* transcriptome sequencing and assembly was performed in 2011 for *C. sinensis* var. *Longjing* (Shi et al., 2011). Transcriptomic data were annotated and used for analysis of secondary metabolic pathways that are crucial for tea quality: biosynthesis of flavonoids, theanine and caffeine. In the same manner, a transcriptomic study of oil-rich *C. oleifera* helped to identify key genes for fatty acid biosynthesis and catabolism in this plant. Moreover, comparative analysis of orthologs between *C. sinensis* and *C. oleifera* revealed 211 genes under the positive selection, which probably could play a major role in the evolutionary processes of the genus *Camellia* (Xia et al., 2014). There are also transcriptomic studies on ornamental plants. The *C. chekiangoleosa* transcriptome was used to investigate anthocyanin biosynthesis pathways, which are responsible for the pigmentation of plant petals (Z. Wang et al., 2014). Photoperiodic flowering and pigment biosynthesis pathways were investigated for ornamental and oil-producing *C. reticulata* (Yao,

Huang, Tong, Xia, & Gao, 2016). While the majority of camellias bloom in winter, endemic to Southern China and critically endangered *C. azalea* is a summer-flowering species (Ren et al., 2014, 2016). To understand the molecular mechanisms of blooming control, RNA-seq analysis of floral tissues was conducted. Expression patterns of *SVP* (SHORT VEGETATIVE PHASE) and *AGL24* (AGAMOUS-LIKE 24), two dormancy-associated genes, were altered in comparison with other plants; also, several hormonal pathways have been shown to play a role in flowering time regulation. Authors suggested that future comparative studies with other *Camellia* species are necessary to understand mechanisms of plant seasonal adaptation and could help to breed new summer-flowering *Camellia* hybrids (Fan et al., 2015).

I analysed transcriptome assembly strategies and resulting transcriptomes from the publications described in this paragraph. Comparison of RNA-seq experiments, transcriptome assemblies, and annotation statistics are presented in the table below (Table 1-1). Interestingly, *Camellia* transcriptomes have large numbers of transcripts, and less than a half of them may be annotated.

Table 1-1 | Comparison of published transcriptome assemblies of plants from the genus *Camellia*.

	Camellia "Nicky Crisp"	*C. lutchuensis*	*C. azalea*	*C. sinensis*	*C. reticulata*	*C. taliensis*	*C. oleifera*	*C. chekiangoleosa*
Publication	Current study and (Denton-Giles, 2014)		(Fan et al., 2015)	(Shi et al., 2011)	(Yao et al., 2016)	(H.-B. Zhang et al., 2015)	(Xia et al., 2014)	(Z. Wang et al., 2014)
Sequencing Method	Illumina HiSeq 2000		Illumina HiSeq 2000	Illumina GA IIx	Illumina HiSeq 2000	Illumina HiSeq 2000	454 GS FLX Platform	454 GS FLX Titanium Platform
Raw reads number*	800 mlns		120 mlns	34.5 mlns (75 bp, paired and single)	394.9 mlns	241.5 mlns	591,033 (average 350 bp)	219,906 (350-600 bp)
Assembly Method	Trinity		Trinity	SOAPdenovo	Trinity	Trinity	Newbler	CAP3
Organs	Flowers	Flowers	Flower buds	Shoots, roots, stems, flowers, leaves and seeds	Leaf buds, leaves, flower buds, flowers, immature fruits	Shoots, leaves, flower buds, flowers	Shoots, leaves, flower buds, flowers	Flowers
Number of transcripts (nr)	133,998	109,291	79,363	127,094	141,460	145,738	104,842	46,279
N50	1076	1204	1196	506	1080	995	771	504
Blastx hits	36,737	33,939	32,826	41,483	68,026	38,947	43,690	23,321
Genes with assigned GO	23,783	30,935	24,086	34,577	39,301	24,988	27,531	NA

**Mlns - millions*

Transcriptomic studies of responses to abiotic stresses. Comparative transcriptomics of different organ tissues or differently treated tissues is a tool to investigate biological processes at the molecular level. Detection of stress-associated genes is of particular interest, because this knowledge can be used to breed resistant plants.

Low temperatures are a critical factor affecting tea plant growth and geographical distribution. Gene expression levels were compared between acclimated and non-acclimated plants. Cold sensor genes, calcium signalling pathways, anti-freezing protein genes and genes of detoxifying enzymes (catalase, superoxide dismutase, peroxidase) were shown to be important for the cold resistance of *Camellia* plants (X.-C. Wang et al., 2013). Mechanisms of winter dormancy of evergreen tea plant involves down-regulation of growth and cell division pathways, and, interestingly, modulation of leaf senescence processes (Paul et al., 2014). *Camellia taliensis*, also known as "wild tea", is an important non-cultivated relative of the tea plant. It grows at high altitudes and demonstrates resistance to many abiotic stresses, which could be used for tea plant improvement. Comparative transcriptomic analysis has shown that *C. taliensis* has more R genes than *C. sinensis*, as well as more *LEA* (LATE EMBRYOGENESIS ABUNDANT) genes, possibly participating in cold resistance (H.-B. Zhang et al., 2015).

Transcriptomic studies of responses to biotic stresses. Blister blight disease is caused by the biotrophic basidiomycete pathogen, *Exobasidium vexans*. Being a leaf disease, it severely affects tea production. Analysis of gene up- and down-regulation in response to the infection in resistant and susceptible plants was used to unravel the molecular basis of resistance to blister blight. In resistant plants, up-regulated genes were in groups of R genes, defence-related enzymes (superoxide dismutase, MPKK6), transcription factors (WRKY, NAM), retrotransposons and chaperones (Jayaswall et al., 2016). The authors make a note that these putative defence mechanisms are close to the resistance responses described in *A. thaliana*; and activation of RPM1 and RPS2-like genes (mentioned in

Chapter 1.1) could suggest that the guard model also works in the resistance to blister blight in tea plants (Jayaswall et al., 2016).

Transcriptomic analysis was also utilized to study the interaction between two cultivars of *C. sinensis* and *Colletotrichum fruticola*, which causes anthracnose – a leaf disease severely affecting the tea industry in China. The results showed that the resistant tea cultivar activated ROS production and induced cell death in response to the pathogen. Further microscopic studies verified the results of the RNA-seq analysis (Yuchun Wang et al., 2018).

Metabolomic studies on *Camellia* plants. Majority of metabolomic studies on *Camellia* plants have been designed to investigate bioactive compounds of tea and *Camellia* oil. For example nuclear magnetic resonance (NMR)-based screening allowed researchers to investigate the influences of light, climate, and geographical location on the accumulation of various metabolites in tea leaves (Ji et al., 2018; Lee et al., 2010, 2015). Often transcriptomic and metabolomic analyses are used together to better describe temporal changes in plant metabolism. Targeted analysis of metabolite content and gene expression analysis was performed to check how pruning activates the accumulation of catechins – bioactive compounds, which are also responsible for the bitter taste of tea. Authors found, that pruning stimulates the accumulation of epigallocatechins, so that tea obtained from wild unpruned tea plants has lower bitterness (Lee et al., 2015). Integrated metabolomics and transcriptomics also were used to study the biosynthesis of terpenoids, which are major volatile contributors to tea aroma (Q. Xu et al., 2018), and flavonoids associated with tea flavour (Huang, Yao, Xia, & Gao, 2018). A study also investigated the role of secondary metabolism in tea resistance to *C. fruticola*, and found that caffeine and catechins can contribute to plant defences, inhibiting pathogen's growth by targeting fungal cell walls and plasma membrane (Y.-C. Wang et al., 2016).

Interactomic studies on *Camellia* plants. Analysis of biological networks, which describe indirect interactions between genes or physical interactions between molecules, provide an insightful way to study various biological processes. To the best of my knowledge, there are no studies investigating physical interactions between proteins in *Camellia* plants. Nevertheless, several biological networks were inferred for *C. sinensis* using two main interactome prediction approaches: co-expression analysis and interologs mapping method. The first one is based on the assumption that if two genes have correlated expressions the products of these genes are likely to be involved in one biological process. This approach was used to investigate the biosynthesis of important biologically active compounds of tea – caffeine, theanine, and catechins. The results indicated that key genes of these pathways had similar expression patterns, and also interacted with MYB, bHLH, WD40, and WRKY transcription factors. Additionally, the tested genes were correlated with enzymes of flavonoid biosynthesis (Tai et al., 2018). The interologs mapping method is based on the assumption that if two proteins were experimentally shown to interact in one organism, one may expect this interaction to be evolutionarily conserved, so the homologs of these proteins also interact in other organisms. Thus, to identify important regulators of tea plant resistance to *E. vexans* (Jayaswall et al., 2016) and *C. fruticola* (Yuchun Wang et al., 2018) authors mapped upregulated plant genes to the interactome of the model plant, *A. thaliana*, using predicted orthology relationships between plants. In summary, both studies identified R genes, MAP kinases and transcription factors, which were key regulators of tea plant resistance against these foliar pathogens (Jayaswall et al., 2016; Yuchun Wang et al., 2018).

Summing up this chapter, RNA-seq analysis coupled with *de novo* transcriptome assembly algorithms is the most common way to study non-model *Camellia* plants and can be utilised to obtain protein coding sequences and analyse gene expression. Combination of RNA-seq approach with metabolomic and interactomic techniques allowed researchers

to investigate various molecular processes behind the unique properties of plants from the genus *Camellia*.

1.6. Background and aims of the project

Macroscopic and microscopic analyses of *Camellia* plant responses to *C. camelliae*, conducted by Matthew Denton-Giles during his PhD studies, demonstrated that the tested plants varied considerably in their resistance to the fungus. The most resistant analysed species was *C. lutchuensis*; the least resistant was *Camellia* 'Nicky Crisp' (Denton-Giles, 2014). The present work describes the molecular mechanisms behind the resistance of *C. lutchuensis* to petal blight disease.

First, it was suggested that the interaction with *C. camelliae* ascospores would induce defence events in *C. lutchuensis*, which can be detected using time-course transcriptomic profiling of infected resistant petals. To test this hypothesis, I established the following objectives for this work:

1. To assemble and annotate transcriptomes of the highly susceptible *Camellia* 'Nicky Crisp' and resistant *C. lutchuensis*.
2. To detect *C. camelliae* responsive genes in the resistant species.
3. To find the main defence pathways using the available knowledge about the model plant, *A. thaliana*.
4. To functionally test the role of detected defence pathways in the susceptible response.

The results of the transcriptomic analysis demonstrated that the phenylpropanoid and jasmonate (JA) pathways were upregulated during the resistant plant response. Thus, the second hypothesis of this project became that the phenylpropanoid compounds contribute to the resistance against *C. camelliae*. The following objectives were set to test this hypothesis:

1. To test the expression of phenylpropanoid genes in the course of the resistance response.

2. To measure the concentration of phenylpropanoid metabolites in infected and mock-treated petal blight resistant petals.
3. To test the effect of phenylpropanoid metabolites on the fungal growth *in vitro*.
4. To determine the ability of phenylpropanoids to protect susceptible *Camellia* flowers.

In order to firmly identify the difference between resistance and susceptibility responses, it is important to know the virulence factors of *C. camelliae*, which trigger and modulate host responses. In a previous study, an *in silico* approach was used to predict secreted fungal proteins, which can contribute to virulence of the petal blight pathogen (Denton-Giles, 2014). In this work, I suggested that a proteomic approach can be used to detect and purify *C. camelliae* proteins, which cause necrosis in plants. Thus, to analyse the fungal proteinaceous secretome, the following objectives were performed:

1. To detect secreted fungal proteins *in planta* and *in vivo* using liquid chromatography–mass spectrometry (LC-MS) analysis.
2. To check the activity of fungal secretome in host and non-host plant tissues.
3. To purify necrogenic components of the secretome using fast protein liquid chromatography (FPLC).

A quick overview of result chapters is presented in Figure 1-8.

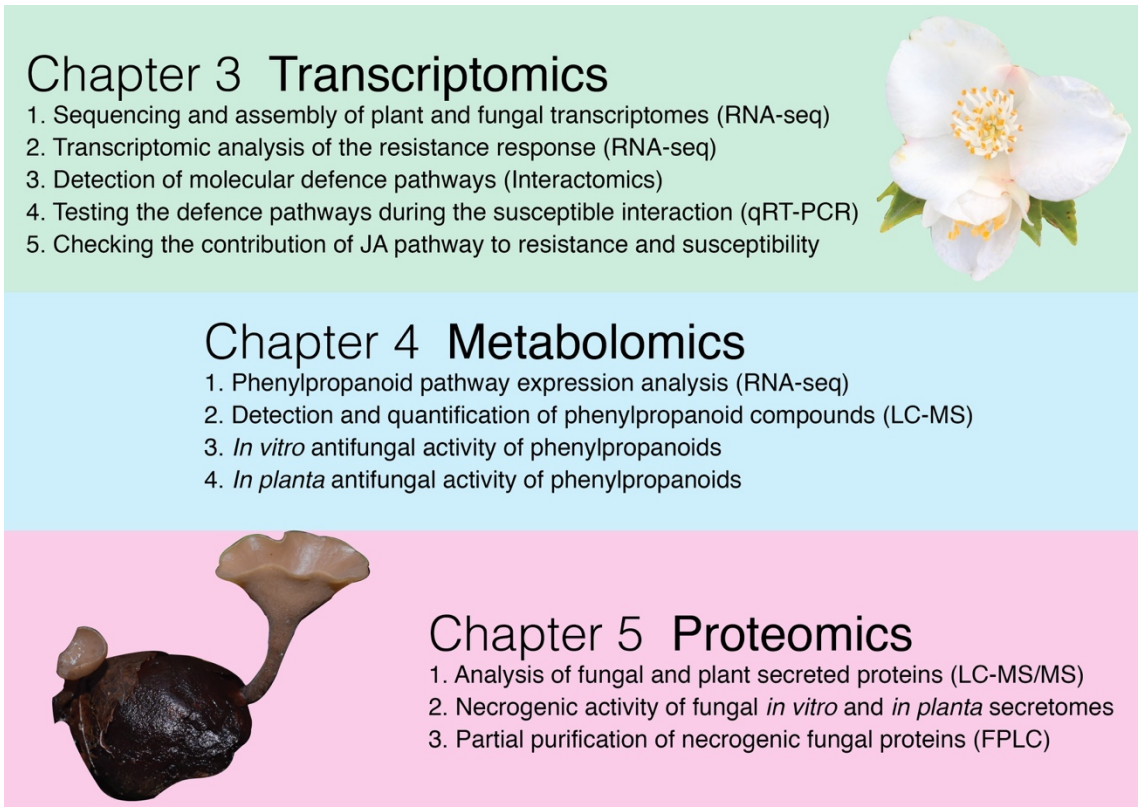

Figure 1-8 | Overview of the presented work.

Chapter 2. Materials and Methods

2.1. Plant and fungal materials and methods

***Camellia* plants.** Twelve *C. lutchuensis* (Wairere Nursery, New Zealand) and twelve *Camellia* 'Nicky Crisp' (*C. japonica* × *C. pitardii* var. *pitardii*) (Kilmarnock Nurseries, New Zealand) were grown in 12 L (size 28) plastic planter bags (Horticom, New Zealand) on the territory of Massey University Ecology Glasshouse (40°23'18.7"S, 175°37'17.9"E), but outside of the glasshouse. The plants were watered 2-3 times per week. Plants were re-potted every year in November-December into Daltons Premium Seed Mix (Daltons, New Zealand) soil. Entangled and dead roots were removed with scissors during the re-potting. On the surface of the soil in each pot, three tablespoons of Scotts Osmocote (Roses, Gardenias, Asaleas & Camellias) fertiliser (Scotts, USA) were added after the re-potting.

During the petal blight season (June-September) shrubs were kept in the Massey University Plant Growth Unit glasshouse (40°22'41.22"S, 175°36'48.73"E) with air inlets covered with 30 mm thick polyester wadding to limit the entry of airborne ascospores of *C. camelliae*. The temperature in the glasshouse was maintained between +1°C and +20°C, mimicking natural conditions in New Zealand for these species (Figure 2-1).

Figure 2-1 | *Camellia* plants used in the study.
Susceptible Camellia *'Nicky crisp' (left) and resistant* Camellia lutchuensis *(right) in the glasshouse.*

Nicotiana benthamiana. Wild-type *Nicotiana benthamiana* plants from the lab stock were grown in Daltons Premium Seed Mix (Daltons, New Zealand) soil in square pots (7mm × 7 mm × 8 mm, Pöppelmann, Germany). Twelve pots were placed on a tray, and trays were kept in a Biosyn Series 6000 plant growth chamber (Contherm Scientific, New Zealand) at 21°C, 12 h/12 h light/dark period and 180 µmol/m^2/s light intensity. Initially, trays with pots were covered with plastic lids to maintain high humidity for seed germination (~ 1 week), and, then, lids were removed and humidity in the growth chamber was maintained around 70%. Plants were watered twice per week covering the bottom of the pots with a 2 cm-high water layer. 4-6-week-old plants were used for the infiltration experiments.

Fungal material. *Ciborinia camelliae* apothecia were collected at Massey University Arboretum (40°22'58.7"S 175°37'11.6"E) between July and September in 2016-2018 (Figure 2-2, left picture). The stipes of collected apothecia were wrapped in a damp paper tissue. Wrapped apothecia were placed in 25 mL glass tubes (3-5 apothecia per tube) in an inverted position with fungal caps hanging down and kept for two days to release ascospores at room condition (Figure 2-2, right picture).

Figure 2-2 | Fully developed apothecium of *C. camelliae* and collection of ascospores.

Infection assay. Apothecia in tissue paper were removed from tubes; released *C. camelliae* ascospores were collected by washing the walls of each tube with 1 mL of sterile milliQ water. Spore concentration of the resulting solution was estimated with haemocytometer. Briefly, a 10 µL aliquot of the suspension was used to quantify the concentration of ascospores with a Neubauer-improved haemocytometer (Marienfeld, Germany). The total number of spores in 16 secondary squares (with a corresponding volume of 6.25×10^{-6} mL) were counted; spores overlapping right and upper borders of a square were counted as spores located inside this square.

To calculate the cell concentration, the following equation was used (1):

(1)

$$Ascospore\ concentration\ (spores/ml) = Total\ number\ of\ counted\ spores \times 10{,}000$$

Whole fully open blooms were collected from *Camellia* shrubs breaking off the flower stems and transferred to the lab in a polystyrene box covered with lid; randomly selected petals were detached from the flowers and placed in plastic trays (640 cm^2) underlaid with damp tissue papers prior to the inoculation. 20 mL of diluted ascospore solution were sprayed on trays with petals using a trigger sprayer from a spray bottle connected to a 50 mL falcon tube. The estimated final coverage was $4.5 – 5 \times 10^4$ ascospores/cm^2. Control petals were sprayed with the same volume of sterile milliQ water. Trays with sprayed petals were covered with plastic wrap and kept in Biosyn Series 6000 plant growth chamber with temperature +21°C, 12 h/12 h light/dark period and 180 μmol/m^2/s light intensity.

***Ciborinia camelliae* mycelial culture.** The strain of *C. camelliae* from the International Collection of Microorganisms from Plants (ICMP), ICMP 19812, previously isolated from sclerotia collected in Massey University Arboretum (40°22'56.2"S 175°37'09.1"E) (Denton-Giles, 2014), was grown in the dark at 20°C on 39 g/L Difco™ Potato Dextrose Agar (PDA) (Difco Laboratories, USA) plates. The media were prepared with milliQ water and autoclaved at 121°C for 15 minutes. The bottles were kept in a water bath at 50°C before pouring.

Hormonal treatment. 1mL aliquots of 1M methyl jasmonate (MeJA) solution were prepared mixing 229 μL of MeJA (Sigma, USA) and 771 μL of ethanol and stored at -20°C. The needed amount of 1M MeJA stock in ethanol was added into the spore solution just prior to spraying to the final concentration of ethanol of 1% (v/v) and 10 mM

of MeJA and mixed by inversion. Control solution was prepared adding the same amount of 100% ethanol to a final concentration of 1% (v/v).

Lesion size measurement. Lesion size measurement was conducted as described previously (Denton-Giles et al., 2013). Briefly, images of infected petals were taken at 48 hpi. Twelve petal replicates (n = 12) from three experiment repeats were used to estimate lesion sizes with 'Colour Threshold' tool of Fiji (distribution of ImageJ) (Schindelin et al., 2012). Briefly, colour space was set to YUV, and parameters Y and U were adjusted to highlight whole petals ($60 < Y < 255$, $50 < U < 170$) or only brown lesions ($60 < Y < 255$, $50 < U < 115$). After the desired area was highlighted, it was measured with the 'measure' function. Relative lesion size was calculated dividing a measured lesion size to the size of the corresponding petal.

The sizes of lesions from the drop-inoculation experiments were measured in absolute values (cm^2). Firstly, the size measurement tool in Fiji software was calibrated using 1 cm on the ruler in the photograph. The lesion borders were highlighted manually with the selection tool, and the resulting area was measured using the 'measure' function.

2.2. Nucleic acid extraction and analysis methods

Plant RNA extraction. About 500 mg of *Camellia* petal tissue (9 petals of *C. lutchuensis* or 1 petal of *Camellia* 'Nicky Crisp') was used to extract RNA with Zymo-Research Quick-RNA™ Miniprep kit (Zymo Research, USA) according to the manufacturer's protocol. Snap-frozen petals were ground into the fine powder using a mortar and pestle for about 30 s with two additions of liquid nitrogen every 10 s. The ground samples were transferred into 2 mL screw cap plastic tubes, and 1 mL of RNA Lysis Buffer was added to the ground tissue. The tubes were kept on ice for 15 min mixing with inversion every 5 min. After centrifugation at 17000 g for 1 min, 500 µl of the resulting supernatant was transferred onto a Spin-Away™ filter-column that was placed in a collection tube. Columns in collecting tubes were centrifuged at 17000 g for 30 s and the columns were discarded. The flow-through in collecting tubes was mixed with the same volume (500 µl) of ethanol. The mixture was transferred into a Zymo-Spin™ IIICG column, which binds RNA, that was placed in a new collection tube and centrifuged at 17000 g for 30 s. Flow-through was discarded and the step was repeated with the remaining 500 µl of the sample-ethanol mixture to maximise RNA yield. Zymo-Spin™ IIICG columns with bound RNA were washed with 100 µL of RNA wash buffer centrifuging at 17000 g for 30 s and the flow-through was discarded. 50 µL of DNase mixture (2 µL of DNase (Roche, USA), 5 µL of 10X DNase buffer, 43 µL of water from the kit) was added to the matrix of each Zymo-Spin™ IIICG column with bound RNA, and the DNA digestion reaction was conducted on a heat block at 37°C for 15 min. Then the columns were washed with 400 µL of RNA Prep buffer, 700 µL of RNA Wash buffer, and 400 µL of RNA Wash buffer, centrifuging at 17000 g for 30 s for each wash step. After the wash steps, Zymo-Spin™ IIICG columns with bound RNA were placed in 1.5 mL tubes, and collection tubes were discarded. RNA was eluted from the columns with 50

µL of DNase/RNase free water (provided in the kit) by centrifugation at 17000 g for 1 min. Resulting samples were stored at -80°C.

RNA quality check. Quality and concentration of RNA samples were checked using 2 µL sample aliquots with a NanoDrop™ 1000 spectrophotometer (Thermo Fisher Scientific, USA). Only samples with 260 nm/280 nm absorbance ratio equal to 1.8 or higher, and 260 nm/230 nm absorbance ratio higher than 1.5 were used for the further analysis. The integrity of RNA samples was checked via the presence of two distinct bright bands without smear, corresponding to 28S and 18S rRNA, by 1% agarose gel electrophoresis.

The quality of the RNA samples extracted for the sequencing experiments were also checked using an Agilent 2100 Bioanalyzer with RNA 6000 Nano kit (Agilent Technologies, USA) at the Massey Genome Service. Only samples with RNA integrity number (RIN) higher than 7 were used for further analysis.

cDNA synthesis. To synthesize cDNA for subsequent gene expression analysis, Transcriptor First Strand cDNA Synthesis Kit (Roche, USA) was used. The volumes of RNA samples that contain 1 µg of total RNA were transferred into 200 µL PCR thin wall plastic tubes. Then, 1 µL of Anchored-oligo (dT_{18}) primers and water (provided with the kit) were added up to a final volume of 13 µL. Mixtures were heated at 65°C for 10 min in a Mastercycler® Pro machine (Eppendorf, Germany). Then, 0.5 µL of RNase inhibitor solution, 0.5 µL of reverse transcriptase enzyme solution, 2 µL of deoxynucleotide mix, and 4 µL of 5X reaction buffer were added to each sample. Tubes were further incubated at 55°C for 30 min, and the reaction was terminated by heating to 85°C for 5 min. Resulting samples were stored at -20°C.

Preparation of primer stocks. Primers used in the study were synthesised by Macrogen (Republic of Korea). 250 µL of sterile milliQ water was added to dissolve primers creating 100 pmol/µL stock solutions. Working primer solutions (10 pmol/µL)

were prepared via ten-fold dilution of the stock solutions. Primer sequences are presented in Appendix A, Table A-1.

General PCR. To 0.5 µL of cDNA samples, 10 pmol (1 µL) of target-specific forward primers, 10 pmol (1 µL) of target-specific reverse primers and 12.5 µL of Taq 2X Master Mix (New England Biolabs, USA) was added into a 200 µL PCR thin wall plastic tube as well as sterile milliQ water up to a final volume of 25 µL. The reaction was conducted on a Mastercycler® Pro machine (Eppendorf, Germany). Initial denaturation at 95°C was conducted for 5 min and followed by 30 cycles of reaction (95°C for 30 s, 60°C for 15 s, 68°C for 10 s) and a final extension step of 68°C for 5 min. The presence and size of PCR products was checked by agarose gel electrophoresis.

Agarose gel electrophoresis. 1% (w/v) and 2 % (w/v) agarose gels prepared with Tris-acetate-EDTA (TAE) buffer (40 mM Tris, 20 mM acetic acid, 1 mM EDTA) were routinely used to separate and visualize RNA and small (< 200 bp) DNA fragments, respectively. The required amount of HyAgarose™ LE Agarose (HydraGene, China) powder was added into 100 mL of TAE buffer in a 200 mL bottle and melted in a microwave with stirring every 30 s until the agarose was completely dissolved. The mixture was poured on a casting tray with a gel comb and solidified (~ 30 min). To each analysed sample, 1/5 of the sample volume of 6X Blue Gel Loading Dye (New England Biolabs, USA) was added, and 20 µL of the resulting mixtures were loaded onto the gel. HyperLadder™ 1kb (Bioline, UK) was used as a molecular weight marker. Gels were run for 40 min at 100 V voltage in TAE buffer and stained in 10 µg/mL ethidium bromide solution in milliQ water for 10 min. Stained gels were visualised using a Bio-Rad Gel Doc XR+ system (Bio-Rad, USA) using Image Lab v6.0 software (Bio-Rad, USA).

Reverse transcription quantitative polymerase chain reaction (qRT-PCR). qPCR was performed on a LightCycler® 480 Instrument II using LightCycler® 480 SYBR Green I Master kit (Roche, USA) and transcript-specific primers (Appendix A, Table A-1).

Reaction mixture of final volume of 10 µL consisted of 0.5 µL forward primer (10 pmol/µL), 0.5 µL of reverse primer (10 pmol/µL), 5 µL 2X SYBR Green I master mix, 1.5 µL water (provided with the kit) and 2.5 µL of ten-fold diluted cDNA. Negative control samples were prepared for each primer pair using water instead of diluted cDNA. Samples were loaded on a 96-well LightCycler® 480 Multiwell Plate (Roche, USA). The reaction was conducted using LightCycler® 480 Software (Roche, USA): the initial denaturation at 95°C for 5 min was followed by 44 cycles of 95°C for 10 s, 60°C for 10 s, and 72°C for 10 s. Raw data was collected from three technical and three biological replicates for each treatment. Quantification cycle (Cq) and primer efficiency values were calculated using LinRegPCR v2015.0 software (Ruijter et al., 2009). Two reference control transcripts were chosen for each plant for their stable expression at all time points and treatments, and from the studies on *C. sinensis* (L.) O. Kuntze (X. Hao et al., 2014). Eukaryotic elongation factor-1 alpha (*EF1α)* and polypyrimidine tract-binding protein 1 (*PTB1)* were used for *C. lutchuensis*, and *PTB1* and Tubulin alpha-3 (*Tub α-3*) for *Camellia* 'Nicky Crisp'. Relative expression fold-change was calculated using the following equation for each tested sample (2):

(2)

$$Relative\ expression\ value = \frac{Primer\ efficiency\ of\ the\ target\ gene^{Calibrator\ Cq_{target} - Treatment\ Cq_{target}}}{Primer\ efficiency\ of\ the\ control\ genes^{Calibrator\ Cq_{control} - Treatment\ Cq_{control}}}$$

Where Calibrator Cq_{target} – mean Cq value of the target-gene in the control treatment samples,

Treatment Cq_{target} – mean Cq value from three technical replicates of the target-gene in the analysed sample,

Calibrator $Cq_{control}$ – mean Cq value of the housekeeping genes in the control treatment samples,

Treatment $Cq_{control}$ – mean Cq value from three technical replicates of the housekeeping genes in the analysed treatment sample.

2.3. Metabolite extraction and analysis methods

Extraction of water-soluble metabolites from *Camellia lutchuensis* petals. The extraction protocol described below was provided by Dr Arvind Subbaraj, AgResearch (New Zealand). Snap-frozen *C. lutchuensis* petals (20 petals per biological replicate) were ground in liquid nitrogen into a fine powder for about 30 s using a mortar and pestle. Samples were transferred into 2 mL screw cap plastic tubes with a hole in the cap (made by punching sharp forceps through the cap) and freeze-dried overnight in a 2 L metal container (100 mTorr, -90°C). 50 mg aliquots of freeze-dried samples were transferred into 1.5 mL tubes and used for the extraction. To each sample, 1 mL of chloroform/methanol (pre-chilled at -20°C) (1:1, v/v) with internal standards (IS) (1.6 mg/L of d_5-L-tryptophan, d_4-citric acid, d_{10}-leucine, d_2-tyrosine, d_{35}-stearic acid, d_5-benzoic acid, $^{13}C_2$-glucose, and d_7-alanine, prepared and provided by Dr Arvind Subbaraj, AgResearch) was added. Each sample was mixed using a vortex for 30 s and incubated at -20°C for 1 h. After that, 500 µL of sterilised milliQ water was added into each tube, and samples were vortexed for 30 s. The samples were centrifuged for 15 min at 12000 g and +4°C. 500 µL of the upper aqueous phase was transferred into a new 1.5 mL tube. Resulting samples were dried in a Savant DNA 110 SpeedVac concentrator (Thermo Fisher, USA) on medium drying rate setting until fully dry (~ 4 h). Samples were re-dissolved in 100 µL of acetonitrile/water (1:9, v/v) (prepared and provided by AgResearch), transferred into insert vials and submitted for the LC-MS analysis.

LC-MS detection and quantification of metabolites from phenylpropanoid pathway. Re-dissolved petal extracts were analysed by Dr Arvind Subbaraj, AgResearch (New Zealand). A pooled mix of all samples was prepared and referred to as the QC (quality control) sample. QC samples were used to monitor any systematic effects of machine performance and/or sample degradation. A high-resolution, accurate mass Exactive™ mass spectrometer with Orbitrap™ technology (Exactive Orbitrap, Thermo,

USA) was used for ultra-high-performance liquid chromatography-mass spectrometry (UHPLC-MS) analysis. For semi-polar compounds, 2 μL of extract was injected into a 1.9 μm Thermo Hypersil Gold C18 column (UHPLC, 100 mm × 2.1 mm, Thermo Fisher Scientific, USA) and eluted over a 16 min gradient with a flow rate of 400 μL/min. The mobile phase was a mixture of water with 0.1% formic acid (solvent A), and acetonitrile with 0.1% formic acid (solvent B). Chromatographic gradient and other LC-MS conditions were as described by Fraser *et al.* (2013).

Samples were analysed in positive and negative ionisation modes. The runs in each mode comprised blanks, a serial dilution of authentic standard, another set of blanks followed by samples, with QC samples interspersed once for every 9 samples. Retention time, signal intensity and mass error of the internal standard were constantly monitored during the runs. Phenolic compounds and amino acids were identified using respective accurate masses, retention times, and a comparison of the elemental composition of the parent ion with that of the actual compound with a tolerance of ± 5 ppm. All UHPLC-MS analyses comprising samples and standards were conducted in triplicate. UHPLC-MS instrument control, data collection and corresponding peak and/or mass spectral analyses were conducted with Thermo Xcalibur software package, and statistical analyses – in Microsoft Excel. The table below shows analysed compounds and their masses (Table 2-1).

Table 2-1 | List of detected and quantified phenylpropanoid compounds.

Compound group	Compound	Molecular weight (PubChem), g/mol	Monoisotopic mass (PubChem), g/mol	Positive ionization mode, g/mol	Negative ionization mode, g/mol
Amino acids	Tyrosine	181.191	181.074	182.082	180.066
	Phenyalanine	165.192	165.079	166.087	164.071
Phenolic acids	Cinnamic acid	148.161	148.052	149.06	147.044
	p-Coumaric acid	164.16	164.047	165.055	163.039
	Caffeic acid	180.159	180.042	181.05	179.034
	Ferulic acid	194.186	194.058	195.066	193.05
	Sinapic acid	224.212	224.068	225.076	223.06
Aldehydes	Coumaraldehyde	148.161	148.052	149.06	147.044
	Caffeyaldehyde	164.16	164.047	165.055	163.039
	Coniferaldehyde	178.187	178.063	179.071	177.055
	Sinapaldehyde	208.213	208.074	209.082	207.066
Alcohols	Coumaralcohol	150.177	150.068	151.076	149.06
	Caffeyalcohol	166.176	166.063	167.071	165.055
	Coniferalcohol	180.203	180.079	181.087	179.071
	Sinapalcohol	210.229	210.089	211.097	209.081
Glycosilated forms	Syringin	372.37	372.142	373.15	371.134
Flavonoid precusors	Naringenin	272.256	272.068	273.076	271.06

Quantification of phenolic compounds and amino acids was based on an internal standard method. A relative response factor (RRF), corresponding to a serial dilution of coumaric acid (10 mg/mL) as the external standard and spiked with the same amount of internal standard as used in the extraction solvent, was determined. Concentration (mg/g) of different compounds in each sample was calculated as follows (3):

(3)

$$Mass_{compound}(mg/g) = \frac{Peak\ area\ _{compound}}{Peak\ area_{IS}} \times RRF \times \frac{Weight_{IS}}{Weight_{sample}}$$

Where $Mass_{compound}$ – concentration of each compound in the sample (mg/g),

Peak $area_{compound}$ – peak area of the target compound

Peak $area_{IS}$ – peak area of the internal standard (d_5-L-tryptophan in positive mode, and d_2-tyrosine in negative mode) in that sample

RRF – Relative Response Factor of coumaric acid standard to internal standard

$Weight_{IS}$ – weight of internal standard in the sample (mg)

$Weight_{sample}$ – weight of the sample (g)

***In vitro* antifungal activity of metabolites from the phenylpropanoid pathway.** To check the effect of selected phenolic acids and coniferyl alcohol on fungal mycelium growth, the compounds were added into the PDA media. 0.1 M stock of the phenolic acids in ethanol and 1 M stock of coniferyl alcohol in acetone were used in the experiment. Details of preparation of the stock solutions are shown in the table below (Table 2-2). Prepared primary stock aliquots were stored at -20°C.

Table 2-2 | Preparation of stock solutions of metabolites from phenylpropanoid pathway.

Compound	Molar mass, g/mol	Amount used, mg	Solvent	Volume of the solvent used, mL	Final concentration of the stock, M
Cinnamic acid (Sigma, USA)	148,2	14.8	Ethanol	1	0.1
p-Coumaric acid (Sigma, USA)	164,2	16.4	Ethanol	1	0.1
Caffeic acid (Abcam, UK)	180,2	18.0	Ethanol	1	0.1
Ferulic acid (Abcam, UK)	194,2	19.4	Ethanol	1	0.1
Sinapic acid (Sigma, USA)	224,2	22.4	Ethanol	1	0.1
Coniferyl alcohol (Sigma, USA)	180,2	18.0	Acetone	0,1	1

50 mM phenolic acid stock solutions were prepared via two-fold dilution of the 0.1 M stocks with 100% ethanol; 10 mM phenolic acid stock solutions were prepared via five-fold dilution of the 50 mM stocks with 100% ethanol. Coniferyl alcohol stocks had concentrations 1M, 0.5 M and 0.1 M, and were prepared via the same dilution procedures using 100% acetone as a solvent. PDA plates with 1 mM, 0.5 mM and 0.1 mM concentrations of the compounds were prepared using phenolic acid and coniferyl alcohol stock solutions according to the table below (Table 2-3). 15 mL of freshly made and autoclaved PDA (maintained at 50°C) was poured into a sterile 50 mL falcon tube; 150 µL of phenolic acid or 15 µL of coniferyl alcohol stock was added into PDA, and the falcon tube content was gently mixed by inversion. The resulting mix was poured onto a Petri dish (90 mm × 15 mm). Control plates were prepared adding 150 µL of 100% ethanol, or 15 µL of 100% acetone.

Table 2-3 | Preparation of PDA plates containing metabolites from the phenylpropanoid pathway.

Final concentration in the plate, mM	Agar volume per plate, mL	Concentration of solution added, M	Volume of solution added, µL
Phenolic acids			
1	15	0.1	150
0.5	15	0.05	150
0.1	15	0.01	150
Coniferyl alcohol			
1	15	1	15
0.5	15	0.5	15
0.1	15	0.1	15

PDA plates were inoculated with 5 mm agar disc-plugs, which were obtained from the edge of actively growing 5-7 days old *C. camelliae* mycelia using a punch. The plates were sealed with parafilm and grown in the dark at 20°C. The mycelium diameter was measured at 4, 5, and 7 days post inoculation (dpi). For each plate, two measurements were performed, as shown in the figure below (Figure 2-3). The final diameter was calculated as an average of these two measurements. Five biological replicates were performed for each treatment, and experiments were repeated twice.

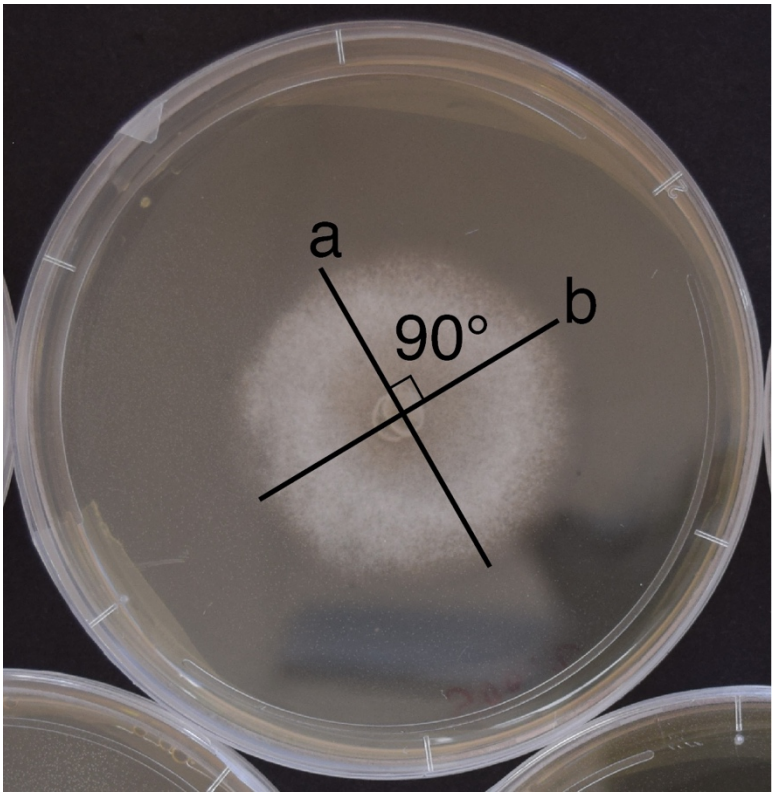

Figure 2-3 | Measurement of fungal mycelium size.
The diameter of a mycelium was measured as an average of two perpendicular diameters (a and b), which intersect at the centre of the initial agar disc-plug.

In planta antifungal activity of metabolites from the phenylpropanoid pathway.

To check the influence of the compounds on petal lesion development, phenolic acids were added into spore solutions prior to the drop-inoculation. 10 µL of 0.1 M stock of phenolic acids in ethanol, or 1 µL of 1 M stock of coniferyl alcohol in acetone were added into 1 mL of spore solution of 10^5 spores/mL concentration. 10 µL drop of the mix were put on right petal halves. Left halves were inoculated with 10 µL of the same spore solution containing corresponding amount of 100% ethanol or 100% acetone instead of the stock. Inoculated petals were placed in trays underlaid with damp paper towels. Trays were covered with a plastic wrap and kept in a Biosyn Series 6000 plant growth chamber with temperature +21°C, 12 h/12 h light/dark period and 180 µmol/m^2/s light intensity.

2.4. Protein extraction and analysis methods

***Ciborinia camelliae* culture filtrate.** *Ciborinia camelliae*, strain ICMP 19812, was grown in the dark at 20°C on PDA plates. To obtain *C. camelliae* culture filtrate, 25-500 mL of 24 g/L Difco™ Potato Dextrose Broth (PDB) (Difco Laboratories, USA) was prepared with milliQ water and autoclaved at 121°C for 15 minutes. The media were inoculated with an agar plaque of the size 1 cm x 1 cm obtained from the edge of one-week-old colony of *C. camelliae*. Cultures were grown at 20°C in the dark for up to 1 month in airtight 50-1000 mL bottles closed with a plastic lid. Culture filtrate was harvested by centrifugation of the cultures at 3000 g for 5 min and resulting supernatant was sterilised through a 0.2 μm filter attached to a 50 mL sterile syringe. 10 mL and 1 mL aliquots of the culture filtrate were stored at -20°C and defrosted when needed.

To check the influence of temperature on necrosis-inducing activity of the culture filtrate, 0.5 mL aliquots in 1.5 mL tubes were kept for 4 h at 37°C, 50°C or 80°C. To perform a proteinase treatment, 25 μL of proteinase K (Roche, Switzerland) stock solution (20 mg/mL) were added to 475 μL of the culture filtrate to a final concentration of the enzyme of 1 mg/mL and the mix was kept at 37°C for 4 h.

Freeze-drying. For anion-exchange chromatography, 100 mL of the culture filtrate was collected and frozen at -20°C in a 250 mL bottle. After that, the lid was loosened, and the bottle was placed in a 2 L metal freeze-dryer container. The freeze-drying was conducted for 48 h at 100 mTorr pressure and -90°C. The obtained lyophilizate was diluted in 15 mL of 20 mM Tris-HCl buffer pH 8.0

Collection of apoplastic fluids from *Camellia* petals. Mock-treated and infected *Camellia* 'Nicky Crisp' petals were collected at 48 hpi after the treatment and fully infiltrated with sterile milliQ water using a 1 mL syringe with needle (Figure 2-4, pictures 1 and 2). Three *Camellia* 'Nicky Crisp' or fifteen *C. lutchuensis* petals were wrapped in Miracloth (Merck, Germany), and inserted in a 50 mL plastic tube. The tubes were covered with lids

to clamp the edges of Miracloth and suspend the petals on the top of the tube (Figure 2-4, picture 3). Tubes with petals were centrifuged at 400 g for 15 min and 1000 g for 5 min. The liquid was collected from the bottom of the 50 mL tubes (~300-500 µL for *Camellia* 'Nicky Crisp' and ~100-200 µL for *C. lutchuensis*, Figure 2-4, picture 4), sterilised using 0.2 µm filters attached to 10 mL syringes and transferred to 1.5 mL tubes to be stored at -20°C. The petals were inspected to ensure the absence of any mechanical damage caused by the procedure (Figure 2-4, picture 5).

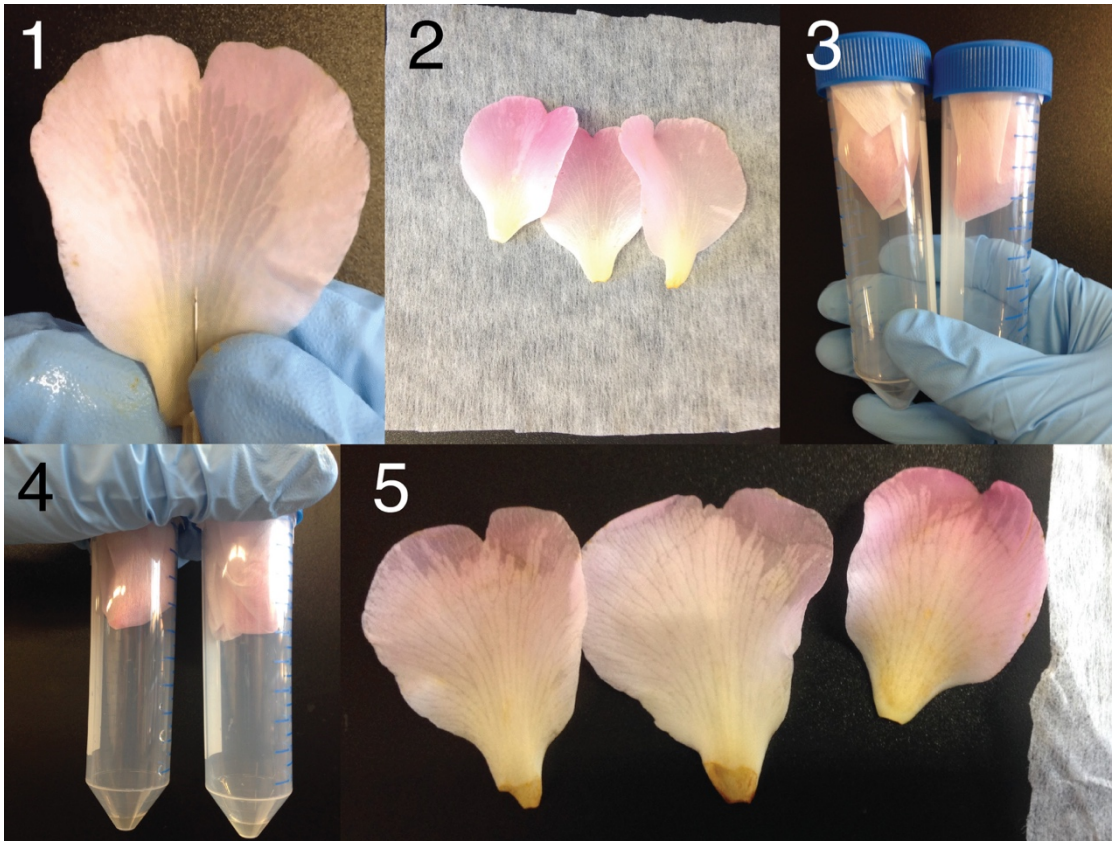

Figure 2-4 | Collection of apoplastic fluids from camellia petals.
Freshly collected Camellia *petals were injected with sterile milliQ water (1) and wrapped in Miracloth (2). Wrapped petals were inserted in 50 mL falcon tubes, and edges of the Miracloth were fixed with a screw cap (3). Tubes were centrifuged and apoplastic fluids were collected (4). After the collection of the fluids, petals were checked for the presence of mechanical damage (5).*

Dialysis of samples. SnakeSkin 3.5K MWCO (3.5 kDa molecular weight cut-off) (Thermo Fisher Scientific, USA) dialysis membrane was routinely used. All dialysis procedures were conducted in two stages: 4-hour dialysis in an amount of buffer 50-100

times more than sample volume at 20°C, and then overnight against the same volume of the buffer at 4°C. Small volumes of the culture filtrate and apoplastic fluids were dialyzed in plastic tubes covered with dialysis membranes instead of the lid and fixed with a small rubber band; big volumes (5 mL or 10 mL) were dialyzed in bags made from the dialysis tubes and closed with rubber bands at both ends.

Fast Protein Liquid Chromatography (FPLC). FPLC was performed at 20°C on an AKTA purifier system using Unicorn v5.31 software (GE Healthcare, USA).

For the anion-exchange chromatography, HiTrapQ HP 1mL column (GE Healthcare, USA) was used. 50 mL of the culture filtrate was dialyzed against 20 mM Tris-HCl pH 8 buffer (buffer A) with SnakeSkin 3.5K MWCO dialysis membrane. For the chromatography of 100 ml of the culture filtrate, it was first freeze-dried, then diluted in 15 mL of the buffer A, and then dialyzed against buffer A overnight. The column was pre-equilibrated with 10 column volumes (10 mL) of buffer A. The culture filtrate was loaded at a flow rate 1 mL/min. Unbound proteins were washed out from the column with 10 column volumes of buffer A. Linear gradient of 1 M NaCl in buffer A (buffer B) up to a concentration of 1 M NaCl was used for the elution. 20 fractions of 1mL were collected at a flow rate of 1 mL/min into 1.5 mL tubes. Fractions were dialyzed against milliQ water and their necrosis-inducing activity was determined.

For the size-exclusion chromatography, Superdex 75 mL column (GE Healthcare, USA) was used. First, the column was equilibrated with 2 column volumes (50 mL) of 10 mM potassium phosphate buffer (pH 6.0) containing also 10 mM NaCl. A sample (0.5 mL of an anion-exchange fraction) was applied at a speed 0.5 mL/min. In total 25 fractions of 1 mL were eluted at a flow rate of 0.5 mL/min. Subsequently, these fractions were tested for the necrosis-inducing activity.

The absorbance was monitored at 205 nm (absorbance of peptide bonds) and 280 nm (absorbance of aromatic amino acids). Only the absorbance at 280 nm is reported due to the better protein-specificity.

Visualization of the chromatography results was performed with Python (Rossum, 1995) using Matplotlib v3.0.3 (Hunter, 2007) and PyCORN v0.19 (github.com/pyahmed/PyCORN) packages.

Necrotising activity test. All necrosis-inducing activities of the culture filtrate and FPLC fractions were tested on at least 2 petals. The culture filtrate and fractions were injected using a 1 mL syringe with needle into *Camellia* petals, and without needle into *N. benthamiana* leaves. One injection volume was about 50-100 µL. In addition to plant species described in Chapter 2.1, susceptible *C. japonica* and *C. reticulata* petals were collected from the shrubs at the Massey University Arboretum (40°22'58.7"S 175°37'11.6"E).

Protein precipitation. 1/4 volume of 100% (w/v) trichloroacetic acid (TCA) was added to the sample, gently mixed and incubated for 30 min at 4°C. Tubes with sample-TCA mix were centrifuged at 17000 g for 5 min and the supernatant was removed. Pellets at the bottom of the tubes were washed twice with 200 µL of cold acetone spinning at 17000 g for 5 min. Then pellets were dried to remove the acetone at a 50°C heat block for 10 min. Dry pellets were dissolved in 15 µL of milliQ water and 5 µL of SDS-PAGE loading buffer mix and mixed using a vortex.

Sodium dodecyl sulphate polyacrylamide gel electrophoresis (SDS-PAGE) by Laemli. For SDS-PAGE analysis, a Bio-Rad Mini-PROTEAN (Bio-Rad, USA) system was used. A spacer plate (8.3 cm × 10 cm, 0.75 mm spacer) and a short plate (8.3 cm × 10 cm) were inserted into a casting frame and placed onto a casting stand. Into the space between two plates, 3-4 mL of separating gel mixture (consisting of 12% (w/v) acrylamide/bis-acrylamide (37.5:1, Bio-Rad, USA), 0, 0.375 M Tris-HCl pH 8.8, 0.1% (w/v) SDS, 0.08% (w/v) of ammonium persulfate and 0.15% (v/v) of TEMED for

polymerisation (Bio-Rad, USA)) was poured and polymerised for 1 h in room conditions. Approximately 1 mL of stacking gel solution (5% (w/v) acrylamide/bis-acrylamide (37.5:1, Bio-Rad, USA), 0.125 M Tris-HCl pH 6.8, 0.1% (w/v) SDS, 0.15% (w/v) of ammonium persulfate and 0.3% (v/v) of TEMED for polymerisation (Bio-Rad, USA)) was added on the top of the solid separating gel; a gel comb was inserted into the stacking solution and polymerisation was conducted for 1 h. Two prepared gels were assembled into a cassette and transferred into a clamping frame. The cassette was filled with running buffer (25 mM Tris, 0.2 M glycine, 0.1% (w/v) SDS) and combs were removed from the gels. The clamping frame with a gel cassette was placed into a tank, and the tank was filled with running buffer up to level indicated on the tank. The assembled system was further used to load samples.

To 3 volumes of a sample in a 1.5 mL tube, 1 volume of reducing loading buffer (4% (w/v) SDS, 40% glycerol (v/v), 0.5 mg/mL bromophenol blue, 200 mM Tris-HCl pH 6.8; 300 μL of β-mercaptoethanol was added to 700 μL of the sample buffer before the use) was added. The tubes were boiled in a water bath (100°C) for 10 min. 20 μL of samples were loaded to gel wells. 2 μL of the pre-stained ladder, PageRuler (Thermo Fisher Scientific, USA), was added as a molecular weight marker. The gels were run at 15 mA for concentrating part and 30 mA for separating part (~ 1 h in total).

Silver stain of protein polyacrylamide gels. Pierce Silver Stain Kit (Thermo Fisher Scientific, USA) was used according to the protocol to stain protein gels. The staining procedure was performed in a glass container covered with a plastic lid. Briefly, gels were fixed at 30 mL of fixing solution (10% acetic acid, 40% ethanol, 50% water) for 30 min or overnight. Then they were washed twice for 15 min with 30 mL of 10% ethanol solution and twice for 15 min with 30 mL of milliQ water. After that, gels were sensitized in 25 mL of sensitizer solution (25 mL of milliQ water and 50 μL of gel sensitizer stock solution from the kit) and washed twice with 30 mL of milliQ water for 1 min. Silver

staining was performed for 30 min in 25 mL of stain solution (25 mL of stain solution with 0.5 mL of stain enhancer from the kit) and gels were washed twice in 30 mL of milliQ water for 20 s. The stain was developed in 25 mL of the developing solution (25 mL of developer with 0.5 mL of stain enhancer) for 2-3 min and the reaction was stopped by the addition of 30 mL of a 5% acetic acid solution.

Mass spectrometry (LC-MS/MS) analysis. To identify proteins extracted from fungal culture filtrate and petal apoplastic fluids, LC-MS/MS analysis was performed by the Auckland University Mass Spectrometry Centre (New Zealand).

Proteins were precipitated from 400 mL of culture filtrate of two-week-old *C. camelliae* liquid culture using the above-described TCA protocol. Analysis of extracted proteins from one biological replicate was performed on an Eksigent 425 nanoLC chromatography system (Sciex, Framingham MA, USA) connected to a TripleTOF 6600 mass spectrometer (Sciex, USA); the system was controlled by the Analyst TF v1.7 software package (Sciex, USA). The sample was injected onto a 0.3 x 10 mm trap column packed with Reprosil C18 media (Dr Maisch, Germany) and desalted before being separated on a 0.075 x 200 mm picofrit column (New Objective, USA) packed in-house with Reprosil C18 media. The following gradient was applied at 250 nL/min using a NanoLC 400 UPLC system (Eksigent): 0 min 1%B; 2 min, 1%B; 105 min, 35%B; 110 min, 98%B; 115 min, 98%B; 116 min, 1%B, 120 min, 1%B (A - 0.1% formic acid in water, B - 0.1% formic acid in acetonitrile).

The picofrit spray was analysed using a TripleTOF 6600 Quadrupole-Time-of-Flight mass spectrometer (Sciex, USA) scanning from 350-1600 m/z for 250 ms; 40 most abundant multiply-charged peptides (m/z 80-1600) were analysed with 40 ms MS/MS scans for a total cycle time of ~1.9 s.

The resulting data was searched against a database containing *C. camelliae* protein sequences (Denton-Giles, 2014) appended with all potato entries (*Solanum tuberosum*) from

Uniprot (70,661 entries in total) using ProteinPilot v5.0 (Sciex, USA). Search parameters were as follows: Sample Type, Identification; Search Effort, Thorough; Cys Alkylation, Iodoacetamide; Special Factors; Urea Denaturation, Digestion, Trypsin.

The same method was used to detect proteins extracted from petal apoplasts (one biological replicate extracted from three sterile-water-sprayed *Camellia* 'Nicky Crisp' petals, and one biological replicate extracted from three infected *Camellia* 'Nicky Crisp' petals). For the LC step, the following gradient was applied at 250 nL/min using a NanoLC 400 UPLC system (Eksigent): 0 min 2%B; 2 min, 2%B; 18 min, 40%B; 20 min, 90%B; 24 min, 90%B; 24.5 min, 2%B, 45 min, 2%B (A - 0.1% formic acid in water, B - 0.1% formic acid in acetonitrile).

Mass spectra scanning was performed on TripleTOF 6600 Quadrupole-Time-of-Flight mass spectrometer (Sciex, USA) from 350-1600 m/z for 150 ms; 30 most abundant multiply-charged peptides (m/z 100-1600) were analysed by 40 ms MS/MS scans for a total cycle time of ~1.5 s.

The resulting peptides were searched against a database containing predicted *Camellia* 'Nicky Crisp' proteins (proteome prediction method is described below in Chapter 2.5) plus *C. camelliae* protein sequences (Denton-Giles, 2014) appended with common contaminant sequences (110,542 entries in total) using ProteinPilot v5.0 (Sciex, USA) with following search parameters: Sample Type, Identification; Search Effort, Thorough; Cys Alkylation, Iodoacetamide; Digestion, Trypsin.

2.5. Bioinformatical and statistical methods

Reference-transcriptome sequencing. For reference transcriptome sequencing, one infected and one uninfected sample were collected at 48 hpi for *C. lutchuensis* and *Camellia* 'Nicky Crisp'. Library preparation and RNA sequencing was performed by New Zealand Genomics Limited (New Zealand) on an Illumina HiSeq 2000 (Illumina, USA). The paired-end reads (2 × 100 bp) were processed and quality-filtered using Cutadapt v1.14 (Martin, 2011) and SolexaQA++ v3.1.7.1 (Cox, Peterson, & Biggs, 2010) with a Phred quality score of 20 (99% base call accuracy). This step was performed in the previous project by Matthew Denton-Giles (Denton-Giles, 2014).

Transcriptome assembly. Fungal reads from infected samples were mapped to the reference *C. camelliae* genome (GenBank GCA_001247705.1) using TopHat v2.1.1 and assembled with Cufflinks v2.2.1 (Trapnell et al., 2012) with default parameters, and unmapped reads were used to assemble plant transcriptomes using Trinity v2.2.0 (Haas et al., 2013) with default parameters. Additional sequences from infected petal transcriptomes were assigned to a fungal origin if those sequences aligned to *S. sclerotiorum* or *B. cinerea* genomes (GenBank GCA_000146945.2 and GCA_000143535.1, respectively) with E-values of 1×10^{-30} or lower. To create reference petal transcriptomes, transcripts assembled from infected and uninfected plant samples were combined and redundant transcripts were removed using CD-HIT-EST v4.6.4 (W. Li & Godzik, 2006) with 90% similarity cut-off. Assembly completeness was tested with BUSCO v3 using the 'odb9' plant single-copy orthologs dataset (Simão, Waterhouse, Ioannidis, Kriventseva, & Zdobnov, 2015). Below is the flowchart of the assembly described in this paragraph (Figure 2-5).

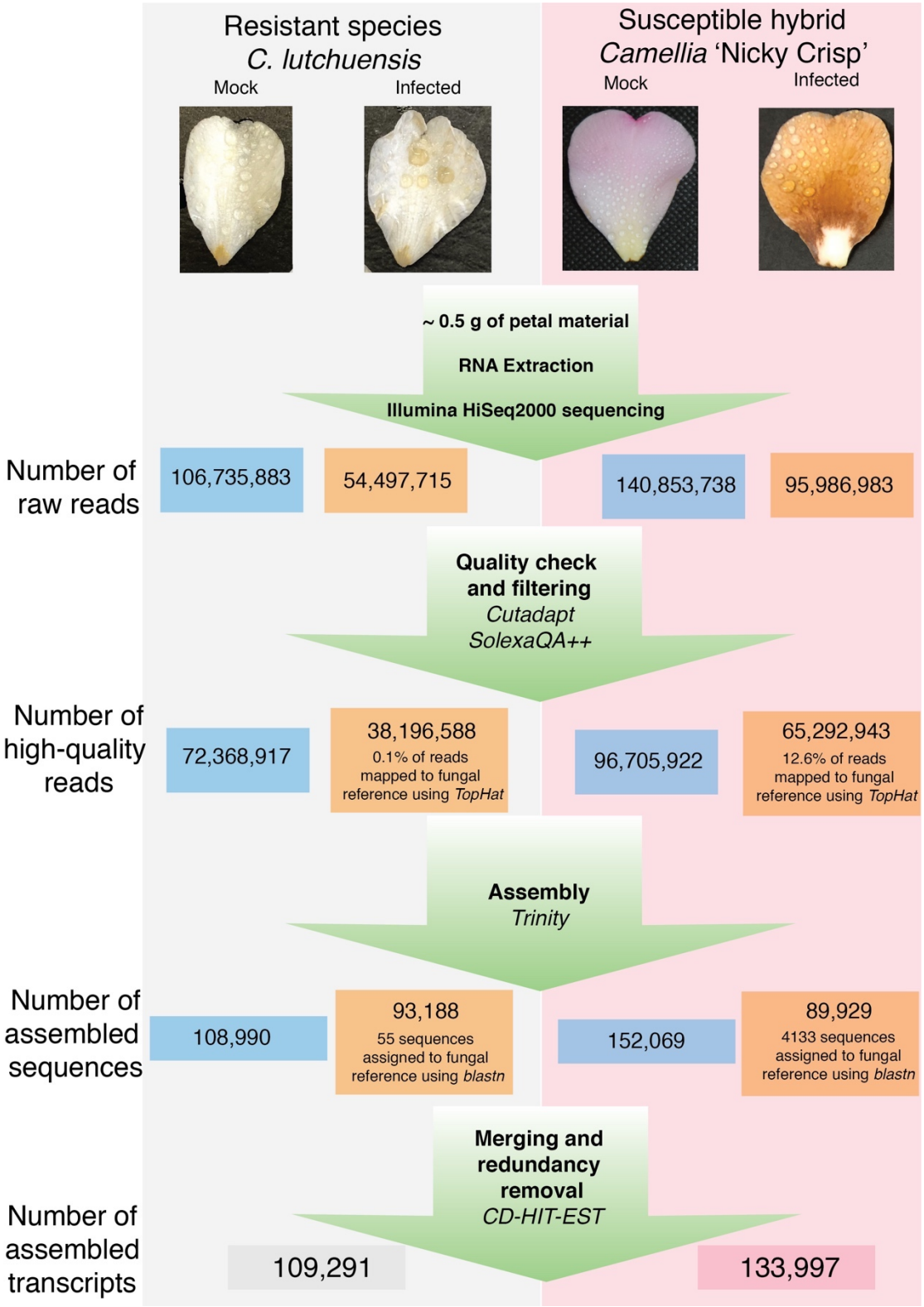

Figure 2-5 | Flowchart of the transcriptome assembly.
Process for C. lutchuensis *(grey) and* Camellia *'Nicky Crisp' (pink), and mock-inoculated samples (blue) and infected samples (brown). Green arrows represent steps in the analysis. Software names are written in italics.*

Transcriptome annotation, and prediction of proteomes. For each transcript, best matching sequences were found in the NCBI nt nucleotide database and UniProtKB/Swiss-Prot using blastn and blastx algorithms (Altschul, Gish, Miller, Myers, & Lipman, 1990), respectively, with E-value cut-off values of 1×10^{-5}. Blast2GO v3.3 (Conesa et al., 2005) was used with default parameters to assign Gene Ontology (GO) Terms (Ashburner et al., 2000) based on the best Swiss-Prot matches. TransDecoder v5 (https://github.com/TransDecoder/TransDecoder/) was used to predict plant proteomes from the assembled transcriptomes and Swiss-Prot search results. Orthologous relationships between two predicted *Camellia* proteomes and the reference proteome of *A. thaliana* (cv. *Columbia*) (UniProt UP000006548) were investigated with Proteinortho v5.16b.

Differential expression analysis. For the quantitative RNA-seq analysis, the Illumina HiSeq 2500 (Illumina, USA) platform was used to generate 2 × 125 bp paired-end reads (New Zealand Genomics Limited, New Zealand). Three biological replicates consisting of nine *C. lutchuensis* petals were collected at 6, 12, and 24 h after infection, and at 12 and 24 h after mock-treatment (18 samples in total). RNA extraction and read processing was performed as for the reference transcriptome assembly described above. High-quality reads from each sample were mapped onto the combined *C. lutchuensis* and *C. camelliae* reference transcriptomes using Bowtie v2.3.0 (Langmead & Salzberg, 2012), and read counts were obtained from the resulting SAM files with the mapcount Perl script (http://mpcox.github.io/mapcount/). Resulting count datasets were imported into the R software environment (R Development Core Team, 2017) and the DESeq2 package v1.17.18 (Love, Anders, & Huber, 2014) was used for differential expression and principal component analyses (PCA). A transcript was considered to be differentially expressed between two compared conditions if the $\log_2$ value of calculated fold-change was less than -1 or greater than 1, and the adjusted *P* value was less than 0.01. Heatmaps were created using R package gplots v3.0.1.1 (Warnes et al., 2019).

Prediction of expression clusters and GO-enrichment analysis. Pearson's correlation was calculated in R for the $\log_2$ fold-change values of each differentially expressed transcript pair; the distance between two transcripts was defined as 1 – correlation coefficient. The resulting distance matrix was used as an input to the hclust() function in R, which was used with default parameters to construct a clustering tree. The resulting tree was cut into ten clusters using the cuttree() function. For each predicted transcript cluster, significantly overrepresented GO terms were found with the BinGO plug-in (Maere, Heymans, & Kuiper, 2005) in Cytoscape v3.6.1 (Shannon et al., 2003). The whole assembled plant transcriptome was used as a background transcript set for each enrichment analysis. Corrected enrichment *P* values were calculated using the BinGO plug-in by means of the hypergeometric test with Bonferroni multiple testing correction.

Orthology-based interactome analysis. Based on the protein orthology analysis results described above, orthologous *A. thaliana* loci were assigned to *C. lutchuensis* differentially expressed transcripts. The lists of TAIR accession numbers, which correspond to *C. lutchuensis* expression clusters, were submitted to the STRING database (Szklarczyk et al., 2017) to search for interactions. 'Experiments', 'Databases' and 'Co-expression' were chosen as active interaction sources, and the minimum required interaction score was set to 0.4 (medium confidence) by default in STRING. Resulting networks were visualized and analysed using Cytoscape v3.6.1 (Shannon et al., 2003) and the igraph R package v1.2.2 (Csárdi & Nepusz, 2006). Network *P* values were calculated in STRING and show the probability of observing a network with the same connectivity if it was built from the same number of randomly sampled *A. thaliana* proteins. In addition, three random networks with sizes comparable to our networks were constructed to illustrate that their *P* values were higher than the significance level of 0.05. Numbers of observed interactions (graph edges) in random networks were almost equal to the expected

number of interactions. The full description of predicted networks is shown in Appendix A, Table A-2.

Annotation of proteins detected using LC-MS/MS. Sequences of proteins detected in *C. camelliae* culture filtrate and apoplastic fluids of *Camellia* 'Nicky Crisp' petals were exported as FASTA files. Resulting files were imported into Blast2GO software (Conesa et al., 2005), and searched against the NCBI non-redundant protein database (nr) using the blastp algorithm with default settings. Proteins were manually assigned into functional groups based on their best blastp hits.

Graphs and diagrams. Bar plots, pie charts, scatterplots, and line graphs were plotted in R programming language using the package tidyverse (Wickham, 2017). Heatmaps were made using the package gplots (Warnes et al., 2019). Pictures were combined and edited for visual clarity using Adobe Illustrator software.

Statistical analysis. Statistical analyses were performed in R programming language. Datasets were analysed using two-tailed Student's *t*-test, or one-way ANOVA analysis with following Tukey's honestly significant difference or Fisher's least significant difference (LSD) tests in R package agricolae (Mendiburu & Simon, 2015). Significance levels used in the analyses and calculated *P* values are shown in the results. Regression analysis of metabolite concentrations was performed using R package mgcv v1.8 (Wood, 2017).

Code. All commands and functions used in this work are presented in Appendix B.

Accession numbers. The original read datasets, which were used for *Camellia* 'Nicky Crisp' reference transcriptome assembly, *C. lutchuensis* reference transcriptome assembly and *C. lutchuensis* differential gene expression analysis, are available in NCBI with BioProject accession numbers PRJNA518146, PRJNA518136, PRJNA506291, respectively.

Chapter 3. Transcriptomic analysis of the resistance response

3.1. Introduction

Plants from the genus *Camellia* have been cultivated and traded since ancient times (H. Lu et al., 2016). In addition to being highly prized ornamental plants, comprising about 300 species and more than 3,000 cultivated varieties (Mondal, 2011), camellias are used to produce the non-alcoholic beverage, tea (*C. sinensis*), as well as seasoning and cooking oils (mainly *C. oleifera* and *C. japonica*). Many *Camellia* species and cultivars are susceptible to the fungal pathogen *C. camelliae* from the family Sclerotiniaceae, which causes petal blight disease. The main effect of this disease is the premature fall of blooms, which can reduce plant reproduction via a decrease in fruit production (Hara, 1919). The disease originated in East Asia and quickly spread throughout the world due to plant trade and wind-borne ascospores (Taylor & Long, 2000). Unfortunately, neither the application of chemical fungicides, nor the use of various biocontrol agents, have been successful in limiting infection rates or disease symptoms to levels that are tolerable by camellia growers (Saracchi, Locati, Colombo, & Pasquali, 2018).

C. camelliae is closely related to two devastating necrotrophic pathogens from the family Sclerotiniaceae with broad host ranges, *B. cinerea* and *S. sclerotiorum*, which cause grey and white mould diseases, respectively (Kohn & Nagasawa, 1984). Despite its close phylogenetic relationship to fungi whose infections are not specific to particular plant organs, *C. camelliae* infects only the floral organs of some *Camellia* species and hybrids, rapidly occupying the whole flower within just days (Denton-Giles et al., 2013).

In earlier research on cellular defence mechanisms, *Camellia* species and cultivars were shown to exhibit various levels of susceptibility and resistance to petal blight; this in turn enabled preferred candidate species and cultivars to be selected for disease resistance breeding. Microscopic analysis showed that the incompatible interaction observed for *C. lutchuensis* and *C. transnokoensis* — the most resistant *Camellia* species tested — includes localized cell death and hydrogen peroxide production. In contrast, the most susceptible *Camellia* 'Nicky Crisp' (*C. japonica* × *C. pitardii* var. *pitardii*), showed no resistance features. In tea crops, both *C. sinensis* var. *sinensis* and *C. sinensis* var. *assamica* have been shown to form a compatible interaction with *C. camelliae* (Denton-Giles et al., 2013).

To develop effective and durable petal blight resistance breeding programs, it is crucial to understand the molecular pathways that resistant *Camellia* plants use for defence. Based on their infection strategies, fungal pathogens can be classified into three groups: biotrophs that acquire nutrients from living plant tissues; necrotrophs that grow and develop on dead tissues; and hemibiotrophs that shift their growth strategy from biotrophic to necrotrophic during the course of their development. The great variation in infection strategies of fungal pathogens forces plants to exploit multiple defence mechanisms. Plant resistance can be considered as a multistep process that includes: (1) recognition of the pathogen by pattern-recognition receptors or R proteins (immune receptors), (2) activation of multiple cellular signalling networks, and (3) activation of biochemical and cellular defence processes (Katagiri & Tsuda, 2010). Transcriptomic studies of tea-pathogen interactions show that R protein immune receptors and transcription factors are master regulators of tea plant defence against the blister blight pathogen, *E. vexans* (Jayaswall et al., 2016), and reactive oxygen species facilitate the resistance to anthracnose, caused by *C. fruticola* (Yuchun Wang et al., 2018).

While activation of defence pathways prevents the development of biotrophic pathogens, perversely, cell death-mediated plant immunity can be deliberately stimulated by

necrotrophs to expand the necrotic area and hence enhance colonization (X. Wang et al., 2014). At the same time, resistance to necrotrophic pathogens still requires sophisticated and coordinated activation of multiple defence mechanisms, such as jasmonate- and ethylene-signalling (Glazebrook, 2005), mitogen-activated protein kinase cascades (X. Li et al., 2014), and the production of secondary metabolites like glycosinolates (Wu et al., 2016), phenylpropanoids (L. Xu et al., 2011), terpenoids (De Cremer et al., 2013) and camalexin (Ferrari, Plotnikova, De Lorenzo, & Ausubel, 2003). This complexity of plant-fungal interactions makes it challenging to select target defence mechanisms for molecular resistance breeding.

Here, I report the plant-fungus interaction between *Camellia* spp. and *C. camelliae*. To identify transcriptional mechanisms underpinning the resistance of *Camellia* plants to necrotrophic *C. camelliae*, I sequenced and assembled transcriptomes of petal blight-resistant *C. lutchuensis*, and petal blight-susceptible *C. japonica* × *C. pitardii* var. *pitardii* 'Nicky Crisp'. I analysed gene expression patterns associated with the resistance response to *C. camelliae*, and found candidate regulator genes of the defence process, as well as genes belonging to secondary metabolic pathways that may also contribute to resistance. Analysis of the susceptible interaction led me to conclude that the timing of the defence response is a key factor defining the outcome of necrotrophic petal blight disease. Based on the results, I suggested a disease control strategy that exploits the early activation of defence pathways in susceptible *Camellia* plants by hormonal treatment.

3.2. Results

Sequencing and assembly of reference *Camellia* transcriptomes. *De novo* assembly of short-read RNA sequences is widely used to build transcriptomes for non-model organisms that lack reference genomes. Transcriptomes for two *Camellia* plants, which differ significantly in their response to the petal blight pathogen *C. camelliae*: petal blight-resistant *C. lutchuensis*, and petal blight-susceptible *C. japonica* × *C. pitardii* var. *pitardii* 'Nicky Crisp', were generated. To construct reference floral transcriptomes, RNA was extracted and sequenced from infected and water-sprayed petals ('mock infection') at 48 h post-inoculation (hpi), generating 110 and 162 million high-quality Illumina 2 × 100 bp paired-end reads for the resistant (NCBI BioProject PRJNA518136) and susceptible plants (NCBI BioProject PRJNA518146), respectively (Denton-Giles, 2014). Since reads from infected petals had mixed species origins, sequences were first mapped onto the *C. camelliae* genome (GenBank GCA_001247705.1) to remove reads derived from the fungus (resulting fungal transcriptome is available in Appendix C, Supplementary File 3). The remaining reads were assembled separately for the infected and uninfected samples using the Trinity *de novo* assembler (Haas et al., 2013). For each plant, transcriptomes obtained from uninfected and infected samples were combined into one file, and redundant sequences removed using CD-HIT-EST (W. Li & Godzik, 2006). The resulting reference transcriptomes consisted of 109,201 assembled transcripts for *C. lutchuensis* and 133,997 transcripts for *Camellia* 'Nicky Crisp' (Appendix C, Supplementary Files 1 and 2). A flowchart of the assembly process is presented in Figure 2-5.

To confirm the quality of the assembled transcriptomes, N50 values (1,204 for *C. lutchuensis*; 1,076 for *Camellia* 'Nicky Crisp') and average GC-content (40.4% for *C. lutchuensis*; 39.9% for *Camellia* 'Nicky Crisp') were measured. These values are similar to published *Camellia* transcriptomes (Fan et al., 2015; Xia et al., 2014; Yao et al., 2016). The

gene-content completeness of the transcriptomes was assessed using BUSCO, which characterizes the presence of 'universal' single-copy plant gene orthologs (Simão et al., 2015). 86% and 89% of these genes were present in the *C. lutchuensis* and *Camellia* 'Nicky Crisp' transcriptomes (Table 3-1), respectively, suggesting that most genes present in both species were successfully sequenced and assembled.

Table 3-1 | Assembly and annotation results

Assembly and annotation statistics	*Camellia lutchuensis*	*Camellia* 'Nicky Crisp'
Number of high-quality read-pairs used (millions)	110	162
Assembly statistics		
Number of assembled transcripts	109,291	133,997
Transcript length range (bp)	201 - 14,732	201 - 15,756
N50	1,204	1,076
% GC	40.4	39.9
BUSCO completeness		
Complete (%)	80.0	82.3
Duplicated (%)	15.1	15.6
Fragmented (%)	6.0	6.4
Missing (%)	14.0	11.3
Annotation results		
With nt hits	35,876	39,927
With Swiss-Prot hits	33,939	36,737
With GO terms	30,935	23,783
Number of predicted proteins	37,239	40,404

Transcriptome annotations and prediction of *Camellia* proteomes. Functional annotations were predicted based on matches to NCBI and Swiss-Prot databases (Table 3-1). Gene Ontology (GO) terms were assigned to 30,935 transcripts of resistant *C. lutchuensis* and 23,783 transcripts of susceptible *Camellia* 'Nicky Crisp'. Protein coding sequences were predicted with TransDecoder (Haas et al., 2013), resulting in 37,239 predicted protein sequences for *C. lutchuensis* and 40,404 for *Camellia* 'Nicky Crisp'. Orthologous proteins were predicted by comparison with the reference proteome of the well-studied model plant, *A. thaliana* (UniProt UP000006548). The two camellia transcriptomes shared 10,125 orthology groups with *A. thaliana*, and an additional 8,410

orthology groups were shared between the two *Camellia* transcriptomes alone. Over half of *A. thaliana* proteins (56%) could not be assigned to any predicted orthology group, while 38% and 41% remained unclassified in the lesser studied *C. lutchuensis* and *Camellia* 'Nicky Crisp' (Figure 3-1).

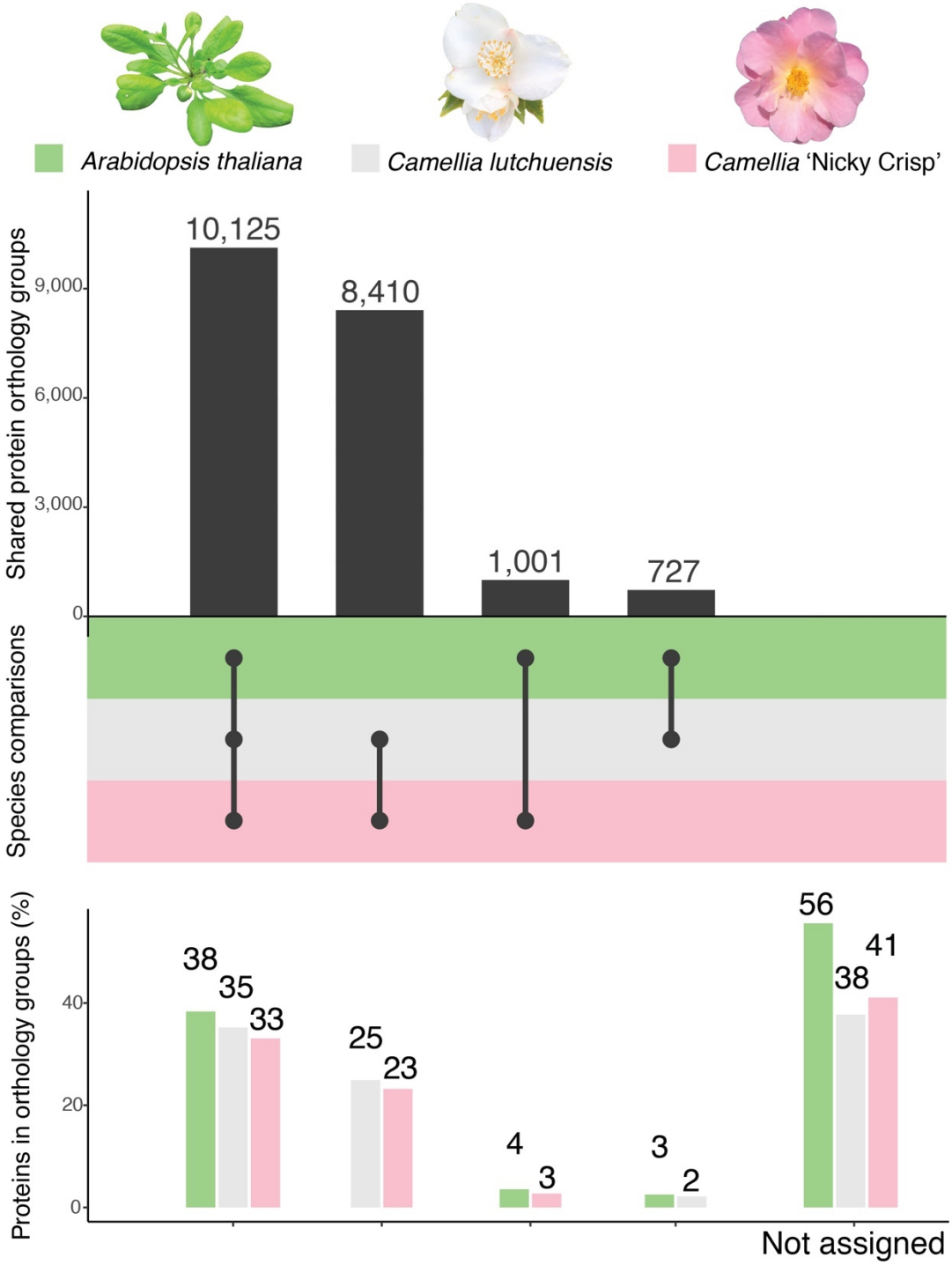

Figure 3-1 | Comparison of predicted *Camellia* proteomes with the reference proteome of *A. thaliana*.

Top bar chart: the number of predicted protein orthology groups. Bottom bar chart: the fraction of all protein sequences in corresponding orthology groups (e.g. leftmost bars show proteins that were classified into orthology groups shared by all three species).

C. camelliae inoculation induces rapid transcriptional responses in resistant *C. lutchuensis*.

To determine the transcriptional resistance response of *C. lutchuensis* following *C. camelliae* infection, a quantitative RNA-seq experiment was performed. RNA was extracted from *C. lutchuensis* petals collected at 0, 6, 12 and 24 h after spraying with fungal spores, and at 12 and 24 h after spraying with sterile distilled water (Figure 3-2a). Approximately 9-12 million high-quality 2 × 125 bp paired-end reads from each sample (NCBI BioProject PRNA506291) were mapped to the fungal and resistant plant reference transcriptomes described above, with mapping rates reaching 95 – 97% (Appendix A, Table A-3). The proportion of fungal reads increased from 0 to 6 hpi, before decreasing again to pre-infection levels at 24 hpi (Figure 3-2b). Principal component analysis (PCA) of transcript read counts showed that the plant underwent dramatic transcriptional reprogramming (Figure 3-2c). Biological triplicates cluster on the PCA graph, emphasizing the consistency of the response to fungal treatment. The biggest transcriptional changes in the plant coincide with the highest fungal transcriptional activity: within the first 6 h following contact with the pathogen, 9,880 transcripts were upregulated and 6,261 were downregulated. From 6 hpi to 12 hpi, 2,240 and 3,872 plant transcripts were up- and downregulated, respectively, while from 12 hpi to 24 hpi, 4,351 transcripts were upregulated and 3,288 downregulated. Fewer differentially expressed transcripts were observed between the mock-inoculated and 0 hpi samples, suggesting that the majority of transcriptional changes observed post-infection at later timepoints were due to responses to the fungus.

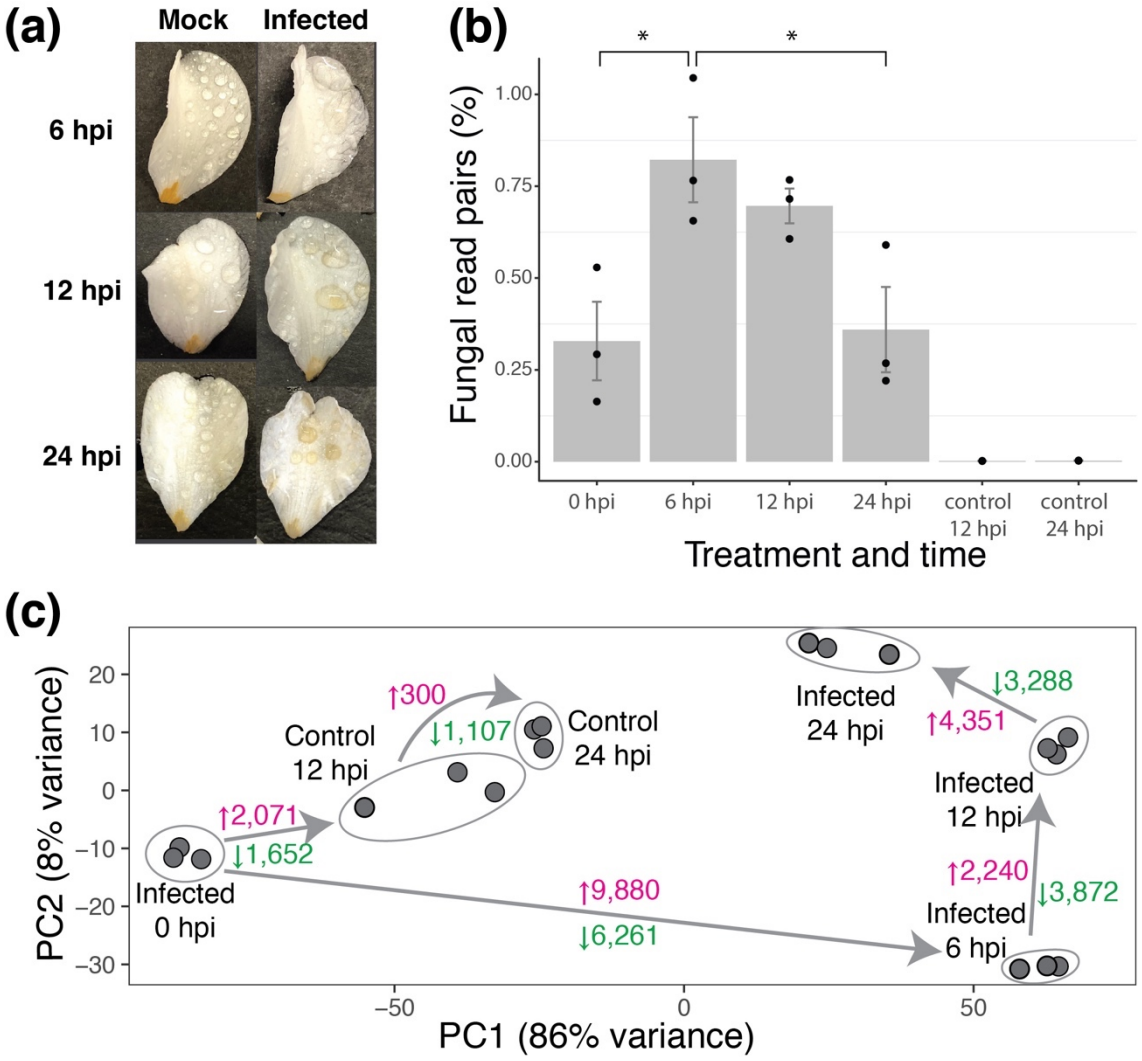

Figure 3-2 | Interactions between *C. camelliae* and resistant *C. lutchuensis*. *(a) Development of the resistance response in* C. lutchuensis. *(b) Proportion of reads mapped to the fungal genome. Each dot represents an observed value, bars represent the average value at each time point and treatment, error bars represent standard error. *, P < 0.05 (two-tailed Student's t-test). (c) Principal component analysis of plant read count data. Each dot represents a biological replicate, circles represent matched biological replicates, arrows indicate the time course, numbers represent upregulated (pink) or downregulated (green) transcripts. hpi = h post-inoculation.*

Functional enrichment of *C. lutchuensis* expression triggered by *C. camelliae*. Identifying functional effects is challenging due to the number of gene interactions involved in most biological processes. *Camellia lutchuensis* transcripts were grouped based on shared patterns of change in their expression levels in response to the petal blight pathogen. Fold changes in gene expression at each time point and treatment condition were calculated relative to 0 hpi levels. A total of 23,083 assembled transcripts

were significantly up- or downregulated during at least one of these analysis points, and 13,598 of these transcripts had functional annotations (Appendix C, Supplementary file 4). Pairwise correlation coefficients for all transcript pairs were submitted to a hierarchical clustering algorithm. GO enrichment analysis was performed on the resulting dendrogram, restricted to ten clusters (Figure 3-3; full results in Appendix C, Supplementary file 5). Clusters 3, 5, and 8 represent genes upregulated in response to inoculation with fungal spores. The biggest cluster (3) contains genes with the earliest responses to the fungus, as well as the most significant enrichment for 'defence response' and 'protein phosphorylation' GO terms. Clusters 5 and 8 demonstrate maximum expression at 12 and 24 hpi, respectively, and are enriched for GO terms associated with secondary metabolism, such as 'secondary metabolic process', 'secondary metabolite biosynthesis process', 'oxidation-reduction process, 'phenylpropanoid metabolic process' and 'flavonoid biosynthesis process'. Clusters 6, 7 and 9 contain transcripts downregulated during the course of infection and are enriched for macromolecule biosynthesis, organ development, and responses to light and hormones. Finally, clusters 1, 2, 4 and 10, which were not specific to the fungal treatment, contain far fewer transcripts, and are enriched for responses to abiotic stimuli, such as 'response to red light', 'temperature compensation of the circadian clock' and 'hypotonic salinity response'. Overall, the observed functional enrichments of differentially expressed genes in resistant *C. lutchuensis* are consistent with typical plant resistance responses.

	Size	Top 5 Enriched Biological Process terms	Corrected *P*	No. transcripts
1	200	10378 Temperature compensation of the circadian clock	3.8×10^{-6}	5
		30834 Regulation of actin filamen depolymerisation	1.6×10^{-5}	8
2	196	51017 Actin filament bundle assembly	1.6×10^{-5}	8
		51693 Actin filament capping	1.6×10^{-5}	7
		9757 Hexose mediated signaling	1.6×10^{-5}	6
		42539 Hypotonic salinity response	3.8×10^{-5}	6
		5513 Detection of calcium ion	3.8×10^{-5}	6
		51592 Responce to calcium ion	6.7×10^{-4}	8
		6971 Hypotonic response	7.5×10^{-4}	6
		8645 Hexose transmembrane transport	1.0×10^{-3}	7
3	4,109	6952 Defense response	2.7×10^{-89}	1,182
		6468 Protein phosphorylation	6.6×10^{-75}	776
		9607 Response to biotic stimulus	4.4×10^{-74}	1,181
		51707 Response to other organism	2.2×10^{-73}	1,164
		6950 Response to stress	3.6×10^{-66}	2,065
4	288	42221 Response to chemical	2.6×10^{-7}	158
		1901700 Response to oxygen-containing compound	2.6×10^{-7}	118
		50896 Response to stimulus	4.2×10^{-7}	208
		9628 Response to abiotic stimulus	4.2×10^{-7}	123
		9725 Response to hormone	1.8×10^{-6}	104
5	2,209	19748 Secondary metabolic process	9.2×10^{-44}	233
		9698 Phenylpropanoid metabolic process	1.2×10^{-31}	172
		44550 Secondary metabolite biosynthetic process	2.1×10^{-28}	141
		1901615 Organic hydroxy compound metabolic process	8.8×10^{-28}	203
		55114 Oxidation-reduction process	4.1×10^{-27}	378
6	1,747	99402 Plant organ development	3.4×10^{-18}	410
		9725 Response to hormone	2.6×10^{-15}	530
		9416 Response to light stimulus	3.4×10^{-15}	297
		9719 Response to endogenous stimulus	5.0×10^{-15}	548
		48364 Root development	5.0×10^{-15}	254
7	2,498	34660 ncRNA metabolic process	1.5×10^{-19}	221
		16072 rRNA metabolic process	1.3×10^{-13}	129
		6399 tRNA metabolic process	3.3×10^{-13}	110
		10467 Gene expression	4.7×10^{-13}	593
		42254 Ribosome biogenesis	5.6×10^{-12}	145
8	531	55114 Oxidation-reduction process	8.0×10^{-8}	92
		19748 Secondary metabolic process	8.0×10^{-8}	48
		44550 Secondary metabolite biosynthesis process	1.5×10^{-3}	36
		9813 Flavonoid biosynthesis process	1.5×10^{-3}	21
		9901 Anther dehiscence	1.5×10^{-3}	10
9	1,380	19219 Regulation of nucleobase-containing compound metabolic process	2.3×10^{-16}	368
		1903506 Regulation of nucleic acid-template transcription	2.3×10^{-16}	327
		2001141 Regulation of RNA biosynthetic process	2.3×10^{-16}	327
		51252 Regulation of RNA metabolic process	2.9×10^{-16}	348
		6355 Regulation of transcription, DNA-templated	8.9×10^{-16}	321
10	440	9628 Response to abiotic stimulus	2.2×10^{-7}	179
		10114 Response to red light	3.6×10^{-6}	20
		50896 Response to stimulus	4.1×10^{-6}	306
		9733 Response to auxin	5.4×10^{-6}	48
		272 Polysaccharide catabolic process	6.1×10^{-6}	21

Figure 3-3 | GO enrichment of *C. lutchuensis* transcripts that respond to *C. camelliae*. *(Left) The heatmap shows row-scaled log_2 fold-change values for 13,598 differentially expressed and annotated* C. lutchuensis *transcripts. Fold-changes are presented relative to 0 h post-inoculation (hpi). Each row corresponds to a transcript, each column to a treatment and time point. Upregulated genes (pink), downregulated (green). White and grey bars correspond to ten predicted transcript clusters, defined on the correlation of their expression values. The table shows the number of transcripts in each cluster, the five most*

significantly enriched GO 'Biological Process' terms, corrected probability values, and the number of cluster transcripts that had the corresponding GO term in their annotation. hpi = h post-inoculation.

Orthologs of *C. lutchuensis* transcripts that respond to *C. camelliae* form non-random interaction networks in *A. thaliana*. Similar expression dynamics for a set of genes may suggest that they are involved in the same cellular process or produce proteins that interact to form a functional complex. Such interactions tend to be evolutionarily conserved (C.-L. Ho, Wu, Shen, Provart, & Geisler, 2012; Musungu, Bhatnagar, Brown, Fakhoury, & Geisler, 2015). Therefore, transcripts with similar expression patterns were identified in *C. lutchuensis* and their predicted orthologs were found in *A. thaliana*. The orthologs of transcripts from each predicted expression cluster form non-random interaction networks with significantly higher rates of interaction than expected by chance (all $P < 10^{-4}$) (Figure 3-4). Thus, it was concluded that predicted *C. lutchuensis* transcript clusters include important defence-associated molecular networks.

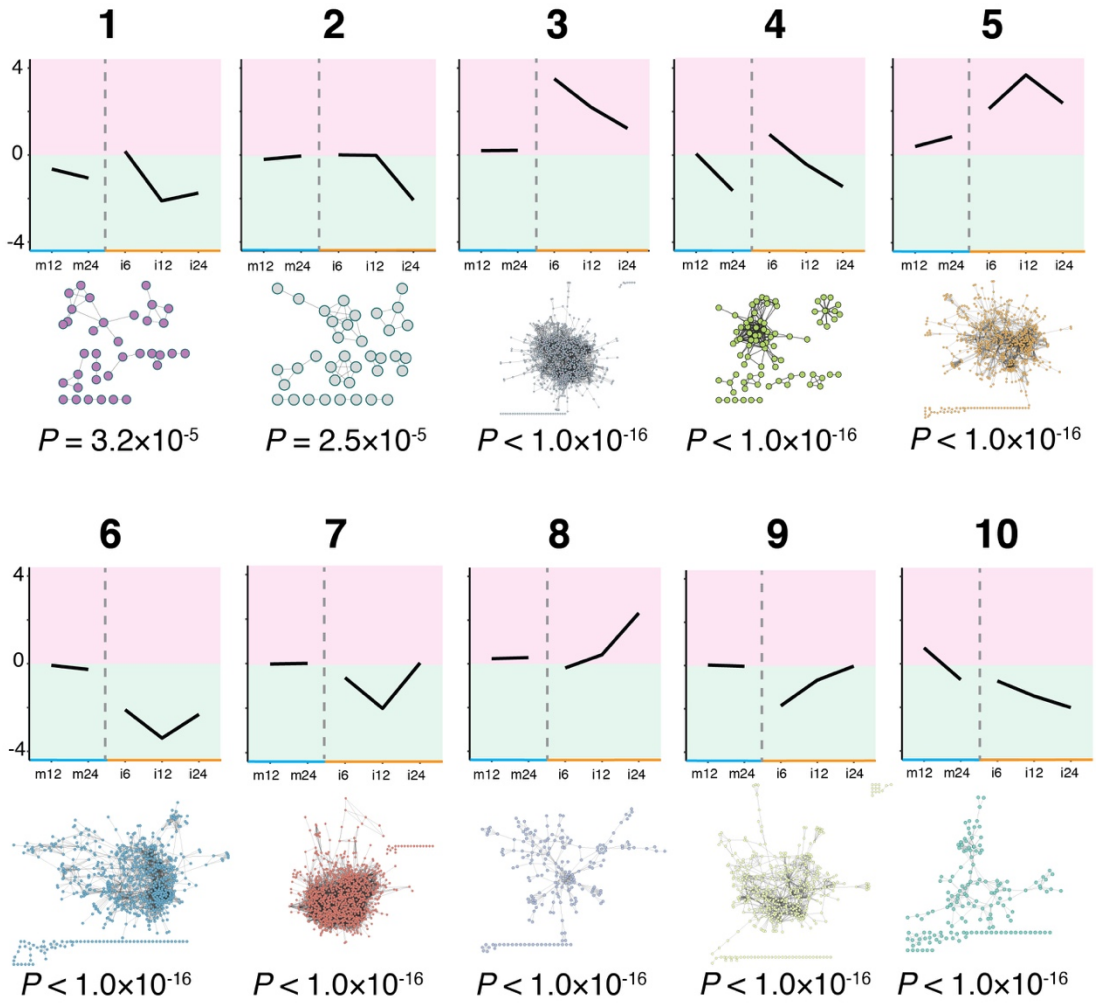

Figure 3-4 | Interaction networks of *A. thaliana* orthologs corresponding to *C. lutchuensis* transcripts that respond to *C. camelliae* infection.
Line charts show average expression pattern of C. lutchuensis *transcript clusters. Red background corresponds to upregulation and green one to downregulation. The y-axes show log_2 fold-change values, and the x-axes show time and treatment ('m12', mock 12 hpi; 'm24', mock 24 hpi; 'i6', infected 6 hpi; 'i12', infected 12 hpi; 'i24', infected 24 hpi). Networks show the interactions between* A. thaliana *genes that are predicted orthologs of* C. lutchunesis *transcripts from indicated clusters. Probability values show the chance of observing a network with the same size and connectivity from a set of randomly sampled* A. thaliana *proteins (all $P < 10^{-4}$). Line chart and network numbering corresponds to the clusters defined in Fig. 3-3.*

***C. camelliae*-responsive interaction networks contain defence-associated hubs and key enzymes of jasmonate and phenylpropanoid biosynthesis.** Functional biological networks contain key hub elements that form multiple interactions. Important regulatory transcripts (hub transcripts) were identified in three predicted networks (3, 5 and 8), which represent *C. lutchuensis* transcripts with the highest upregulation at 6, 12 and 24

hpi, respectively (Figure 3-4). Each node (transcript) in these networks can be represented on a scatterplot (Figure 3-5, see Supplementary file 6 in Appendix C for full results), where the *x*-axis shows the number of interactions that each transcript forms within the predicted network, and the *y*-axis shows the $\log_2$ fold-change value of each transcript at 6, 12 or 24 hpi for networks 3, 5 and 8, respectively. Transcription factors (blue), kinases (red) and ubiquitin-ligases (green) are involved in a range of cellular processes and are expected to interact with multiple gene targets. These three functional groups are enriched in transcripts with maximal upregulation at 6 hpi vs 12 and 24 hpi (χ^2 independence test, both $P < 0.01$, df = 3, Appendix A, Table A-4), especially at high-frequency interaction hubs. Three of transcripts that were highly upregulated at 6 hpi, *WRKY33*, *MPK3* and *MYB15,* are essential for disease resistance in *A. thaliana* (Beckers et al., 2009; Birkenbihl, Diezel, & Somssich, 2012; Chezem, Memon, Li, Weng, & Clay, 2017).

Production of secondary metabolites is an essential part of plant resistance to various pathogens (Pusztahelyi, Holb, & Pócsi, 2015). Indeed, networks corresponding to the highest expression levels at 12 and 24 hpi contain enzymes associated with secondary metabolite biosynthesis, such as 4-coumarate-CoA ligase (*4CL*) and cinnamate-4-hydroxylase (*C4H*), which are enzymes central to the phenylpropanoid pathway; ferulate 5-hydroxylase (*F5H*), which is the rate-limiting enzyme of syringyl lignin biosynthesis; and elicitor-activated gene 3 (*ELI3-2*), which encodes an aryl-alcohol dehydrogenase and participates in lignin biosynthesis. The high-frequency interaction hubs with maximal upregulation at 12 and 24 hpi were enzymes related to secondary metabolism: aldehyde dehydrogenases (*ALDH2B4*, *ALDH3H1*), oxidoreductase *BRI1-5* ENHANCED 1 (*BEN1*), and dihydroflavonol 4-reductase (*DFR*).

Jasmonic acid (jasmonate, JA), a plant hormone, also mediates resistance to necrotrophic pathogens (Han, 2017). Transcripts involved in JA metabolism, signalling and response to JA appear in all three networks (shown as triangles, Figure 3-5), including the

main enzymes of the JA biosynthesis pathway: 13S-lipoxygenase (*LOX*), 12-oxophytodienoate reductases (*OPR*), allene oxide synthase (*AOS*), OPC-8:0 CoA ligase 1 (*OPCL*), allene oxide cyclase (*AOC*), and acyl-CoA oxidase (*ACX*). In summary, this interactome-based analysis highlights that ascospore-treated resistant *C. lutchuensis* petals activated multiple interaction hubs that play a role in resistance to petal blight disease.

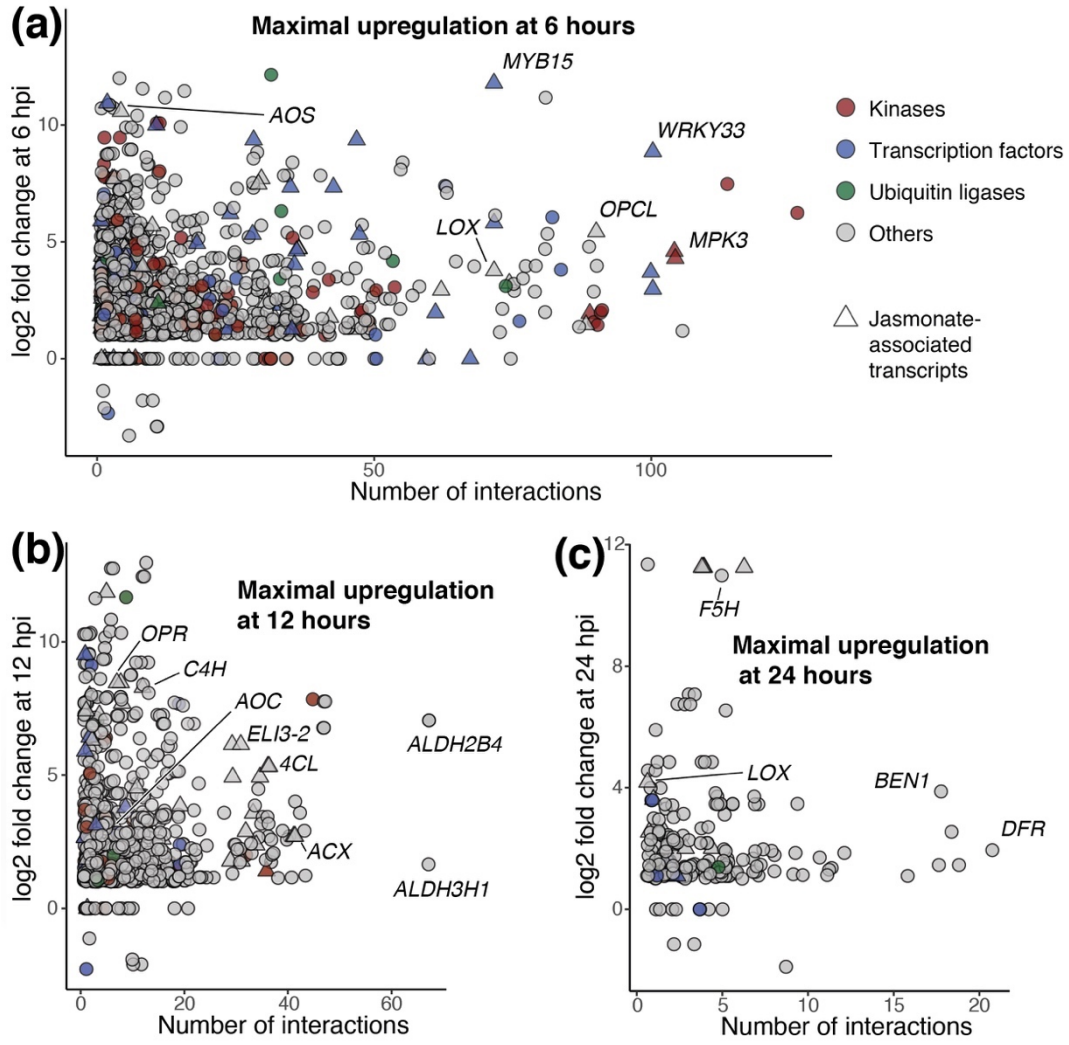

Figure 3-5 | Predicted interactome nodes.
Dots represent C. lutchuensis *transcripts from expression clusters 3, 5 and 8 (panels a, b and c, respectively). The x-axes show the number of interactions for the ortholog of each transcript in the corresponding* A. thaliana *interaction network. The y-axes show* log_2 *fold-change of transcription at 6, 12 or 24 h post-inoculation (hpi) for clusters 3, 5 and 6, respectively. Functional groups are denoted by different colours, transcripts with GO terms that contain key word 'jasmonic acid' are shown as triangles, key genes of note that are described in the text are labelled.*

qRT-PCR validates the results of quantitative RNA-seq analysis. The quantitative RNA-seq results were verified in resistant *C. lutchuensis* by measuring the expression levels of genes belonging to resistance-associated hubs. *WRKY33*, *MPK3* and *MYB15* genes, which are the hub genes that form multiple interactions and are highly expressed at an early stage of the infection in resistant plants, were tested. I also analysed the expression of *BAK1*, *SOBIR1* and *RIN4*, which are upregulated at 6 hpi, and whose involvement in *A. thaliana* immunity has been reported previously (Liebrand, van den Burg, & Joosten, 2014; Toruño, Shen, Coaker, & Mackey, 2018), as well as *LOX*, *AOS*, *OPCL* and *OPR*, which are involved in JA biosynthesis. qRT-PCR expression data for all ten tested genes correlated highly with the results obtained from the quantitative RNA-seq analysis, validating these key observations (all $P < 0.05$, Pearson's correlation test; Figure 3-6a).

Resistance-associated hubs have elevated expression levels at late stages of infection in susceptible *Camellia* 'Nicky Crisp'. I surveyed the expression of a subset of genes in the highly susceptible *Camellia* 'Nicky Crip' using qRT-PCR to determine whether they show different expression dynamics relative to the resistant species. Six early resistance hub genes (*WRKY33, MPK3, MYB15, SOBIR1, BAK1, RIN4*), three genes that encode phenylpropanoid pathway enzymes (*C4H*, *4CL*, *F5H*), and four JA biosynthesis genes (*LOX, AOS, OPCL, OPR*) were analysed. All thirteen genes showed divergent expression patterns in the susceptible plants (Figure 3-6b). None were significantly upregulated after the mock treatment at any time point, validating that their expression only responded to fungal spores. However, after fungal treatment, the transcripts had slightly elevated expression levels at 6 hpi, but this was only significant for *BAK1* and *SOBIR1*. The highest upregulation for all transcripts was seen at 24 hpi, in contrast to the rapid and strong upregulation observed at 6 hpi in *C. lutchuensis*. Activation of resistance hubs in susceptible *Camellia* "Nicky Crisp" occurs later than in the resistant *C. lutchuensis*.

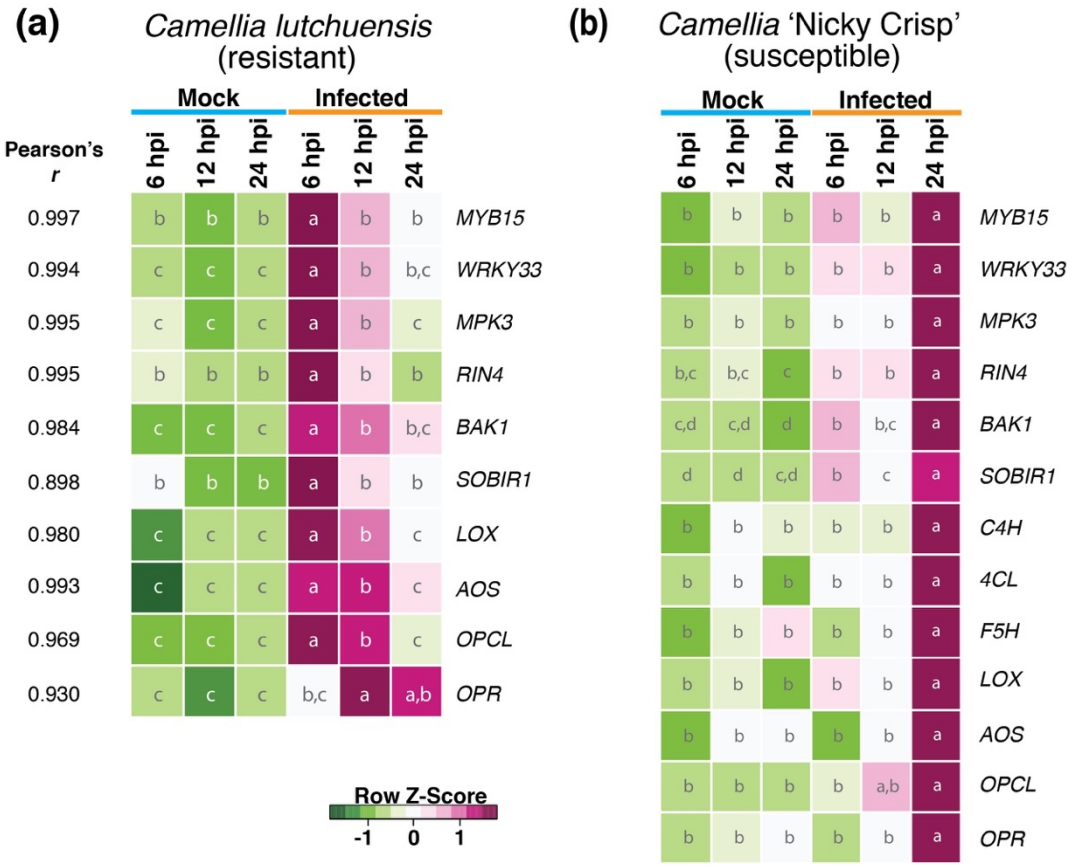

Figure 3-6 | qRT-PCR analysis of selected transcripts.
Two row-scaled heatmaps represent expression levels in (a) C. lutchuensis *and (b)* Camellia *'Nicky Crisp'. Each row represents a gene transcript, each column a treatment and time point. Upregulated genes (pink), downregulated (green). Relative expression levels were measured against two reference transcripts (PTB1 and EF1-α for* C. lutchuensis*, and PTB1 and Tub α-3 for* Camellia *'Nicky Crisp'). Expression levels are presented as the mean of three biological replicates. Data were analysed with two-way ANOVA (Time × Treatment) and Tukey's Honest Significant Difference tests separately for each transcript. The same letter in two heatmap cells within a row indicates that expression levels did not differ significantly between those two conditions ($P < 0.05$). For* C. lutchuensis*, correlations between RNA-seq and qRT-PCR expression values (left column in a) were tested with Pearson's correlation coefficient (all $P < 0.05$). hpi = h post-inoculation.*

Methyl jasmonate treatment suppresses petal blight infection and upregulates resistance-associated hubs in susceptible *Camellia* 'Nicky Crisp'.

Methyl jasmonate (MeJA), a volatile derivative of JA, is widely used to protect plants against fungal diseases (K. Wang, Liao, Kan, Han, & Zheng, 2015; Z. Zhu & Tian, 2012). Since the resistance-associated hubs observed in *C. lutchuensis* include JA production, signalling and JA-induced responses, it is likely that JA influences petal blight resistance in

C. lutchuensis and the lack of early JA biosynthesis in *Camellia* 'Nicky Crisp' might be a reason for its susceptibility. To test this hypothesis, I sprayed petals with the same fungal spore solution, but added either MeJA or ethanol (control) (Figure 3-7a-b). At 48 hpi, lesions fully covered ascospore-treated petals, while lesion sizes were significantly smaller in petals treated with MeJA ($P = 2.9\times10^{-5}$, two-tailed Mann-Whitney U test). Expression levels of the *MPK3* and *WRKY33* genes were assayed in susceptible plant petals 6 h following the treatment; while the MeJA-treated petals showed higher gene expression than ascospore-treated ones, only the infection with ascospores combined with the hormone treatment resulted in a significantly higher expression levels of both of these key defence genes (Figure 3-7c). Taken together, these observations suggest that early activation of resistance-associated hubs by JA likely contributes to the *Camellia* defence against petal blight disease.

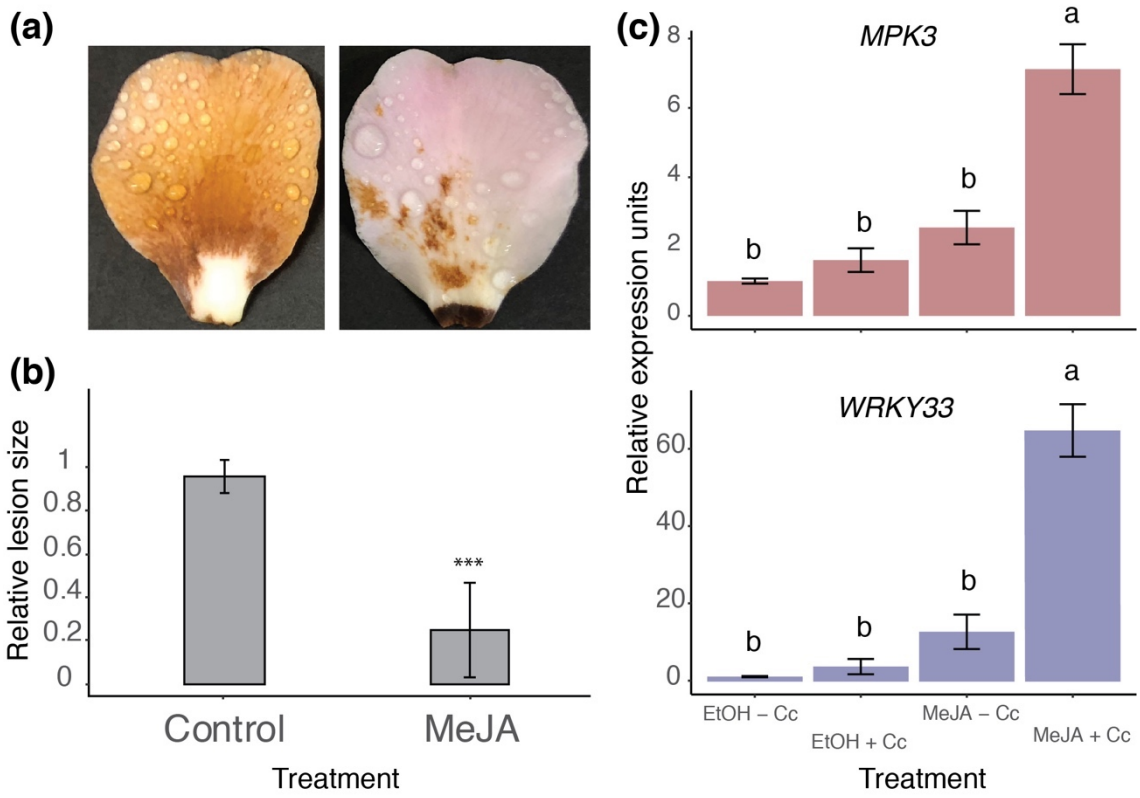

Figure 3-7 | Effects of methyl jasmonate treatment on petal blight infection in susceptible *Camellia* 'Nicky Crisp'.
(a) The petals on the left were treated with C. camelliae *spores in 1% ethanol solution (left) or with fungal spores in a 10 mM methyl jasmonate in 1% ethanol solution (right) and incubated for 48 h. (b) The bar*

*chart shows the relative lesion sizes on petals at 48 hpi. Bars indicate mean relative lesion areas as a proportion of the whole petal, error bars indicate the standard deviation calculated from twelve biological replicates. ***, P < 0.001 (two-tailed Mann-Whitney U test). (c) Bar charts show the effect of methyl jasmonate and spore treatment on the expression levels of WRKY33 and MPK3 transcripts at 6 hpi. The x-axis shows the treatments applied: 'EtOH – Cc', 1% ethanol only; 'EtOH + Cc',* C. camelliae *spores in 1% ethanol solution; 'MeJA – Cc', 10 mM methyl jasmonate in 1% ethanol solution; and 'MeJa + Cc', 10 mM methyl jasmonate in 1% ethanol solution containing* C. camelliae *spores. Relative expression levels were measured against two reference transcripts (PTB1 and Tubulin α-3) and normalized to the average value of the 1% ethanol-treated control samples. Bars show mean expression values; error bars show the standard error calculated from three biological replicates. The data were analysed with a two-way ANOVA (Ascospores × MeJA) and Tukey's Honest Significant Difference test separately for each tested transcript. The same letter above two bars indicates that expression levels did not differ significantly between those two conditions (P < 0.05).*

3.3. Discussion

When pathogens circumvent pre-existing structural and chemical defences, plants must rely on their innate immune system, which is based on the recognition of non-self (Heise et al., 2003). More specifically, extracellular or intracellular plant immune receptors must recognize molecular patterns of invasion (i.e., pathogen-associated molecular patterns (PAMPs), damage-associated molecular patterns (DAMPs), or effectors) to activate defence responses that halt the growth of these pathogens (Cook et al., 2015). This is certainly true for biotrophic pathogens, which require a living plant host for growth and development. Unlike biotrophs, however, necrotrophs explicitly exploit the host defence responses activated by receptor-invasion pattern interactions to trigger plant susceptibility via the stimulation of host-mediated necrosis in plant tissues (Ciuffetti et al., 2010; Gilbert & Wolpert, 2013). Here, in the *Camellia* spp.-*Ciborinia camelliae* interaction, I demonstrate that the timing of defence activation can play a crucial role in plant resistance to the necrotrophic fungus and define the outcome of the disease process.

Global gene expression analysis showed the major functional patterns of *C. lutchuensis* resistance to petal blight disease. Management of limited resources forces plants to increase the efficiency of their physiological processes (Huot, Yao, Montgomery, & He, 2014), and the defence response of resistant *Camellia* petals follows a growth-defence trade-off. In response to ascospore treatment, resistant plant petals downregulated transcripts associated with growth and development, and upregulated stress- and defence-related genes. These defence-associated processes were temporally segregated, with early kinase-activity and signalling, and later secondary metabolite production (Heise et al., 2003). Similarly, *Brassica napus'* resistance to *S. sclerotiorum* included the activation of mitogen-activated protein kinase signalling cascades and resulted in the production of glucosinolates (Wu et al., 2016). *Camellia lutchuensis* transcript co-expression groups also had orthologous

interaction networks in *A. thaliana*, showing that the resistance of *C. lutchuensis* to *C. camelliae* may be typical of the defence mechanisms to pathogens found in other plants.

The main regulatory pathways of the defence response were identified using an interactome-based approach. Key genes were upregulated in resistant *C. lutchuensis* after ascospore treatment, with the strongest interaction hubs containing orthologs of known resistance- and stress-associated genes, such as *WRKY33* (Birkenbihl et al., 2012), *MPK3* (Mao et al., 2011) and *MYB15* (Holl et al., 2013). The *WRKY33* transcription factor and *MPK3* kinase are involved in a common defence regulatory loop in *A. thaliana*, which contributes to systemic acquired resistance (Yiming Wang et al., 2018). The *MYB15* transcription factor is a positive regulator of the phenylpropanoid pathway (Chezem et al., 2017). I also observed enriched expression of phenylpropanoid pathway genes, which may contribute to *C. camelliae* resistance via the production of compounds with direct antifungal activity (König et al., 2014) or as precursors of lignin monomers that reinforce plant cell walls (Yin Wang et al., 2013). Oxylipin pathway genes involved in the biosynthesis of JA, a plant hormone that mediates resistance against necrotrophic pathogens (Han, 2017), were upregulated in several interaction hubs.

A distinctive feature of petal blight disease is its rapid spread of infection: while other fungal infections develop over days or weeks, a single *C. camelliae* lesion spreads over the whole petal within 48 h (Denton-Giles et al., 2013). Indeed, as suggested by RNA-seq results, the proportion of fungal RNA in infected samples doubled in the first 6 h of the infection. The transcriptional response of resistant plants was similarly quick, with maximal activity at 6 hpi. This accords with microscopic observations showing that the resistance response occurs within the first 12 hours of interaction, during the asymptomatic phase, with localized plant cell death and accumulation of reactive oxygen species (ROS) (Denton-Giles et al., 2013). Plant resistance thus appears to be most effective during the biotrophy-like asymptomatic growth stage of the fungus (Denton-Giles et al., 2013) — the initial

phase found even in "classic" necrotrophs such as *S. sclerotiorum* (Kabbage, Yarden, & Dickman, 2015) and *B. cinerea* (Veloso & van Kan, 2018). Like our observations, necrotrophic *Macrophomina phaseolina* infection of a resistant plant line of *Seasamium indicum* showed a prompt host response to the pathogen at initial biotrophy-like steps of the interaction (Chowdhury, Basu, & Kundu, 2017). Thus, it can be concluded that rapid activation of the resistance response can be essential for resistant *Camellia* plants to stop the development of *C. camelliae*.

Comparative studies between susceptible and resistant plant species or lines often help to highlight the most important factors of the defence against pathogens. For example, resistant *Brassica* and *Solanum* plants showed more intensive upregulation of defence pathways in response to necrotrophs than susceptible plants (Smith, Mengesha, Tang, Mengiste, & Bluhm, 2014; Wu et al., 2016). Expecting to observe differences between resistant and susceptible *Camellia* species, I tested the expression dynamics of three defence pathways – *MPK3-WRKY33*, *MYB15*-phenylpropanoid and JA biosynthesis – in the susceptible hybrid *Camellia* 'Nicky Crisp'. All three pathways were significantly upregulated only at the latest step of the infection, which corresponds to the start of lesion formation in susceptible petals. These pathways thus contribute not only to resistance, but strikingly, also to susceptibility. Nevertheless, the exogenous application of MeJA, which led to the upregulation of two important resistance hubs, *WRKY33* and *MPK3*, within the first 6 h of infection, did reduce lesion sizes in susceptible petals. This further verifies that the early defence activation contributes to the petal blight resistance. This increased resistance appears to be driven by the simultaneous activation of multiple defence pathways by exogenous MeJA and elicitor compounds from ascospores, leading to integrated upregulation of the *MPK3* and *WRK33* resistance hubs, in agreement with the quantitative disease resistance model (Roux et al., 2014). Similar observations have been made for several defence-associated genes in strawberry fruits infected with the necrotroph

B. cinerea (Saavedra, Sanfuentes, Figueroa, & Figueroa, 2017). Therefore, the approach using hormonal treatment coupled with natural or synthetic fungal invasion pattern elicitors seems worth investigating further, as it may result in more effective priming of plants against numerous diseases.

According to the Invasion Model (Cook et al., 2015), plants generally interact with biotrophs and necrotrophs using the same molecular pathways, but with different outcomes: inhibition of biotrophic infection and acceleration of necrotrophic infection. In the *Camellia* spp.-*C. camelliae* interaction, both resistant and susceptible plants trigger the same defence pathways. However, the timing of pathway induction defines the nature of the interaction. If defence is activated early during the biotrophy-like step of fungal development, it leads to host resistance. The activation of plant defence pathways when the fungus reaches its necrotrophic stage instead leads to susceptibility (Figure 3-8). This conclusion is based on the comparative analysis of just one resistant and one susceptible host, and further work with other *Camellia* cultivars is needed to confirm the suggested model.

It is still unclear what the main factors are that regulate the timing of *Camellia* defence. Susceptible *Camellia* species may lack the immune receptors needed to detect *C. camelliae*, hence preventing early recognition. The pathogen might then activate host defence pathways in its favour using DAMPs released from cell wall destruction (Denoux et al., 2008) or secreted fungal carbohydrate-active enzymes (CAZymes) similarly to *B. cinerea* (Minz-Dub et al., 2017). Alternately the secretome of *C. camelliae* produced during the early biotrophy-like stage may contain compounds that suppress the immune response of susceptible plants, such as effector proteins (W. Zhu et al., 2013) or oxalic acid (Williams et al., 2011) (Figure 3-8), as produced by the related pathogen *S. sclerotiorum*.

Whether infection is more a function of the pathogen or the host plant is important for effective treatments. For rapid infection by necrotrophic pathogens, the timing of the

host response may be the more crucial factor for resistance than the nature of the defence itself and should be considered in the design of disease-control strategies.

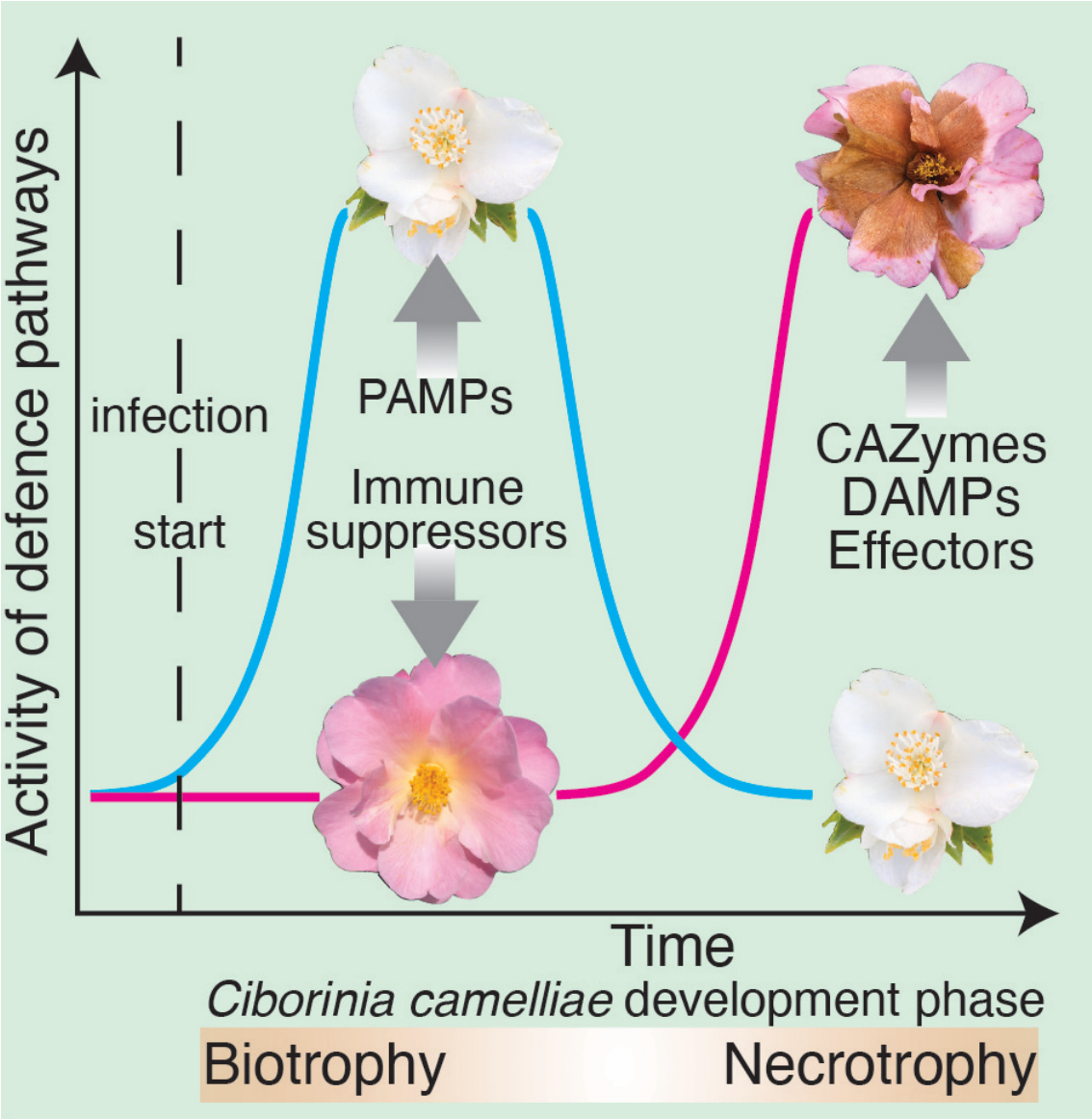

Figure 3-8 | Putative model of plant-fungus interaction for *Camellia* petal blight disease. *The line chart shows the transcriptional activity of tested defence pathways in resistant* C. lutchuensis *(blue) and susceptible* Camellia *'Nicky Crisp' (red). Grey arrows show fungal molecules that can modulate plant defence pathways. The orange bar (bottom) shows the development phases of the petal blight pathogen. PAMPs – pathogen-associated molecular patterns; CAZymes – carbohydrate-active enzymes; DAMPs – damage-associated molecular patterns.*

Chapter 4. The role of phenylpropanoid metabolites in resistance to camellia petal blight

4.1. Introduction

Contact with the petal blight pathogen induces a dramatic transcriptional reprogramming of *C. lutchuensis* petals, which also leads to the activation of secondary metabolism (Chapter 3). The enrichment analysis of the transcripts that were upregulated at 12 and 24 hours after the inoculation showed the upregulation of phenylpropanoid pathway genes in infected petals of resistant plants. This chapter further examines the role of the phenylpropanoid pathway in the resistance of *C. lutchuensis* to *C. camelliae*.

Commencing from the aromatic amino acids phenylalanine and tyrosine, the phenylpropanoid pathway supplies numerous plant secondary metabolites such as flavonoids, monolignols and coumarins (C. M. Fraser & Chapple, 2012). The first reaction in the biosynthesis pathway, deamination of phenylalanine, is performed by phenylalanine ammonia lyase (PAL), and leads to production of *trans*-cinnamic acid. Other phenolic acids are derived from *trans*-cinnamic acid via oxidation and methylation reactions which are catalysed by trans-cinnamate 4-monooxygenase (C4H), p-coumaroyl shikimate/quinate 3'-hydroxylase (C3H), caffeate O-methyltransferase (COMT), and ferulate 5-hydroxylase (F5H). The next step in the pathway is the synthesis of aromatic CoA-esters catalysed by 4-coumarate-CoA ligase (4CL), after which these esters either can be used for the production of flavonoids via chalcone (performed by naringenin-chalcone synthase (CHS)), or undergo two step reduction forming lignin monomers (performed by cinnamoyl-CoA reductase (CCR) and cinnamyl-alcohol dehydrogenase (CAD)) (Vogt, 2010). The map of the pathway is presented in Figure 4-1.

The phenylpropanoid pathway has a vast biological functionality. Multiple observations showed that plants activate the pathway in response to various abiotic and biotic stresses. For example, phenylpropanoids are produced in tea crop (*C. sinencis*) and highbush blueberry (*Vaccinium corymbosum*) in response to light and UV-B, respectively (Luengo Escobar et al., 2017; Y. S. Wang et al., 2012). In white grapes (*Vitis vinifera*), the content of phenylpropanoids was increased during drought stress. The positive effect of phenylpropanoid compounds, which helps plants to cope with abiotic stresses, is often explained by their antioxidative properties (Peterlunger et al., 2016).

When it comes to biotic stresses, metabolites from the phenylpropanoid pathways can contribute to plant resistance against various pathogens. For example, UV-B-induced response in *A. thaliana* led to the accumulation of sinapates and increased resistance to *B. cinerea* (Demkura & Ballaré, 2012). Deposition of lignin in secondary cell walls is crucial for the prevention of pathogen penetration (Miedes, Vanholme, Boerjan, & Molina, 2014). The previous studies on camellia petal blight showed that cell wall lignification was involved in the resistance response to *C. camelliae* too (Taylor, 2004). Interestingly, phenolic acids produced by the phenylpropanoid pathway were shown to be promising antifungal agents even against human pathogens from the genus *Candida* (Canturk, 2018; Teodoro, Ellepola, Seneviratne, & Koga-Ito, 2015).

In order to determine the contribution of the phenylpropanoid pathway to the resistance of *C. lutchuensis* to petal blight, I started from the analysis of expression profiles of phenylpropanoid pathway enzymes. Then, using LC-MS, the levels of several metabolites from the pathway were measured to determine the dynamics associated with the resistance response. Finally, some phenylpropanoid pathway compounds were tested for antifungal activity against *C. camelliae*, suggesting a direct contribution in the defence of *Camellia* plants against the petal blight pathogen.

4.2. Results

Ascospore treatment upregulates phenylpropanoid pathway genes in *C. lutchuensis* petals. Quantitative RNA-seq analysis, described in Chapter 3, showed the enriched expression of the phenylpropanoid pathway in infected resistant *C. lutchuensis* petals. To further understand how the plant pathway activity was affected by the pathogen-inoculation, I found the expression patterns of pathway genes in the RNA-seq data (Figure 4-1). Indeed, expression levels of many genes were elevated in infected petals, including core pathway genes like PAL, C4H and 4CL. Despite the fact that some of the genes, including PAL, C4H and 4CL, were upregulated in mock-treated samples, the majority of differentially expressed phenylpropanoid pathway genes showed higher folds of upregulation after ascospore-treatment. Remarkably, CHS genes, encoding the first enzyme of flavonoid biosynthesis, were mainly downregulated in response to *C. camelliae*. Overall, the results indicated that the activation of phenylpropanoid genes is a part of the resistance response of *C. lutchuensis* to *C. camelliae*.

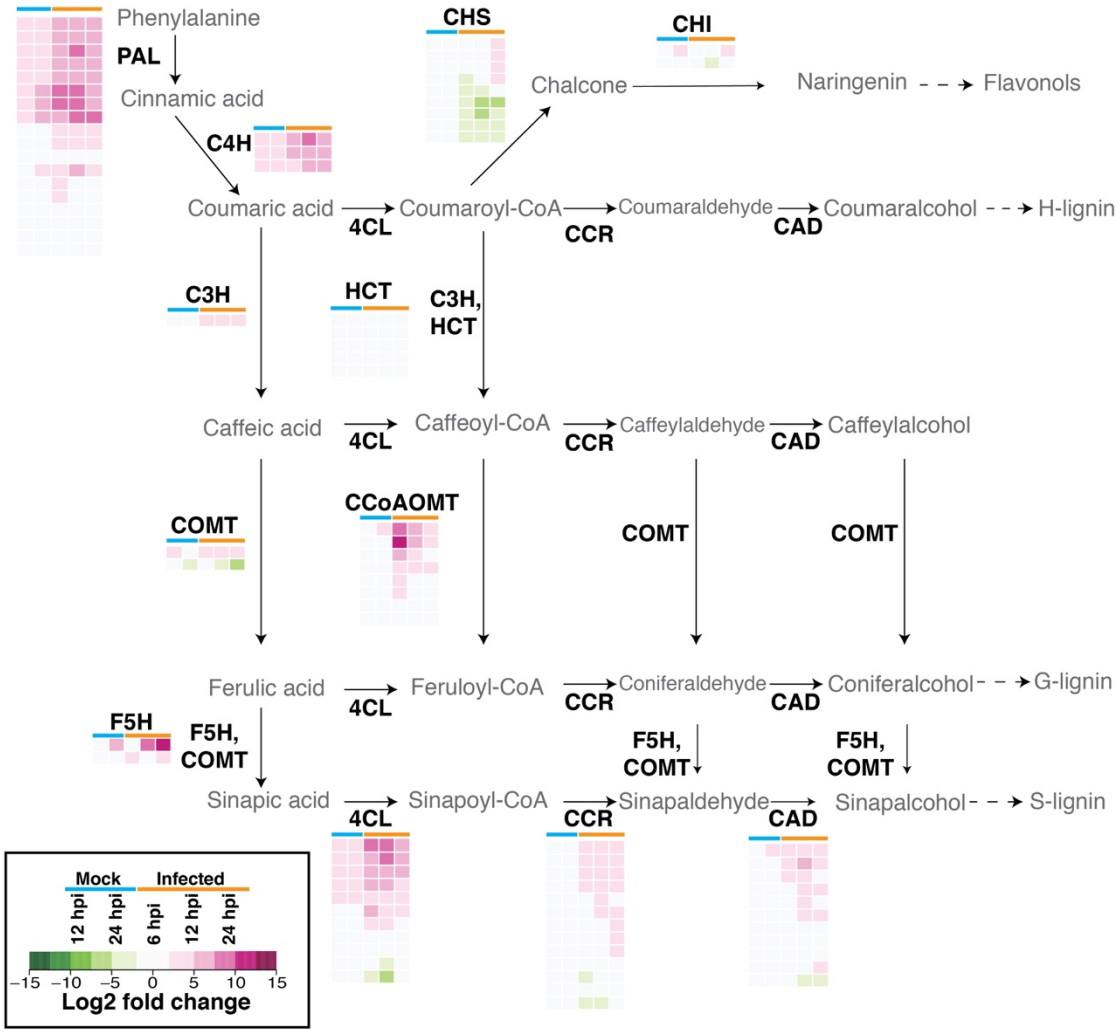

Figure 4-1 | Expression map of the phenylpropanoid pathway in mock- and ascospore-treated *C. lutchuensis* petals.
Heatmaps show expression of the transcripts annotated as phenylpropanoid biosynthesis genes, where rows represent the transcripts and columns show treatment and timepoints. Cell colouring shows the log_2 of fold-change values calculated against 0 hpi timepoint. Enzyme abbreviations: PAL, phenylalanine ammonia lyase; C4H trans-cinnamate 4-monooxygenase; 4CL, 4-coumarate-CoA ligase; C3H, p-coumaroyl shikimate/quinate 3'-hydroxylase; HCT, hydroxycinnamoyl-CoA:shikimate/quinate hydroxycinnamoyltransferase; COMT, caffeate O-methyltransferase; CCoAOMT, caffeoyl-CoA O-methyltransferase; F5H, ferulate 5-hydroxylase; CCR, cinnamoyl-CoA reductase; CAD, cinnamyl-alcohol dehydrogenase; CHS, naringenin-chalcone synthase; CHI, chalcone isomerase. The table-dataset used to prepare heatmaps, which contains transcript IDs, log_2 of expression fold-change values, and transcript annotations, is available in Appendix C as a Supplementary file 7.

Phenylpropanoid content of resistant petals is affected by petal blight infection. The changes in pathway gene expression are expected to alter concentrations of corresponding metabolites. To check the effect of petal blight infection on the *C. lutchuensis* petal phenylpropanoid contents, the concentration of several metabolites was measured in

the course of the resistance response using LC-MS. The table below shows the concentrations of detected metabolites in mock-treated and infected *C. lutchuensis* petals at different time points after inoculation (Table 4-1). One-way ANOVA was performed to find the compounds whose concentrations changed significantly after the mock- or ascospore-treatments. As a result, the concentrations of both tested aromatic amino acids, all tested phenolic acids, three aldehydes (coumar-, caffey-, and sinapaldehyde), caffeyalcohol, and one isomer of syringin (glycosylated form of sinapic acid) were shown to be significantly affected by the treatment ($P < 0.05$). At the same time, the content of naringenin — the first precursor of flavonoids — was not affected by either mock or ascospore treatment. In brief, LC-MS analysis showed that the content of phenylpropanoid metabolites of *C. lutchuensis* petals was affected by the ascospore treatment, as suggested by the RNA-seq results.

Table 4-1 | Results of LC-MS quantification of compounds from phenylpropanoid pathway.

Compounds	0 hpi	6 hpi		12 hpi		24 hpi		48 hpi		ANOVA *P* value	
	Mock	Mock	Infected	Mock	Infected	Mock	Infected	Mock	Infected		
Amino acids											
Phenylalanine, µg/g	3.30±0.41	3.64±0.06	4.60±0.71	4.47±0.57	3.54±0.34	4.59±0.21	**2.98±0.05**	4.43±0.33	**2.59±0.18**	**0.01**	**
Tyrosine, µg/g	0.48±0.03	0.67±0.03	0.80±0.08	0.97±0.21	0.72±0.13	0.67±0.04	**0.37±0.03**	0.77±0.04	**0.35±0.07**	**0.00**	**
Phenolic acids											
Cinnamic acid, mg/g	0.05±0.01	0.03±0.00	0.04±0.00	0.05±0.01	**0.03±0.00**	0.02±0.00	0.01±0.00	0.01±0.00	0.01±0.00	**0.00**	***
p-Coumaric acid, mg/g	0.88±0.33	0.75±0.31	**1.58±0.08**	1.01±0.27	1.31±0.10	0.85±0.12	**1.51±0.16**	0.37±0.04	0.35±0.02	**0.00**	**
Caffeic acid, µg/g	2.74±0.33	3.14±0.12	**2.38±0.28**	3.03±0.29	2.47±0.14	2.44±0.04	2.61±0.16	2.07±0.06	2.62±0.13	**0.03**	*
Ferulic acid, mg/g	0.17±0.05	0.17±0.05	**0.29±0.04**	0.24±0.04	0.28±0.01	0.28±0.02	0.27±0.05	0.37±0.04	0.38±0.03	**0.01**	*
Sinapic acid, mg/g	1.02±0.23	1.09±0.18	**1.75±0.10**	1.57±0.05	1.36±0.09	1.20±0.06	1.09±0.17	1.48±0.20	1.26±0.00	**0.02**	*
Aldehydes											
Coumaraldehyde, mg/g	0.04±0.02	0.06±0.01	0.05±0.01	0.06±0.01	0.06±0.01	0.09±0.02	**0.22±0.05**	0.13±0.03	0.17±0.00	**0.00**	***
Caffeyaldehyde, mg/g	0.72±0.08	0.46±0.18	0.22±0.04	1.33±0.23	**0.16±0.00**	0.17±0.02	0.15±0.02	0.23±0.08	0.30±0.04	**0.00**	***
Coniferaldehyde, mg/g	0.04±0.01	0.03±0.00	0.05±0.00	0.05±0.00	0.04±0.00	0.04±0.00	0.04±0.00	0.04±0.00	0.04±0.00	0.24	
Sinapaldehyde, mg/g	0.05±0.02	0.06±0.01	0.06±0.01	0.07±0.00	0.06±0.01	0.09±0.02	**0.23±0.06**	0.15±0.03	0.19±0.01	**0.00**	***
Alcohols											
Coumaralcohol, mg/g	0.03±0.01	0.03±0.01	0.05±0.00	0.05±0.00	0.04±0.00	0.04±0.00	0.04±0.01	0.04±0.00	0.04±0.00	0.27	
Caffeyalcohol, mg/g	0.03±0.01	0.04±0.00	0.04±0.01	0.04±0.01	0.04±0.01	0.06±0.01	**0.14±0.03**	0.09±0.02	0.12±0.01	**0.00**	***
Sinapalcohol, mg/g	0.04±0.02	0.04±0.00	0.07±0.02	0.04±0.01	0.07±0.03	0.06±0.01	0.08±0.02	0.07±0.02	0.04±0.01	0.58	
Glycosilated forms											
Syringin a, mg/g	0.22±0.04	0.31±0.06	0.49±0.08	0.50±0.08	0.51±0.11	0.43±0.04	0.42±0.08	0.62±0.12	0.50±0.01	0.06	
Syringin b, mg/g	0.51±0.23	0.32±0.06	0.48±0.08	0.54±0.05	0.45±0.06	0.17±0.01	0.25±0.02	0.25±0.03	0.15±0.02	**0.03**	*
Flavonoid precursor											
Naringenin, mg/g	0.01±0.00	0.01±0.00	0.01±0.00	0.01±0.00	0.01±0.00	0.01±0.00	0.01±0.00	0.00±0.00	0.00±0.00	0.36	

The concentrations are shown per 1 g of dry petal weight. Values are mean ± SE; n = 3. Highlighted values of infected samples are significantly different from corresponding mock-treated ones according to Fisher's LSD test, P < 0.05. Purple colour shows that the infected samples had higher concentration, and green colour – lower concentration – than the mock-treated ones.

Phenylpropanoid compounds show various concentration patterns in the course of the resistance response. Overall, the metabolites, whose content was significantly affected by the treatment, showed complex dynamics during the experiment. To assess expression dynamics of phenylpropanoid metabolites in the course of the resistance response, they were grouped according to their temporal concentration patterns. Then, a regression analysis with cubic splines was performed for each compound, which permitted analysis of the complex non-linear relationship between time and compound concentrations. Unlike linear regression models, cubic splines are defined as piecewise functions, so they take into account that the concentration of analysed metabolites can increase and decrease multiple times in the course of observations. (Ahn, Kumar, Mukha, Tzur, & Shlomi, 2017; Leaf et al., 2018; Leupold et al., 2018; Semba et al., 2016) (Figure 4-2).

The compounds formed five correlation groups (A-E), based on their concentration patterns. Three compounds from group A showed different patterns between mock and ascospore-treatments. Amino acids – phenylalanine and tyrosine – slightly increased in concentration at 6 hpi in infected samples, but then their levels were reduced to lower than those of the mock-treated samples at 24 and 48 hpi ($P < 0.05$, Fisher's LSD test). At the same time, infected petals maintained elevated concentrations of p-coumaric acid at 6 and 24 hpi of the treatment ($P < 0.05$, Fisher's LSD test). The group B contained ferulic and sinapic acids, whose concentration was higher in infected samples at 6 hpi ($P < 0.05$, Fisher's LSD test), but the trends did not differ significantly between mock-treatment and infection process at the later time points. The group C consisted of three highly correlated metabolites – coumaraldehyde, sinapaldehyde, caffeyalcohol – which had significantly higher concentrations in the infected petals at 24 hpi ($P < 0.05$, Fisher's LSD test). Syringin b, cinnamic acid and caffeyaldehyde showed a downward trend in infected petals, and the maximal concentration of these compounds was observed in

mock-treated samples at 12 hpi ($P < 0.05$ only for cinnamic acid and caffeyaldehyde, Fisher's LSD test). The last group, E, contained only caffeic acid, which had a constant concentration in infected petals but increased at 6 and 12 hpi in mock-treated petals ($P < 0.05$ only at 6 hpi, Fisher's LSD test) with subsequent decline at 24 and 48 hpi. Overall, the correlation and regression analyses showed that the phenylpropanoid metabolites demonstrate various concentration patterns during the resistance response of *C. lutchuensis*.

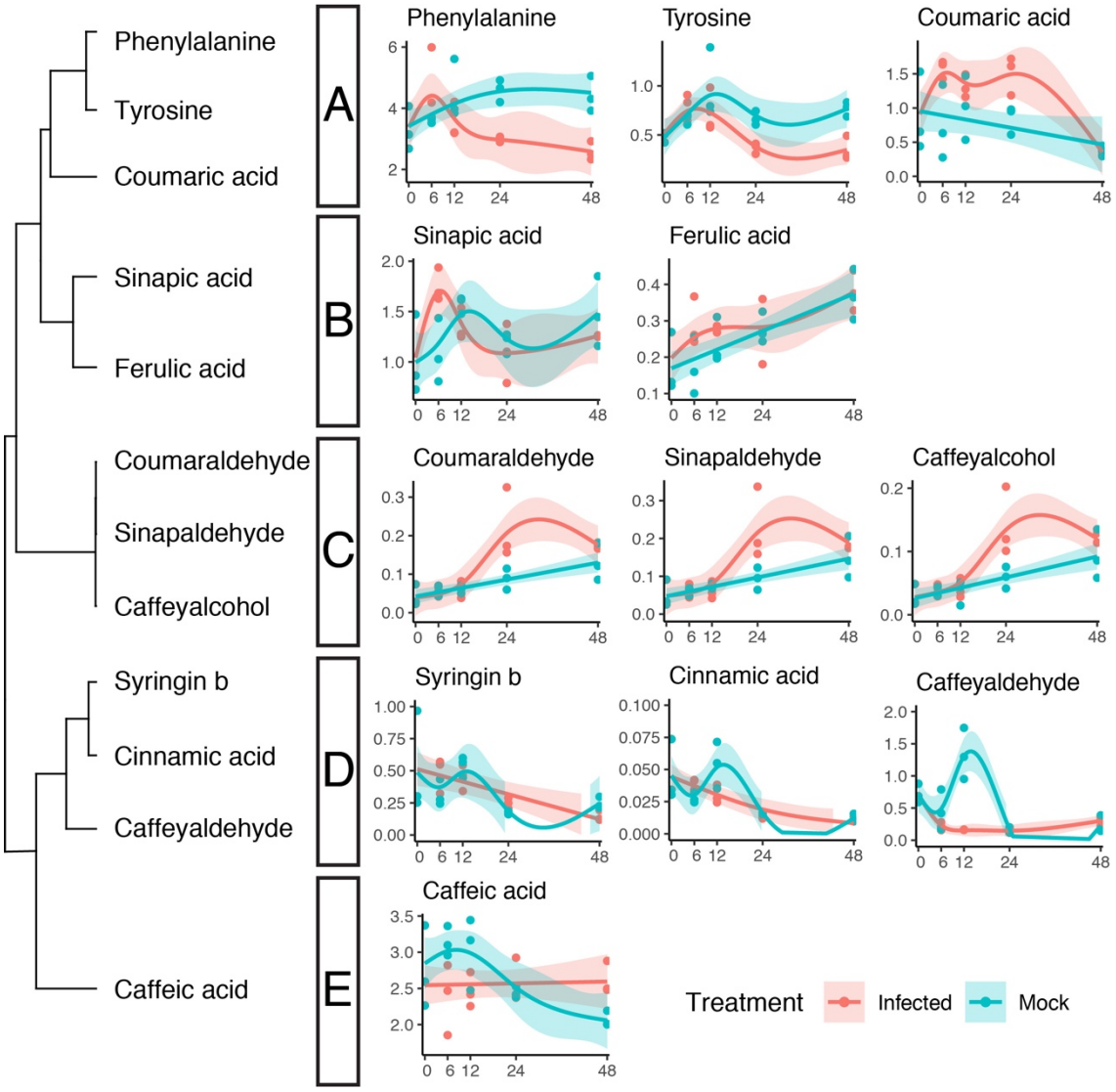

Figure 4-2 | Time-course profiles of phenylpropanoid metabolites in infected and mock-treated *C. lutchuensis* petals.
The dendrogram on the left shows the results of the correlation clustering for the concentration patterns of the pathway compounds affected by the treatment. Bar plots on the right show the detected concentrations of corresponding compounds. X-axis shows timeline of the treatment, y-axis shows the measured content of the corresponding compounds, the concentration units are μg/g for phenylalanine, tyrosine and caffeic acid, and mg/g for the other compounds; dots represent individual observations; lines show fitted cubic splines, and ribbons show 95% confidence intervals of the fitted model.

***In vitro* antifungal activity of phenylpropanoid compounds.** Antimicrobial activity was reported for several phenylpropanoid compounds (Canturk, 2018; Hemaiswarya & Doble, 2010; Piotrowski et al., 2015). Here I hypothesize that phenylpropanoids may contribute to petal-blight defence in resistant plants. To test this hypothesis, several phenylpropanoid compounds were added into the fungal growth media. *Ciborinia camelliae* colonies were grown on PDA plates supplemented with 100, 500 and 1000 μM concentrations of phenylpropanoid compounds, which correspond to concentration ranges used in similar studies with other fungal species (Cuperlovic-Culf, Rajagopalan, Tulpan, & Loewen, 2016; König et al., 2014). Measurement of colony sizes was performed at 5 dpi (Figure 4-3). The strongest antifungal activity was observed for ferulic acid at all tested concentrations. Coniferyl alcohol, which is synthesized via the two-step reduction of ferulic acid, also inhibited the fungal growth at all tested concentrations. Cinnamic and coumaric acids showed significant reduction in colony sizes at concentrations of 500 μM and 1000 μM, while sinapic and caffeic acids showed growth inhibition only at 1000 μM. To sum up, all tested phenylpropanoid compounds showed various rates of *in vitro* antifungal activity against *C. camelliae*.

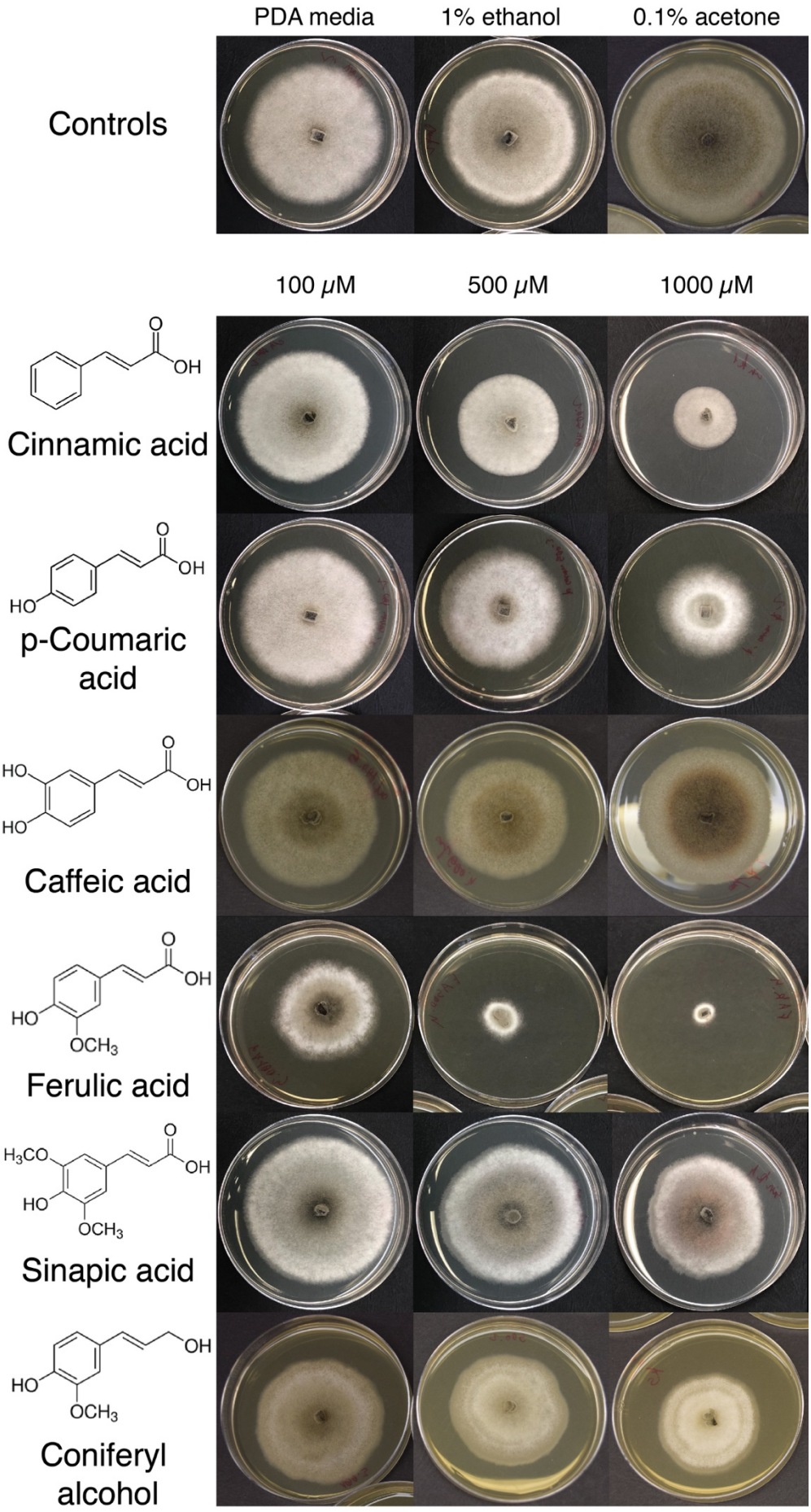
PDA media
1% ethanol
0.1% acetone
Controls
100 μM
500 μM
1000 μM
Cinnamic acid
p-Coumaric acid
Caffeic acid
Ferulic acid
Sinapic acid
Coniferyl alcohol

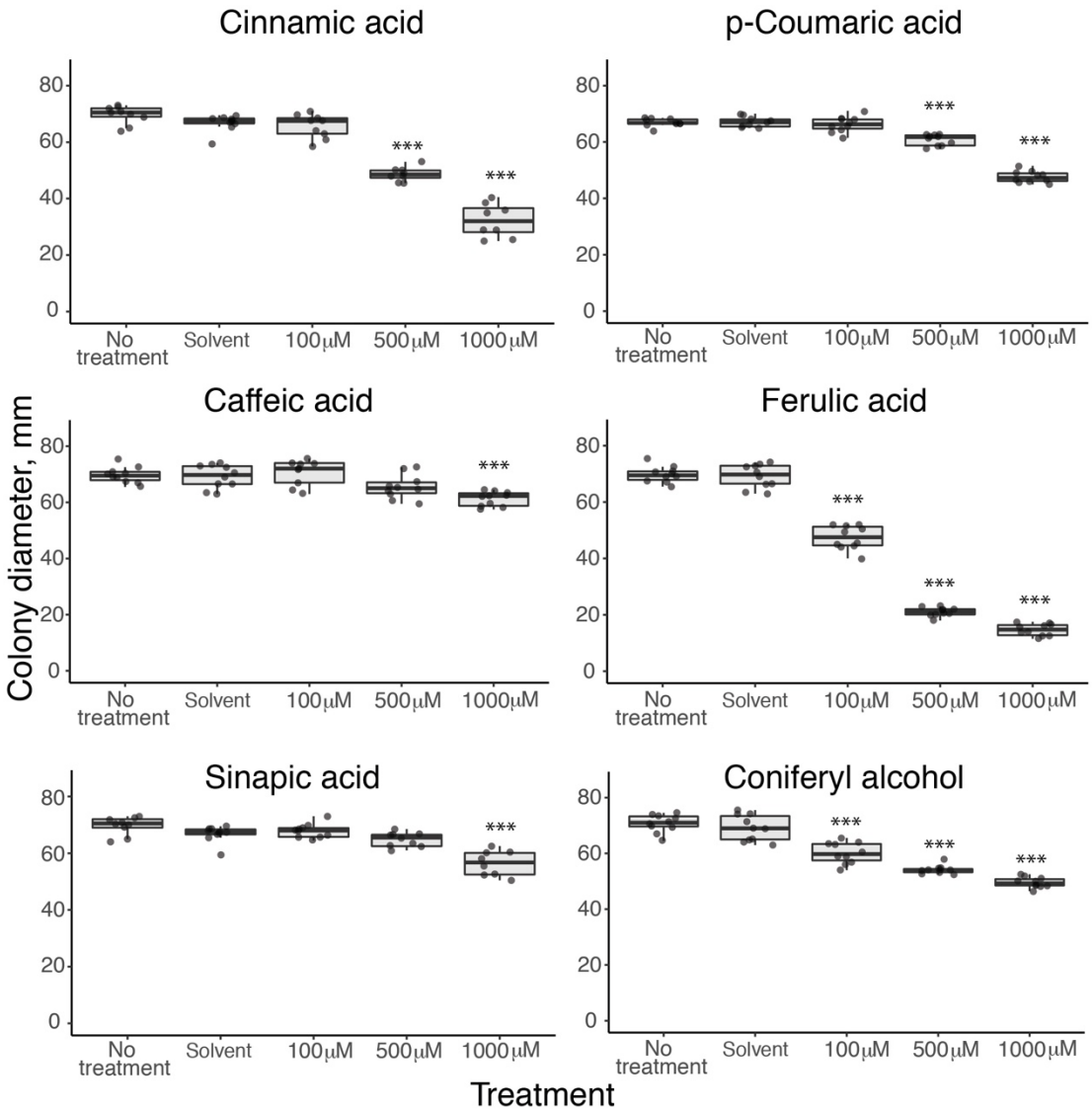

Figure 4-3 | *In vitro* activity of phenylpropanoids against petal blight pathogen. *Left figure shows radial growth of fungal colonies in potato dextrose agar plates in the presence of phenylpropanoid compounds at 5 days post inoculation (dpi). Boxplots above show the measured colony diameters at 5 dpi. The measurements were performed for 10 biological replicates from two independent experiment repeats. ***, P < 0.001 (two-tailed Student's t-test), compared to corresponding solvent control.*

Phenylpropanoids inhibit petal blight development on susceptible petals. *In vitro* tests described above demonstrated that phenylpropanoid compounds can inhibit the growth of *C. camelliae* mycelium. My next hypothesis was that these compounds might suppress development of the blight on *Camellia* petals. To check this, highly susceptible *Camellia* 'Nicky Crisp' petals were drop-inoculated with ascospore solution with either added phenylpropanoid compounds or corresponding solvents. Resulting lesions were

measured at 48 hpi (Figure 4-4). Unlike the results of *in vitro* test, coniferyl alcohol did not affect the fungal growth on petals, showing no significant difference from the control ethanol and acetone treatments. Caffeic and sinapic acid considerably reduced disease development, while addition of cinnamic, p-coumaric or ferulic acids completely prevented lesion development. Overall, the experiment demonstrated that phenolic acids have antifungal activity against *C. camelliae* ascospores.

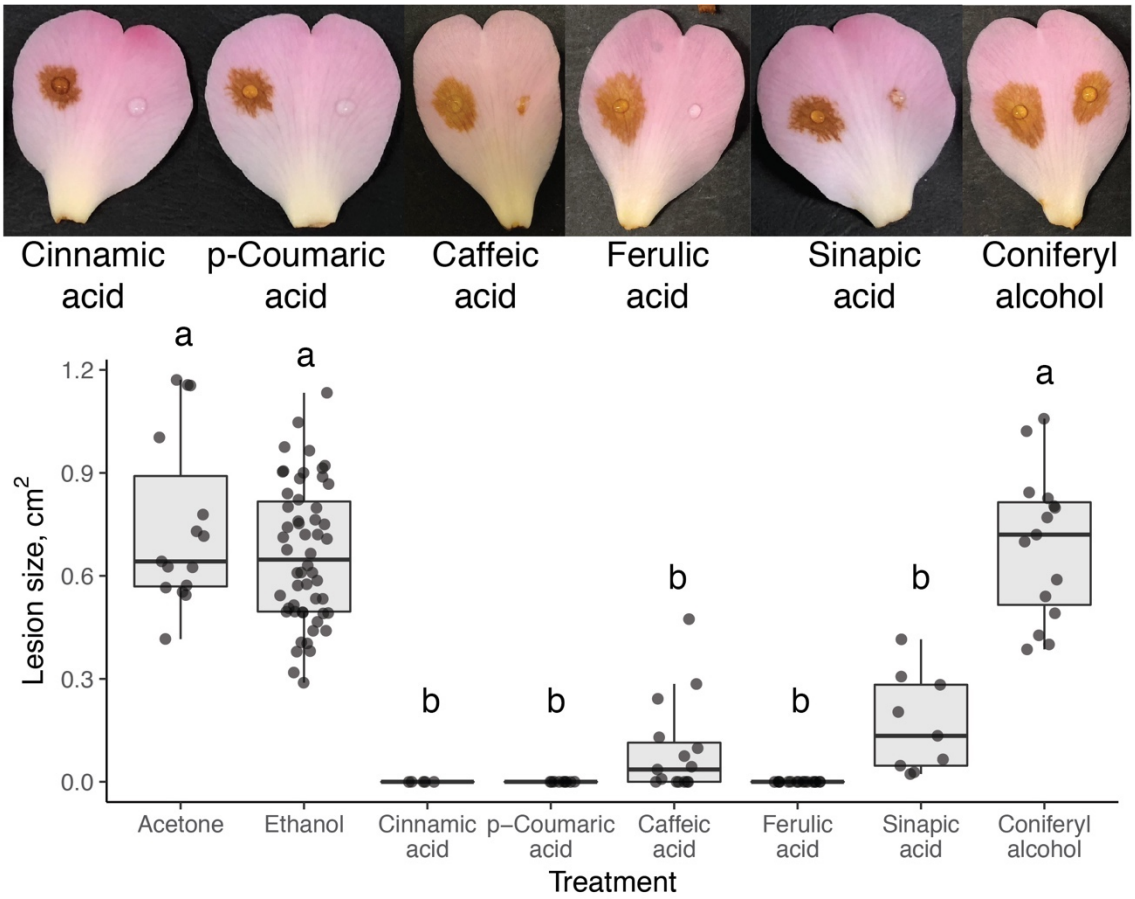

Figure 4-4 | The effect of phenylpropanoid metabolites on the petal blight development on *Camellia* 'Nicky Crisp' petals.

Petals were infiltrated with 10 μl of ascospore solution. Solution used on the right side of a petal contained 1mM concentration of the phenylpropanoid compound and 1% of ethanol or 0.1% of acetone as a solvent, while the solution on the left side contained only a corresponding solvent. Lesions were measured at 48 hpi, and boxplots show the obtained lesion sizes. Dots represent individual observations. Results were analysed with one-way ANOVA with repeated measures and Tukey's Honest Significant Difference test. The same letter above two boxes indicates that lesion sizes did not differ significantly between two treatments ($P < 0.05$). Upper pictures show representative petals.

Ferulic acid treatment is more effective on the early stages of the infection.

In the previous test, phenylpropanoid metabolites were added directly in the ascospore solution right before the inoculation. To check, whether the later addition of a compound can still reduce lesion development, ferulic acid was added after inoculation with ascospore solution. First, both sides of petals were drop-inoculated with ascospore solution in sterile water. Inoculated petals were incubated for 6, 12 or 24 hours. After the incubation time, the initial solution was gently removed with a paper towel, and the inoculation point was covered with 50 µl of 1% ethanol solution on the left side, and 1 mM ferulic acid (ferulate) in 1% ethanol on the right side. Figure 4-5 shows the resulting lesion sizes at 72 hpi. While the addition of ethanol solution after 6 hpi did not stop the lesion formation, 1 mM ferulic acid fully suppressed the development of the infection. The effect was less pronounced for the 12 hpi treatment, but still, the addition of ferulic acid resulted in significantly smaller lesions than the ethanol-treatment applied at the same time point. The two treatments did not result in significant differences in lesion sizes, when applied at 24 hours after the initial ascospore inoculation. According to the results, ferulic acid can inhibit the blight development even if not added in the initial ascospore solution, although the activity of the treatment decreases during later stages of the infection.

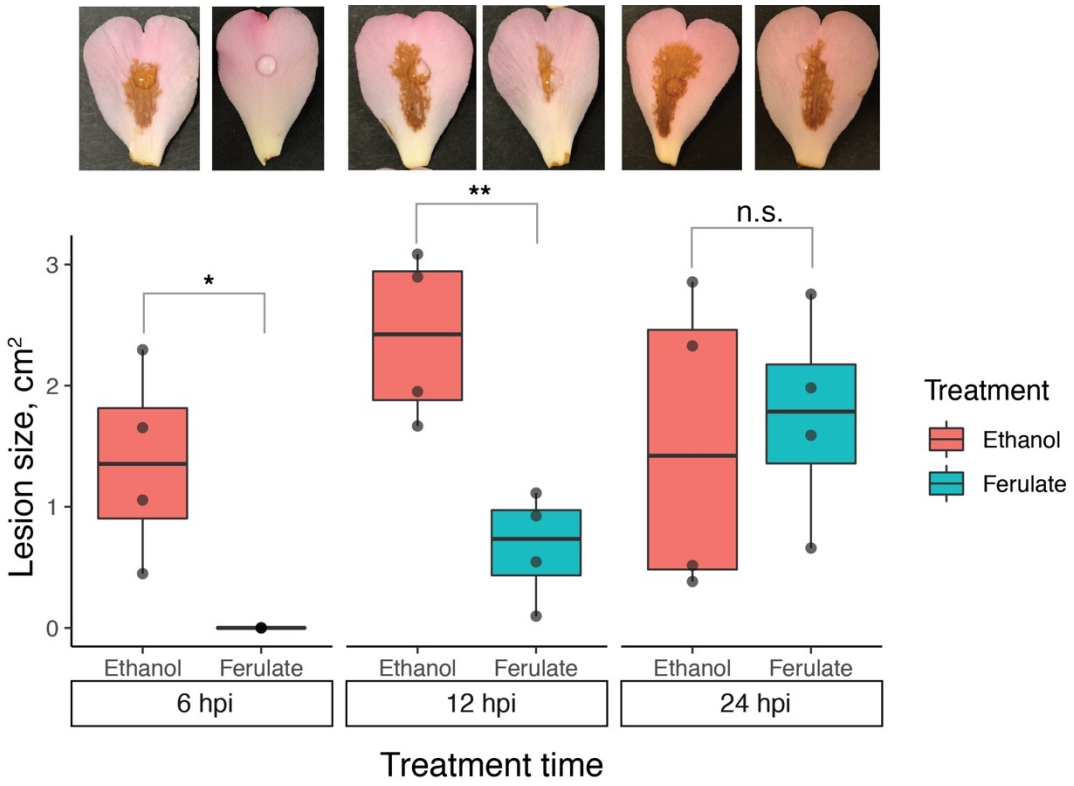

Figure 4-5 | The effect of ferulate-treatment time on lesion development in susceptible *Camellia* 'Nicky Crisp'.

*The boxplot represents the lesion sizes after the treatment, and dots represent individual observations. Colours correspond to the treatment, and boxes are grouped according to the treatment time. *, $P < 0.05$; **, $P < 0.01$ according to two-tailed Student's t-test. The pictures above the boxplots are representatives of four biological replicates.*

4.3. Discussion

Induced plant defence mechanisms include production of various secondary metabolites. Even though the phenylpropanoid pathway was mostly viewed as a source of lignin, which fortifies plant cell walls blocking the invasion of pathogens, recent studies have shown the direct antimicrobial effects of phenylpropanoid compounds (König et al., 2014). Here, using the *C. lutchuensis*-*C. camelliae* pathosystem, I demonstrate that phenylpropanoid metabolites may contribute to the rapid resistance response of *Camellia* plants against the necrotrophic petal blight pathogen.

The phenylpropanoid pathway showed an enriched upregulation in *C. lutchuensis* after the treatment with *C. camelliae* ascospores. The activation of this pathway in response to various pathogens was previously observed on a transcriptomic level in other plants (De Cremer et al., 2013; Y. Hao et al., 2016; L. Xu et al., 2011). Many genes of the pathway were upregulated also in mock-treated petals, but still had lower fold-change values than the infected petals, suggesting that they partially responded to background stress associated with detachment of petals and their prolonged incubation in artificial conditions. That is not unexpected since the phenylpropanoid pathway contributes to the resistance to abiotic stresses as well (Abdollahi Mandoulakani, Eyvazpour, & Ghadimzadeh, 2017; Gori et al., 2015).

Unlike the other enzymes of the pathway, naringenin-chalcone synthase (CHS) was significantly downregulated in resistant petals after the fungal treatment. Apparently, this works as an important mechanism allowing to modulate the flux through the pathway and shift it towards the production of monolignols that are important for the defence, but not the precursor of flavonoids, naringenin. Interestingly, the pathogenic fungus *U. maydis* can override this fine-tuned balance using a specific effector, Tin2, which conversely stimulates anthocyanin (flavonoid) production and decreases lignin biosynthesis, subsequently facilitating colonization of maize plants by the pathogen (Tanaka et al., 2014).

To understand how observed transcriptomic changes in the pathway affect the production of metabolites, LC-MS measurements were performed for infected and mock-inoculated petals. As expected, the concentrations of the majority of detected compounds were affected by the treatment. The production of the aromatic amino acids, phenylalanine and tyrosine, was slightly elevated at 6 h in infected petals, but dropped to the levels that were lower than in the mock-treated petals, which is likely due to the elevated consumption of them by the upregulated phenylpropanoid pathway in infected petals (Manela et al., 2015).

The content of three phenolic acids increased over the course of the infection. Coumaric acid had higher production in infected petals at 6, 12 and 24 hpi; sinapic acid only at 6 hpi; ferulic acid had a higher concentration in infected petals at 6 hpi, but also an increasing temporal trend in ferulic acid concentration was observed for both infected and uninfected petals. The results presented here are consistent with observations from other works. For example, in response to infection with the necrotroph *B. cinerea*, the resistant apple cultivar, *Malus domestica* var. *Qinguan*, produces significantly higher amounts of ferulic acid, while the susceptible cultivar, *Malus domestica* var. *Fiji*, does not change ferulic acid content. Moreover, susceptible cultivar fruits have generally lower content of ferulic acid than the resistant ones (Ma, He, Liu, & Zhou, 2018). To further support the hypothesis that phenylpropanoid compounds contribute to petal blight resistance, an analysis of susceptible *Camellia* cultivars needs to be performed. Two hypothetical outcomes could further support my model: susceptible *Camellia* cultivars always have a lower content of phenylpropanoids, or they fail to induce the pathway in response to the infection. The second statement was already partially supported by the observations from the previous chapter, where I showed that the upregulation of *C4H* and *4CL* genes, core enzymes of the pathway, occurs in susceptible *Camellia* 'Nicky Crisp' petals later than in the resistant *C. lutchuensis*.

In vitro and *in vivo* tests showed that compounds from the phenylpropanoid pathway can suppress the development of the petal blight pathogen. The compounds with the highest *in vitro* antifungal activity – cinnamic acid, coumaric acid, and ferulic acid – completely inhibited development of lesions on susceptible petals as well. Interestingly, the only tested alcohol, coniferyl alcohol, demonstrated antifungal activity *in vitro*, but had no significant effect on lesion development *in planta*. One explanation for this observation could be that, in a plate culture, coniferyl alcohol slowly oxidizes back to a more toxic ferulic acid by oxygen or fungal enzymes (as demonstrated before for fungal liquid culture (König et al., 2014)), while the petal surfaces may have different chemical and physical conditions.

The testing of the treatment application time showed that early treatment was more effective in the inhibition of the petal lesion development. This is in accord with results of the transcriptomic observations that the early defence response is a key factor enabling resistance against petal blight. The results of LC-MS analysis further supported this hypothesis: the accumulation of coumaric, ferulic and sinapic acids – compounds that demonstrated *in vitro* and *in planta* fungistatic activity – takes place already at 6 hpi. Thus, these three compounds may contribute to the early resistance with different efficacy. However, it is not yet possible to conclude whether the later application of ferulic acid was not effective due to higher ferulate-resistance of the fungal necrotrophic stage, or just because the penetration of ferulic acid was not efficient enough to inhibit the growth of fungal mycelium growing deep in petals.

Antifungal activity of many detected compounds was not tested in this study due to their unavailability. It remains unclear if three compounds highly upregulated at 24 hpi – coumaraldehyde, sinapaldehyde, and caffeyalcohol – have any antifungal activity. Nevertheless, the sudden drop in their content at 48 hpi may suggest that they are metabolized downstream in the pathway to produce lignin (observed at 24-96 hpi (Taylor,

2004)), or other types of antifungal compounds such as coumarins, phytoalexins, and stilbenes (Malinovsky, Fangel, & Willats, 2014).

At present, there are few publications on the mode of antimicrobial action of phenylpropanoid compounds. Ferulic and gallic acids were demonstrated to affect plasma membrane of bacterial cells and induce cell content leakage (Borges, Ferreira, Saavedra, & Simoes, 2013). A study on pathogenic *Candida albicans* showed that phenylpropanoids decrease cell adhesion, inhibiting biofilm formation (Raut, Shinde, Chauhan, & Karuppayil, 2014). Caffeic acid was demonstrated to have inhibiting activity on glyoxylate cycle in *C. albicans* (Cheah, Lim, & Sandai, 2014). Poacic acid, a dimer of ferulic acid, binds β-1,3-glucan and inhibits fungal growth. Taken together, I suggest that the tested phenylpropanoids might have inhibited the growth of *C. camelliae* by targeting the fungal cell wall. Then, it is possible that the observed variation of antifungal activity may be due to the levels of structural compatibility between the phenylpropanoid compounds and a fungal target molecule. It also cannot be excluded that phenylpropanoids may have affected the adhesion of ascospores to the susceptible plant petal surface. Further tests are required to check these hypotheses.

The study presented in this chapter further extends the significance of the phenylpropanoid biosynthesis pathway for plants. To the best of my knowledge, it is the first study showing the early events occurring in the pathway, since usually metabolomic studies investigate patterns in time steps of days, not hours. Using the example of the *C. lutchuensis*-*C. camelliae* interaction, I demonstrated that the pathway produces fungistatic metabolites which may facilitate the rapid defence response of the plant. Based on current observations and previous microscopic studies (Denton-Giles, 2014; Taylor, 2004), I suggest a model of how the phenylpropanoid pathway contributes to the defence of *C. lutchuensis* against *C. camelliae* in multiple ways (Figure 4-6). The early response to the fungus includes the accumulation of coumaric, ferulic and sinapic acids, which may have a toxic

effect on the nascent hyphae of the pathogen. Later polymerization of lignin monomers and cell wall thickening creates a physical barrier, preventing the penetration of the fungus and further suppressing the establishment of the infection.

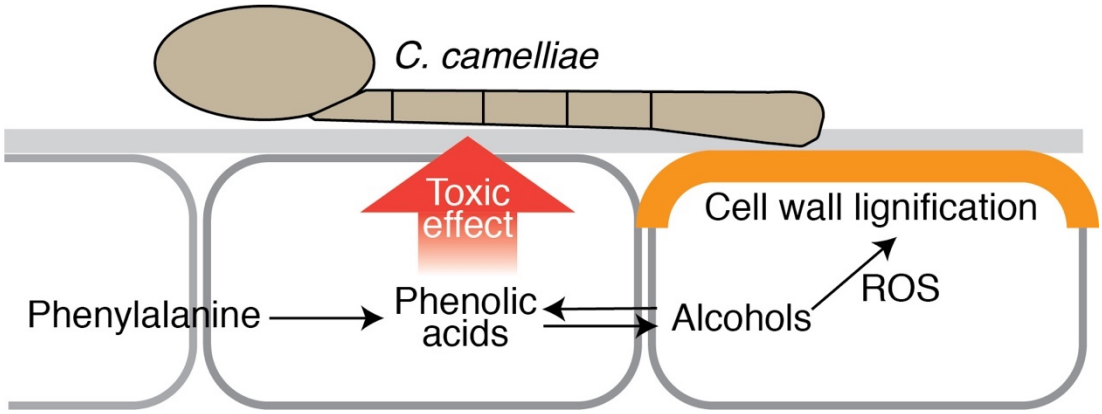

Figure 4-6 | Putative roles of the phenylpropanoid pathway in the resistance of *C. lutchuensis* to petal blight disease.
In response to the petal blight infection, resistant C. lutchuensis *petals produce phenolic acids, which have a toxic effect on the pathogen. The acids are metabolized further to produce aldehydes and alcohol, which form lignin in the presence of reactive oxygen species (ROS) and specific enzymes or get oxidized back to phenolic acids via the non-specific oxidation processes.*

Chapter 5. Towards the proteomic analysis of *Camellia* spp.-*C. camelliae* interaction

5.1. Introduction

The interaction between hosts and pathogens is facilitated by the secretion of compounds of various molecular size and chemical nature. Secreted proteins play a significant role in plant-fungus interactions and attract researchers' interest. Proteins produced by pathogenic fungi help to circumvent physical barriers and degrade complex organic compounds to acquire nutrients (e.g. cutinases, cellulases, endopolygalacturonases (Kubicek, Starr, & Glass, 2014)), and also to manipulate host responses (toxins and immune suppressors (Frías, González, & Brito, 2011; W. Zhu et al., 2013)). The composition of fungal proteinaceous secretomes is linked to the lifestyle of the fungus: necrotrophic fungi tend to exploit more CAZymes than biotrophic ones (Zhao, Liu, Wang, & Xu, 2014). In turn, plants also secrete proteins into the intercellular space of their organs to detect and stop the invasion of pathogens. These proteins reinforce plant cell walls and control oxidative balance (Delaunois et al., 2014). Many plant proteins directly target pathogens (e.g. chitinases (Kumar et al., 2018)) or neutralize their cell wall degrading enzymes (Juge, 2006).

Genomic, transcriptomic, and proteomic approaches combined with bioinformatic analysis are used to study plant and fungal secreted proteins. For example, an indirect analysis of the *C. camelliae* secretome was conducted in the previous study (Denton-Giles, 2014). The fungal secretome was predicted from the newly sequenced fungal genome and compared to the secretomes of closely related *S. sclerotiorum* and *B. cinerea*, demonstrating the enrichment of *C. camelliae* secretome with so called small-secreted proteins (SSPs). An

example of the transcriptomic approach is a study on *D. septosporum*, which identified important fungal secreted proteins, including CAZymes and cysteine-rich SSPs, based on their temporal expression patterns in the course of a pine needle blight infection (Bradshaw et al., 2016).

The direct investigation of secretomes uses proteomic methods which allow to detect, quantify and purify proteins from various biological samples. Quantitative proteome analysis of *Xanthomonas oryzae*, which causes bacterial blight of rice, identified a secreted cysteine protease XoCP contributing to the virulence of the pathogen (Yiming Wang et al., 2017). Proteomic analysis of apoplastic interaction occurring between rice and *M. oryzae* combined with subsequent transient protein expression methods showed that fungal glycosyl hydrolases can work as apoplastic pathogenicity effectors. The proteomic methods allow not only identification but also purification of proteins for functional studies. For example, a fast protein liquid chromatography (FPLC) method was used to purify and characterize necrosis-inducing proteins from *B. cinerea* (Y. Y. Zhang et al., 2015) and *Z. tritici* culture filtrates (Ben M'Barek et al., 2015).

This chapter describes the analysis of camellia petal blight infection based on a proteomic approach. In the course of *Camellia* spp.-*C. camelliae* interaction, the penetration of the pathogen is followed by the growth of fungal mycelium in the intercellular space of petals (petal apoplast) (Denton-Giles et al., 2013). To investigate the interaction between plants and fungus occurring in the intercellular space of petals, apoplastic fluids of *Camellia* 'Nicky Crisp' petals were extracted and used for the identification of secreted plant and fungal proteins. I also tested the *in vitro* secretome of *C. camelliae* using fungal culture filtrate and compared its protein composition with *in planta* secretome of the fungus. Both fungal culture filtrate and apoplastic washes of infected plants had necrosis-inducing activity, suggesting that they contain components contributing to the virulence of *C. camelliae*. Moreover, an FPLC method was exploited to partially purify the components of the

culture filtrate, which induced necrosis in *Camellia* petals. Overall, the results of this chapter further demonstrate the necrotrophic type of the interaction between *Camellia* plants and *C. camelliae* and characterize proteinaceous secretome of the pathogen.

5.2. Results

Petal blight infection affects the apoplast proteome of susceptible *Camellia* 'Nicky Crisp'. After passing the petal cuticle and epidermis, *C. camelliae* continues its growth in the intercellular space of the petal mesophyll (Denton-Giles et al., 2013). The presence of the pathogen would be expected to induce changes in the plant apoplast and affect the apoplastic proteome. To test this hypothesis, I compared the proteomic compositions of apoplastic fluids from mock-treated and infected susceptible *Camellia* 'Nicky Crisp' petals at 48 hpi.

Proteins were precipitated from 50 µL aliquots of apoplastic fluids using TCA precipitation. SDS-PAGE analysis of the resulting pellets showed that the infected petals contain significantly less protein than the mock-treated ones (Figure 5-1a): many protein bands were absent in the infected samples and the intensity of the remaining bands was lower.

To conduct a qualitative comparison between proteomes of mock-treated and infected petal apoplasts, proteins were extracted from 300 µL of apoplastic fluids (one uninfected and one infected sample) and analysed using LC-MS/MS. The previously predicted *Camellia* 'Nicky Crisp' proteome was used to detect plant proteins from the obtained mass spectrometry data (the proteome is described in Chapter 3). As a result, 164 plant proteins were identified in the mock-treated sample and 98 proteins in the infected one. The two samples shared 48 proteins in common (Figure 5-1b). All detected proteins were annotated using blastp search against the NCBI non-redundant protein database. The full list of detected proteins and their annotation is presented in Appendix C, Supplementary file 8. Based on the annotation results, plant proteins were assigned into functional groups. Counts of proteins in these groups further highlighted the differences between mock-treated and infected samples. The two count tables differed significantly ($P = 0.027$, according to a χ^2 independence test (Appendix A, Table A-5) suggesting that the

petal blight infection affects the proteomes of infected petals. The mock-treated sample had a higher proportion of enzymes associated with plant cell wall biosynthesis and modification, and of proteases compared to the infected sample. Relative numbers of oxidoreductases, pathogen-resistance and signalling proteins were higher in the infected sample. Remarkably, in the apoplastic fluids of the infected sample, two typically cytosolic proteins – ubiquitin and glyceraldehyde-3-phosphate dehydrogenase (GAPDH) – were detected. Diagrams that show the enzymes belonging to the described functional groups are presented in Appendix A (Figure A-1 and Figure A-2). In summary, SDS-PAGE and LC-MS/MS analyses showed that the petal apoplastic proteome of *Camellia* 'Nicky Crisp' undergoes dramatic changes during the susceptible interaction with *C. camelliae*.

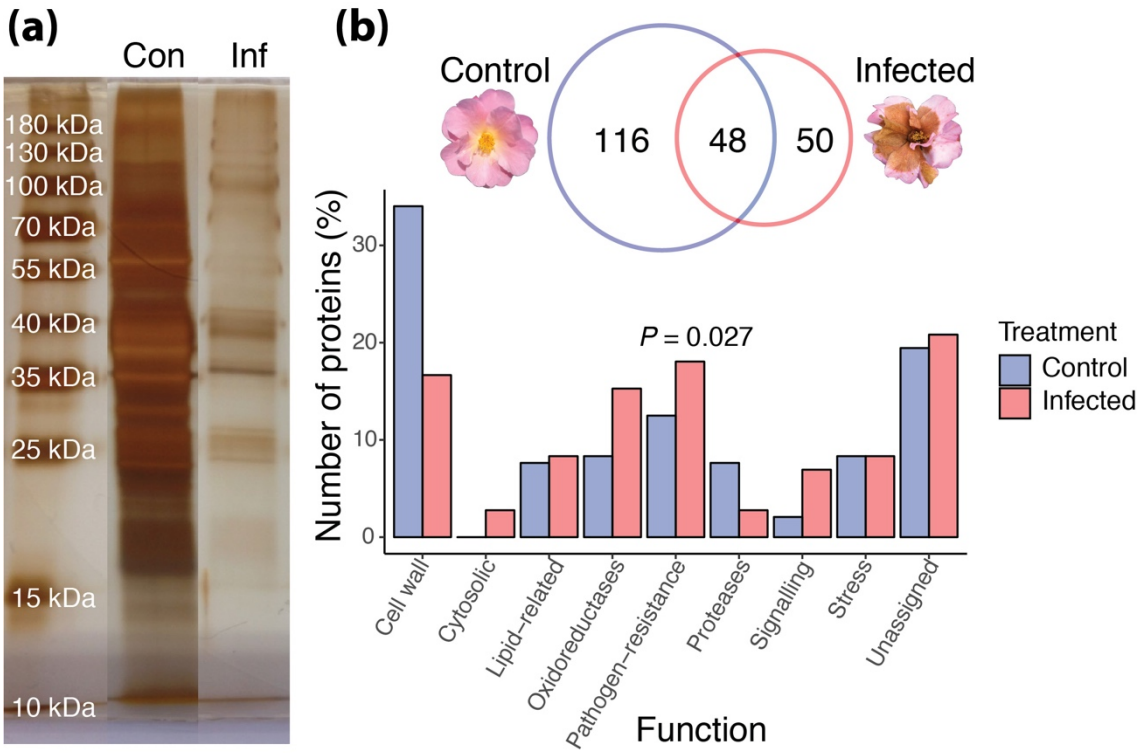

Figure 5-1 | Comparison of apoplastic proteomes of mock-treated and infected *Camellia* 'Nicky Crisp' petals.

(a) SDS-PAGE analysis of proteins extracted from 50 µL of mock-treated (Con) and infected (Inf) Camellia *'Nicky Crisp' petals at 48 hpi. Lanes show representatives of three biological replicates.*

(b) The Venn diagram shows the number of shared and unique proteins detected in apoplastic fluids of mock-treated (control) and infected petals. The bar plot shows the distribution of proteins across functional groups, with differences between petals in the relative amounts of proteins in the control and infected petals (χ^2 independence test, $P = 0.027$).

***C. camelliae* culture filtrate and apoplastic fluids of infected *Camellia* 'Nicky Crisp' petals contain *C. camelliae* proteins.** During the growth in petal apoplast, *C. camelliae* should produce proteins, which facilitate fungal growth and virulence. Indeed, the secreted fungal proteins were detected in apoplastic fluids of infected petals. *Ciborinia camelliae* proteins were identified in infected *Camellia* 'Nicky Crisp' petal apoplast, using a mass-spectrometry dataset reported in the previous section. As result, 55 fungal proteins were detected in intercellular space of infected petals. This set of proteins hereafter is called the *in planta* secretome.

The mycelial stage of the fungus, which grows in *Camellia* petals, can be cultivated in liquid culture. It was proposed that *C. camelliae* secretes proteins in a liquid culture as well as in petal apoplasts. SDS-PAGE analysis of *C. camellia* culture filtrate indicated that it contains proteins of the various molecular sizes (Figure 5-2a). To check their origin, 400 mL of the culture filtrate was used to extract proteins using the TCA method, and the resulting pellet was analysed using the LC-MS/MS method. In total, 94 fungal proteins were detected in the culture filtrate, using previously predicted fungal proteome (Denton-Giles, 2014), and annotated with blastp and NCBI non-redundant protein database. The obtained list of proteins from fungal culture filtrate hereafter called *in vitro* secretome.

The comparison of obtained datasets showed that *in vitro* and *in planta* secretomes share 25 fungal proteins, while 69 and 30 proteins were unique for the culture filtrate and plant apoplast, respectively (Figure 5-2b). Based on the annotation, all proteins were classified into five functional groups: CAZymes, hypersensitive response elicitors (HR-elicitors), oxidoreductases, proteases, and other proteins (full list of *in vitro* and *in planta* fungal secreted proteins is in the Appendix C, Supplementary file 8). The percentage of CAZymes was higher *in planta* than *in vitro*, while the culture filtrate contained more oxidoreductases and proteases. Surprisingly, HR-elicitors were detected only in the culture

filtrate. Although, numbers of proteins in functional groups did not differ significantly between *in vitro* and *in planta* secretomes ($P = 0.745$, according to a χ^2 independence test, Appendix A, Table A-6), suggesting that the observed differences are likely to be due to chance. To sum up, secreted *C. camelliae* proteins were detected in the fungal culture filtrate and infected petals apoplast, and these protein sets had similar functional distributions.

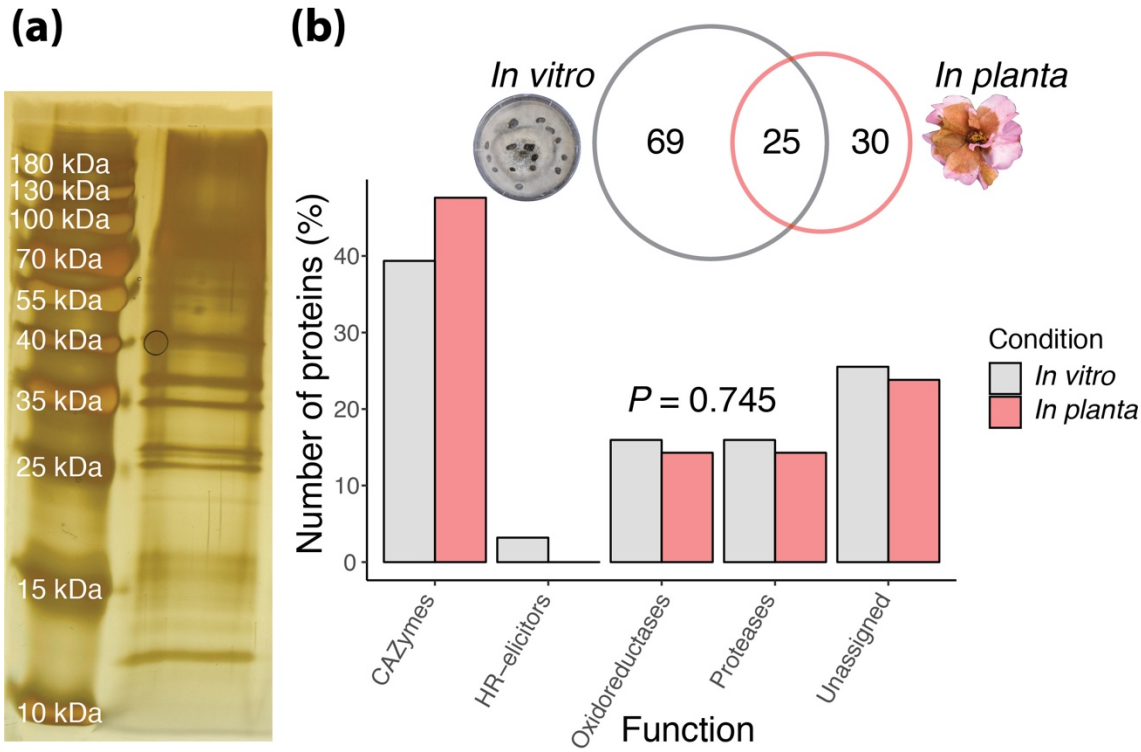

Figure 5-2 | Comparison of *C. camelliae in vitro* and *in planta* secretomes.

(a) SDS-PAGE analysis of proteins extracted from 500 µL of two-weeks-old C. camelliae *culture filtrate.*

(b) The Venn diagram shows the number of shared and unique proteins detected in the fungal culture filtrate (in vitro) and infected Camellia *'Nicky Crisp' apoplast (in planta) at 48 hpi. The bar plot shows the distribution of proteins into functional groups, and P value shows that the difference between protein counts in the groups does not vary substantially (χ^2 independence test, $P = 0.745$).*

***C. camelliae* culture filtrate and apoplastic fluids of infected *Camellia* 'Nicky Crisp' has necrogenic activity.** Secreted fungal proteins have numerous functions, including the induction of plant tissue necrosis. To test the effect of *C. camelliae* secreted proteins on plants, fungal culture filtrate and apoplastic fluids of infected petals were injected into *Camellia* petals and *N. benthamiana* leaves (Figure 5-3). Two-weeks-old sterile

PDB media and apoplastic fluids of mock-treated petals were used as control injections. Susceptible *Camellia* 'Nicky Crisp' petals demonstrated a rapid and strong response to the culture filtrate injection, showing visible browning within the first hour after infiltration. The response to the infected apoplastic fluids occurred later, at 20 hpi. Similarly, both culture filtrate and apoplastic fluids caused necrosis in petal blight-resistant *C. lutchuensis* petals and non-host *N. benthamiana* leaves, but none of the observed responses were as rapid and strong as a response of the *Camellia* 'Nicky Crisp' petals to the culture filtrate. No necrosis in petals or leaves was observed in response to the PDB-media or apoplastic fluids of mock-treated petals, suggesting that the necrosis-inducing agents were produced due to the fungal activity. Further experiments in this chapter were performed using fungal culture filtrate due to its availability and ability to produce bigger quantities of proteins.

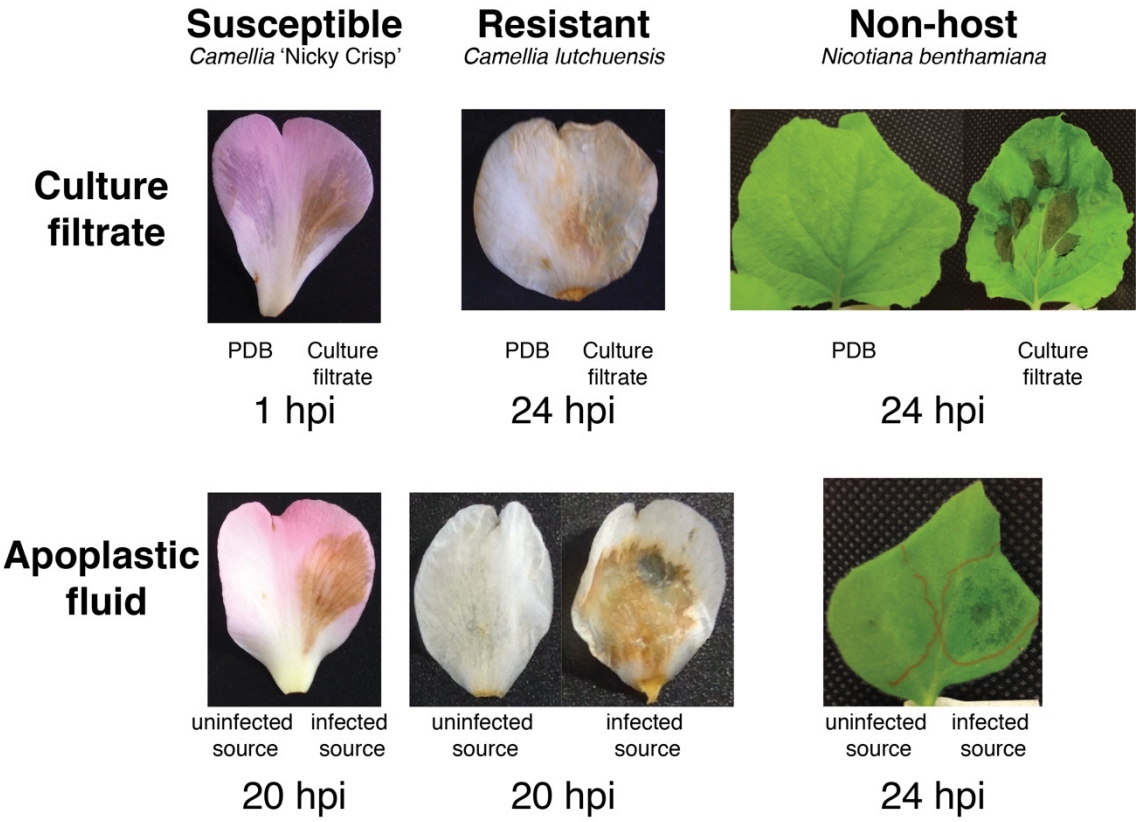

Figure 5-3 | Necrogenic activity of *C. camelliae* culture filtrate and apoplastic fluids of infected *Camellia* 'Nicky Crisp' petals.
Approximately 50-100 µL of tested liquid was infiltrated into petals and leaves. The first row shows the results for the culture filtrate injections, where sterile Potato Dextrose Broth (PDB) was used as a control. The second row shows the injection results of apoplastic fluids from infected Camellia *'Nicky Crisp' petals extracted at 48 hpi. Apoplastic fluids of mock-treated petals extracted at 48 hpi were used as a control.*

Hours under the photographs indicate the time which was required for the necrosis to develop. The photographs show the representatives of at least two biological replicates.

Necrogenic factors of *C. camelliae* culture filtrate are heat-sensitive proteins.

Secondary metabolites that fungi produce, as well as proteins, may be necrosis-inducing agents of *C. camelliae* culture filtrate. If necrogenic agent(s) of the culture filtrate are protein(s), the activity of the culture filtrate can be heat-sensitive and also be affected by proteinases. To test this, temperature and proteinase treatments of the culture filtrate were performed and the effects of these treatments on the necrosis-inducing activity were determined. While the treatment at 37°C slightly affected the activity of the culture filtrate (Figure 5-4, left parts of petals on the first row), delaying the development of the necrosis, the addition of proteinase K and incubation at the same temperature totally compromised the necrosis-inducing activity (Figure 5-4, right parts of petals on the first row). High-temperature treatments such as 50°C and 80°C also fully inactivated the culture filtrate (Figure 5-4, second and third rows). Taken together, these observations supported the suggestion that necrogenic agent(s) of *C. camelliae* culture filtrate are proteinaceous in nature.

Figure 5-4 | The effect of proteinase K and temperature treatment on the necrosis-inducing activity of *C. camelliae* culture filtrate.
Time course shows the time after injection. First row shows the effect of proteinase K treatment. Left parts of petals were infiltrated with the culture filtrate incubated at 37°C for 4 hours, right parts – with the culture filtrate with addition of proteinase K at the concentration 1 mg/mL. Second and third rows show the influence of the temperature treatment. Left halves of petals were infiltrated with untreated culture filtrate, right halves with the culture filtrate incubated at 50°C and 80°C for 4 hours. Photographs show representatives of three biological replicates.

Anion-exchange FPLC produces fractions of *C. camelliae* culture-filtrate which have necrogenic activity. The experiment described in the previous paragraph showed the presence of the necrogenic proteins in the culture filtrate. If this suggestion is true, liquid chromatography methods can be used to purify the proteins from the culture filtrate, and the resulting fractions would also have a necrosis-inducing activity. Anion-exchange chromatography was chosen as the first strategy for the fractionation of the culture filtrate: the method allows to bind and concentrate negatively-charged proteins form big volumes of the culture filtrate and subsequently separate them based on the strength of their charge.

Initially, 50 mL of the two-weeks-old culture filtrate was loaded onto the column, and 20 protein fractions were eluted with an increasing gradient of sodium chloride. The chromatogram had two distinctive peaks of absorbance at 280 nm (Figure 5-5a). Resulting fractions were back-dialyzed against sterile milliQ water to desalt and injected into *C. sasanqua* petals to test the necrosis-inducing activity. After 24 hours, fraction E6 corresponding to the first absorbance peak, and fractions E9 and E10 from the second absorbance peak demonstrated necrogenic activity (Figure 5-5a). No necrogenic activity was observed in other fractions, including the ones with compounds, which were not bound to the column.

To obtain new fractions with higher concentration of proteins, 100 mL of the culture filtrate was freeze-dried, diluted in 15 mL of the loading buffer and loaded onto the column. As previously, 20 fractions were eluted with an increasing sodium chloride gradient, and the absorbance was monitored at 280 nm. The resulting chromatogram had two distinctive peaks, but, unlike in the previous run, the first peak was higher than the second one (Figure 5-5b). The colour intensity of obtained fractions varied, and the fractions with the highest protein contents had distinctive yellow colour (Figure A-3 in Appendix A). Analysis of individual desalted fractions showed that necrogenic activity was found in fractions B3, B2, C2 and C3. Interestingly, these new injections induced necrosis within the first 5 hours of inoculation, which is likely to be due to the higher content of the necrogenic proteins in obtained fractions than in the previous run. No necrogenic activity was observed for the flow-through fractions that did not stay bound to the column medium at the lowest salt concentrations (e.g. Figure 5-5b, fractions A10 and A15). Elution times of the necrogenic fractions was similar to the previous run which validated both obtained results.

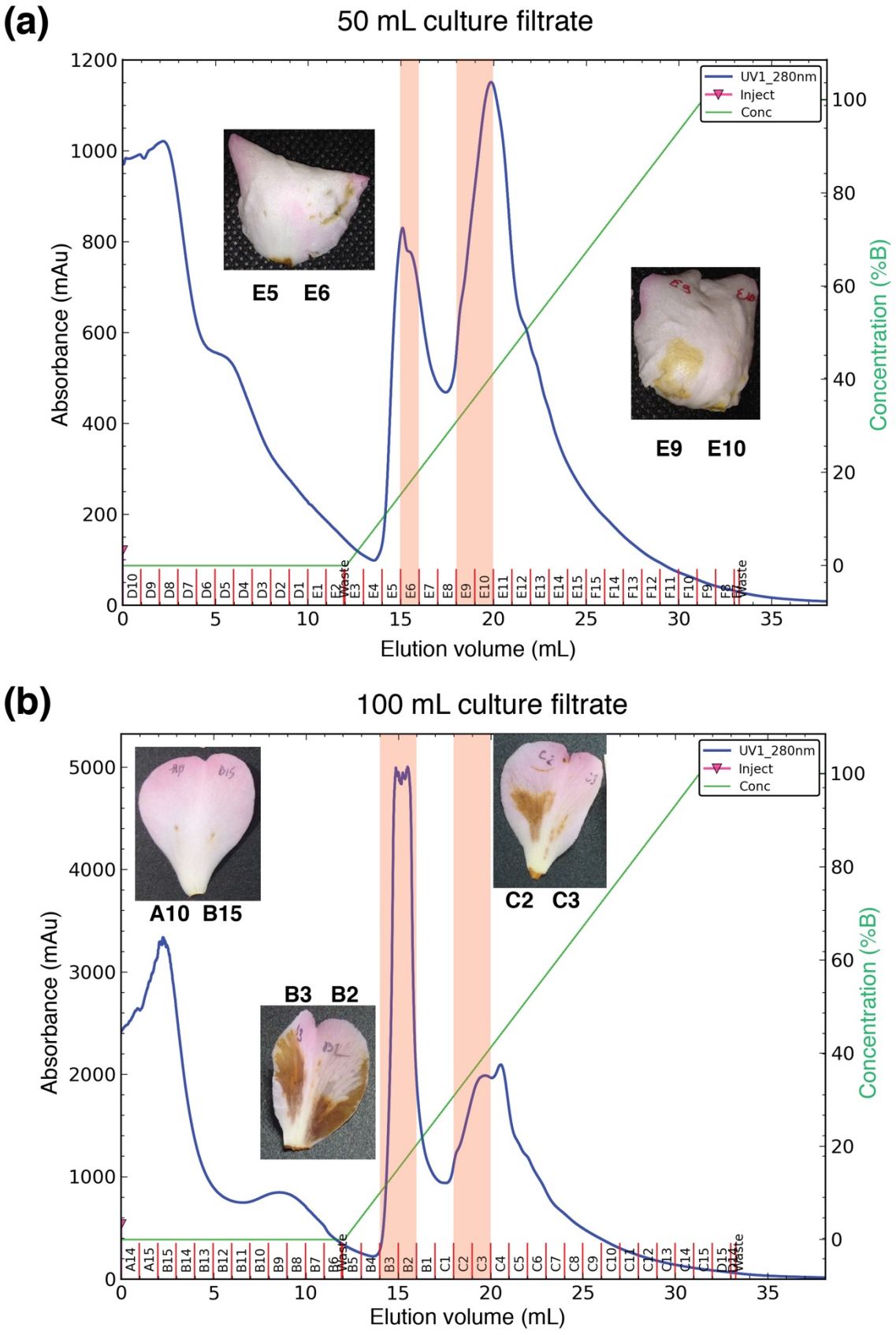

Figure 5-5 | Results of anion-exchange FPLC.
50 mL and 100 mL (freeze-dried and diluted in 15 mL) C. camellia *two-week-old culture filtrates were analysed with anion-exchange chromatography (graphs (a) and (b), respectively). The x-axis shows the*

elution volume, and y-axis – the absorbance at 280 nm. Highlighted areas of the plots show the fractions with necrosis-inducing activity, and pictures shows infiltrated Camellia sasanqua *(a) and* Camellia 'Nicky Crisp' *(b) petals at 24 hpi and 5 hpi, respectively. Labels show the fractions which were injected into the corresponding petal lobes. The activity of the fraction E10 in the picture (a) could not been fully demonstrated due to the curly shape of the petal and softening of the necrotic area which makes the petal handling challenging.*

Size-exclusion FPLC demonstrates that necrosis-inducing anion-exchange fractions contain multiple proteins and can be used to further purify necrosis-inducing proteins. To further purify the necrogenic proteins in the anion-exchange fractions, size-exclusion chromatography was used. The method separates proteins based on their molecular size. 0.5 mL aliquots of fractions B3 and B2 that were obtained from the anion-exchange chromatography of 100 mL of the culture filtrate were used for two separate experiments. In total, 25 fractions were collected while the absorbance was monitored at 280 nm. Both resulting chromatograms had more than one peak, which suggested that tested fractions may contain more than one protein (Figure 5-6). Due to the limited supply of petals at the end of *Camellia* flowering season, only the activity of fractions from B2 was tested. Necrogenic activity was observed for two fractions, A10 and A11, and did not correspond to the highest peak of the chromatogram. Moreover, the necrosis was visible on petals only at 48 hpi. To sum up, it was shown that size-exclusion chromatography approach can be used to further purify necrogenic proteins from the culture filtrate.

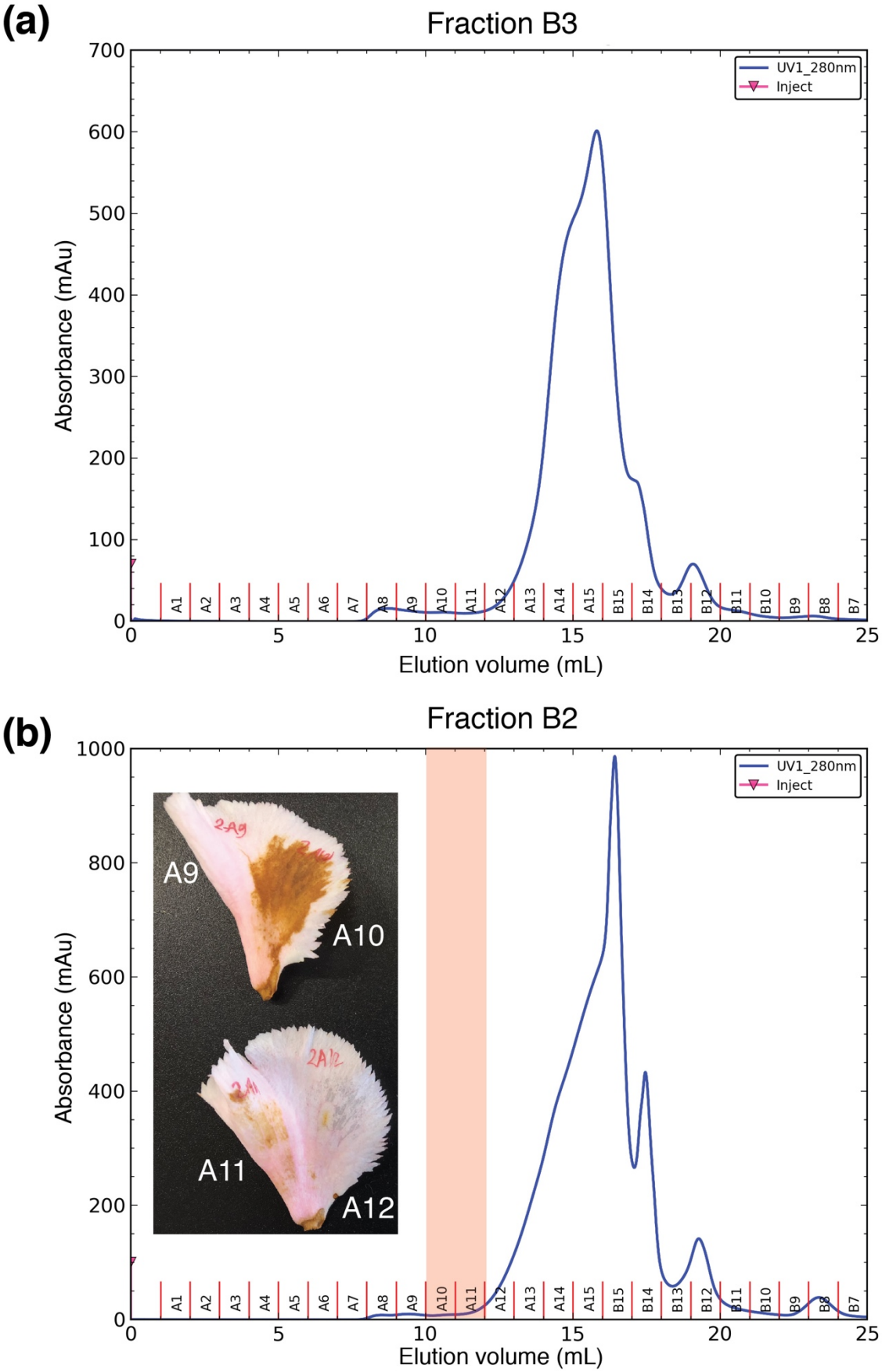

Figure 5-6 | Results of size-exclusion FPLC.

Two fractions obtained from anion-exchange chromatography of 100 mL of C. camelliae *culture filtrate, B3 and B2, were analysed using size-exclusion chromatography (graphs (a) and (b), respectively). The x-axis shows the elution volume, and y-axis – the absorbance at 280 nm. The necrosis-inducing activity was tested only for the fractions of B2 due to the end of the* Camellia *flowering season. Highlighted area of the plot shows the fractions with necrosis-inducing activity, and the picture shows infiltrated* Camellia japonica *petals at 48 hpi. Labels show the fractions which were injected into the corresponding petal lobes.*

5.3. Discussion

This chapter further characterises *Camellia* spp.-*C. camelliae* interaction using proteomic methods. Using the LC-MS/MS approach, together with *in silico* predicted plant and fungal proteomic datasets, allowed me to detect secreted *C. camelliae* and *Camellia* 'Nicky Crisp' proteins. The fungal proteins secreted *in vitro* and *in planta* demonstrated necrogenic activity, suggesting that they can contribute to the virulence of the pathogen.

Compared fungal and plant sets of detected proteins varied considerably: the observed differences in proteome compositions could be due to the effect of treatment as well as sampling bias and large variation between replicates, which are generally strong for LC-MS/MS-based proteomic analysis (Berg et al., 2010). Even if the sampling affects the detection of a particular protein, one may expect that obtained LC-MS/MS observations will reflect a true distribution of proteins among functional groups. In this case, the comparison of these distributions can be more reliable than the comparison on the level of individual proteins.

The functional distribution of plant apoplastic proteins was significantly affected by the petal blast infection. To the best of my knowledge, this is the first study showing a dramatic decrease in apoplastic protein content of plants infected with pathogens. It is unclear if it is the result of the proteolytic activity of fungal secretome (Jashni, Mehrabi, Collemare, Mesarich, & de Wit, 2015) or the decrease of plant protein production caused by the stress. In agreement with the necrotrophic nature of camellia petal blight disease, the infected petal apoplast had a higher percentage of various PR-proteins, including PR-1, which could facilitate the propagation of the pathogen-induced necrosis. For example, the necrotrophs *S. nodorum* and *P. nodorum* produce effectors, which specifically target plant PR-1 proteins and mediate necrosis in wheat (Breen, Williams, Winterberg, Kobe, & Solomon, 2016; S. Lu, Faris, Sherwood, Friesen, & Edwards, 2014). Moreover, the appearance of cytosolic ubiquitin and GAPDH in plant apoplast suggests that the petal blight causes

leakage of the cytoplasm – characteristic of the necrotrophic stage of the infection (Dickman & de Figueiredo, 2013).

Fungal secreted proteins were detected both in the infected petal apoplasts and culture filtrates. Interestingly, the functional distribution of proteins did not differ for *in planta* and *in vitro* fungal secretomes. As predicted with *in silico* approach by Matthew Denton-Giles (Denton-Giles, 2014), CAZymes had the highest abundance in both *in vitro* and *in planta* secretomes which reflects the necrotrophic nature of *C. camelliae* (Bellincampi, Cervone, & Lionetti, 2014). Homologs of three small necrosis-inducing proteins – cerato-platanin (Frías et al., 2011), NLP2 (Schouten et al., 2008), and 22kDa glycoprotein EC91 (UniProt A0A166VV93) – were detected only in the culture filtrate (sequence IDs au3244, au2222, au4906 in the Supplementary file 8, Appendix C, respectively). Whether these proteins were not produced *in planta* or could not have been detected in the apoplast due to the low concentration of fungal proteins remains unclear. *In vitro* and *in planta* secretomes had in common three fungal endopolygalacturonases (sequence IDs au4598, au9824, au774 in the Supplementary file 8, Appendix C) – homologs of important virulence factors of *B. cinerea*, which are recognized as invasion patterns by *A. thaliana* (Kars et al., 2005; L. Zhang et al., 2014).

The present work does not include quantitative aspects of proteomic analysis. The quantification of secreted proteins in culture filtrates and apoplastic washes could not have been performed with regular protein assays (e.g. Bio-Rad Protein Assay, Bio-Rad, USA) due to the low protein concentrations and small sample volumes obtained. LC-MS/MS can be used for quantitative comparisons, but the analysis must be performed with biological replicates to obtain reliable results. Analyses based on iTRAQ (isobaric tags for relative and absolute quantification) method, when proteins are labelled with sample-specific tags, can allow amounts of proteins to be determined from different samples in a single LC-MS/MS run, which would allow time-series screening of the resistant and susceptible interaction

events (Guo, Wang, Gu, Jin, & Yang, 2017; Zeng et al., 2017). However, the technique requires around 50 μg of protein per sample, so, in the case of *C. lutchuensis*, apoplastic washes from about 170 petals have to be extracted to produce just one biological replicate (estimation of protein content in *C. lutchuensis* apoplastic washes is shown in Appendix A, Table A-7 and Figure A-4).

The necrogenic activity of infected apoplastic fluids and fungal culture filtrate was demonstrated via the injections into plant tissues. Interestingly, necrotic responses were observed in all tested plants, which included highly susceptible *Camellia* 'Nicky Crisp', resistant *C. lutchuensis* and non-host *N. benthamiana*. Similarly, in the wheat-*Z. tritici* pathosystem, the culture filtrate of the pathogen-induced necrosis both in susceptible and resistant plant lines (Ben M'Barek et al., 2015). In contrast, only susceptible wheat cultivars demonstrated a necrosis-response to *S. nodorum* culture filtrate (Z. H. Liu et al., 2004). In the described experiment, *C. camelliae* culture filtrate and infected apoplastic washes had a necrotrophic *repertoire* of secreted proteins, which shares multiple conserved protein groups with broad-host *B. cinerea* and *S. sclerotiorum* (Denton-Giles, 2014). This may explain the observed effect on resistant and non-host plants. Thus, apparently, the early defence response strategy exploited by resistant *C. lutchuensis* (discussed in Chapter 3) averts the release of multiple CAZymes, which are still harmful to resistant plants. Another observation supporting this hypothesis was reported in an unpublished PowerPoint presentation by Jose Luis Couselo, University of Vigo, Spain: mycelial inoculum of *C. camelliae* was able to initiate necrotrophic fungal growth on resistant *C. lutchuensis* petals as well as on petals of non-host plants. Taken together, it suggests that the plant susceptibility and resistance to *C. camelliae* are likely to be defined by the interaction occurring at the early stages of the infection, during the initial biotrophy-like growth.

Small cysteine-rich effector proteins have a highly stable molecular structure and were shown to keep their necrogenic activity even after the exposure to high-temperatures

(Z. Liu et al., 2012). In contrast, the activity of CAZymes can be inhibited by heat-treatment: a secreted xyloglucanase of *B. cinerea*, BcXYG1, has a heat-sensitive tertiary structure, which is important for the induction of necrosis. (W. Zhu et al., 2017). Moreover, the plant recognition of polygalacturonases (L. Zhang et al., 2014) and xylanase 11A (Noda, Brito, & González, 2010) molecules of *B. cinerea* in their native conformation was required for full fungal virulence. Thus, according to observations made on *C. camelliae* culture filtrate, it is tempting to speculate that heat-sensitive CAZymes are its main necrogenic components. When it comes to the activity of infected apoplastic washes, their necrogenic activity could have been caused not only by fungal proteins but also by DAMPs that are released in the course of cell wall destruction (Benedetti et al., 2015).

Further investigation of fungal secretome components is essential to uncover the virulence mechanisms of *C. camelliae*. Recombinant proteins, which can be produced in *E. coli* or *P. pastoris*, may have altered, non-native protein structures; the usage of additional molecular tags, which help to detect and purify target proteins, can also affect the activity of tagged proteins (Denton-Giles, 2014). FPLC was used as a method to identify necrogenic proteinaceous components of culture filtrates which are naturally produced by pathogens (Ben M'Barek et al., 2015; Friesen, Meinhardt, & Faris, 2007; Z. H. Liu et al., 2004). Indeed, the fractions obtained from anion-exchange chromatography had necrogenic activity similarly to the original fungal culture filtrate. The presence of the activity in two distinct peaks suggested that the culture filtrate is likely to contain more than one necrogenic protein. The activity of anion-exchange fractions was increased using higher amounts of the initial culture filtrate possibly due to the concentration-dependent manner of the necrogenic activity. As suggested by the elution times of necrogenic size-exclusion fractions, necrosis-inducing proteins of *C. camelliae* culture filtrate a more likely to be high-molecular weight proteins or protein complexes than SSPs. That supports the hypothesis that CAZymes may have been the main contributors to the necrosis-inducing

activity of the culture filtrate. The activity of size-exclusion fractions – resulting from the second step of purification – dropped significantly and was observed only after 48 hpi; in comparison, the activity of the initial culture filtrate was visible at 1 hpi. This could be caused by the decreased protein concentration of size-exclusion fractions or inactivation of proteins associated with multiple purification and dialysis steps. The first problem can be addressed using a second anion-exchange step instead of the size-exclusion purification, which would further increase the concentration of target proteins (Ben M'Barek et al., 2015), or using an ultrafiltration approach to concentrate proteins from size-exclusion fractions. Protein inactivation might be minimized if FPLC is performed in low-temperature conditions. It should be noted that the high activity of the original culture filtrate can be facilitated by functional complexes of fungal secreted proteins (Badhan, 2016). The separation steps performed in high-salt solutions will inevitably lead to the dissociation of native complexes and, as result, may decrease the necrogenic activity.

The seasonal character of *Camellia* flowering is another challenge for this project to address. In order to compare necrogenic activities of different components from *C. camelliae* secretome, experiments should be conducted on one *Camellia* species or hybrid. Alternatively, leaves of *N. benthamiana* may be routinely used for necrogenic-activity testing, although, this approach is not applicable for the detection of *Camellia*-specific fungal virulence factors.

Overall, the results presented in this chapter further verify the necrotrophic nature of the petal blight disease. *Ciborinia camelliae* produces a range of proteins contributing to the virulence of the fungus. As shown with the transcriptomic approach, a successful resistance strategy of *Camellia* plants is likely to stop fungal growth before it reaches the necrotrophic phase of the infection and releases multiple necrosis-inducing CAZymes. In the later stages of the infection, activation of apoplastic immunity may only facilitate the propagation of the pathogen in the petal tissues.

Chapter 6. General discussion, conclusions and future plans

Camellia petal blight disease is not considered as a direct threat to food security or natural environment of affected countries. Nevertheless, it gives us an example of how plant fungal diseases can rapidly spread and become a global-scale problem that can only be addressed by collective efforts of scientists and plant breeders.

Petal blight resistance as an early defence activation. The present study originates from the PhD project of Matthew Denton-Giles, which demonstrated the magnitude of natural petal blight resistance variation within the genus *Camellia* (Denton-Giles, 2014). To understand molecular mechanisms behind the resistance, defence responses of *C. lutchuensis* – the most resistant species tested – were analysed in the current study using transcriptomic and network analysis approaches. The study allowed me to overview the dynamics of the defence response which showed the strong and early upregulation of multiple plant genes. The main molecular pathways involved in the resistance appeared to be *WRKY33-MPK3* pathway, oxylipin and JA, and phenylpropanoid biosynthesis pathways. Same pathways were shown to be involved in the late stages of the susceptible interaction, likely contributing to the tissue necrosis. Overall, this result has a considerable impact for current plant disease management strategies: the timing of the treatment should be taken into consideration to maximize the effectivity of it. Thus, it can be recommended that the future petal blight control methods should target the fungus on the early asymptomatic stages of the infection – a strategy utilized by resistant *Camellia* plants in nature.

While the breeding of new resistant *Camellia* hybrids is a long-term objective, the present study suggests a way to protect existing susceptible *Camellia* cultivars. The highest activity of *WRKY33-MPK3* pathway in *Camellia* 'Nicky Crisp' petals was observed after the combined treatment with MeJA and ascospores (Figure 3-7). Therefore, it may be possible that the hormone can be used together with elicitor compounds, such as chitosan (El Hadrami, Adam, El Hadrami, & Daayf, 2010).

Unfortunately, the current study does not provide an answer to the question what the main triggers of the early defence activation in *C. lutchuensis* are. First of all, the suggested interaction model should be expanded further by including other *Camellia* cultivars with intermediate levels of the resistance. Two candidate cultivars for this analysis are *C. sinensis* var. *assamica* and *C. sinensis* var. *sinensis*. According to previous research results (Denton-Giles, 2014), *C. sinensis* var. *assamica* was more resistant to petal blight than *C. sinensis* var. *sinensis*. Genomes of both plants have been sequenced and published (*C. sinensis* var. *assamica* (Xia et al., 2017), *C. sinensis* var. *sinensis* (Wei et al., 2018)), which makes it possible to conduct effective comparative genomic and transcriptomic studies using these two cultivars. The first question to address can be whether the more resistant *C. sinensis* var. *assamica* would demonstrate stronger and earlier upregulation of resistance hub-genes, such as *WRKY33* and *MPK3*, than *C. sinensis* var. *sinensis*. Ultimately, comparative genomic analyses between these two cultivars may result in detection of quantitative trait loci associated with petal-blight resistance, which can be used as markers for *Camellia* breeding (Palanga et al., 2017; Yang, Islam, et al., 2018; Yang, Sood, Luo, Todd, & Wang, 2018).

Conclusions

- Resistance to *C. camelliae* is a complex process requiring rapid and simultaneous activation of multiple defence pathways.
- Jasmonate biosynthesis, *WRKY33-MPK3*, and the phenylpropanoid pathways are key regulators of the *Camellia* spp.-*C. camelliae* interaction.
- Early activation of *Camellia* defence pathways leads to resistance, while the late activation contributes to susceptibility.

Future directions

- Test the effectivity of combined MeJA and fungal elicitor treatments on *Camellia* plants in laboratory and field conditions.
- Test the early defence model on *C. sinensis* cultivars with intermediate levels of resistance.
- Screen *C. sinensis* populations for resistance-associated quantitative trait loci.

Practical applications: disease prevention using early defence response activation

- Susceptible *Camellia* flowers can be primed against the blight using a combined treatment with MeJA and fungal elicitors.
- Extending the genomic and transcriptomic studies on *C. sinensis* cultivars may lead to the discovery of genetic markers for petal blight resistance breeding.

Phenylpropanoid metabolites as fungistatic agents of the early defence.

Observed dynamics of phenylpropanoid biosynthesis in *C. lutchuensis* petals further highlighted the importance of the first hours of the *Camellia* spp.-*C. camelliae* interaction for successful induction of resistance. The concentrations of the three compounds were elevated early during the resistance response – p-coumaric, ferulic and sinapic acids. These compounds demonstrated different levels of fungistatic activity against *C. camelliae* if the treatment was applied within the first 12 hours after the infection with fungal ascospores. It should be further checked whether the susceptible *Camellia* petals sampled at different stages of the blight infection would have lower concentrations of phenolic acids than resistant plants. The importance of the pathway's contribution to the petal blight resistance can be further estimated using the inhibitors of the phenylpropanoid enzymes, which hypothetically should increase the susceptibility of *C. lutchuensis* to *C. camelliae* (A. M. P. Jones, Chattopadhyay, Shukla, Zoń, & Saxena, 2012; Schalk et al., 1998).

The present study analysed only a small fraction of plant metabolites. Activation of the phenylpropanoid pathway may result in the increased biosynthesis of other known and yet undiscovered antimicrobial plant compounds (e.g. stilbenes, coumarins, phytoalexins (Piasecka, Jedrzejczak-Rey, & Bednarek, 2015), diferulates (Piotrowski et al., 2015)). Another crucial aspect to investigate can be a spatial distribution of the pathway activity. Both transcriptomic and metabolomic analysis required 10-15 whole petals of *C. lutchuensis* for one biological replicate, thus, obtained results represent an averaged picture of the phenylpropanoid pathway activity. However, microscopic analysis of the resistance response demonstrated that many plant defence events, including ROS accumulation and cell death, are localized around the germinating ascospores of *C. camelliae* (Denton-Giles et al., 2013). Thus, hypothetically, *C. lutchuensis* petals also can accumulate phenylpropanoid compounds specifically around the attempted fungal penetration zones, so the local concentrations of phenolic acids would quickly reach the levels that are toxic for nascent *C.*

camelliae hyphae. There is a precedent for localized activity of the phenylpropanoid pathway: the cell-type-specific transcriptomic analysis of *Picea glauca* bark tissue showed that the epithelial cells of cortical resin ducts displayed a higher transcriptional activity of core phenylpropanoid genes than phloem or cortex cells (Celedon et al., 2017).

The mechanisms of action of how phenolic compounds provide fungistatic properties are yet to be discovered. Microscopic analysis of lesion development in treated and untreated infected petals may help to identify the stages of *C. camelliae* development which are the most susceptible to the treatment. Comparative transcriptomics may help to identify *C. camelliae* genes whose expression is affected by phenylpropanoids. *In silico* target prediction tools, which search for binding sites of small molecules in protein databases, also can be used to find the enzymes which are interacting with phenolic acids (Byrne & Schneider, 2019). Unfortunately, as for now, many of these methods offer a prediction of human target proteins by default (Figure 6-1). An alternative approach would be to test the toxicity of phenolic acids on *Saccharomyces cerevisiae* deletion mutants, which would allow us to find genes conferring the resistance or susceptibility of yeasts to these compounds (C. H. Ho et al., 2011; Piotrowski et al., 2015). Consequently, enzymes of *C. camelliae* homologous to yeast targets of phenolic acids would be tested as candidate-targets of phenylpropanoids. Thus, regardless of the chosen strategy, the first step in target screening would be to improve the annotation of *C. camelliae* proteins in order to find the orthology relationships with proteins of model organisms, including the proteins from Protein Data Bank (PDB, www.rcsb.org) that have resolved 3D structures.

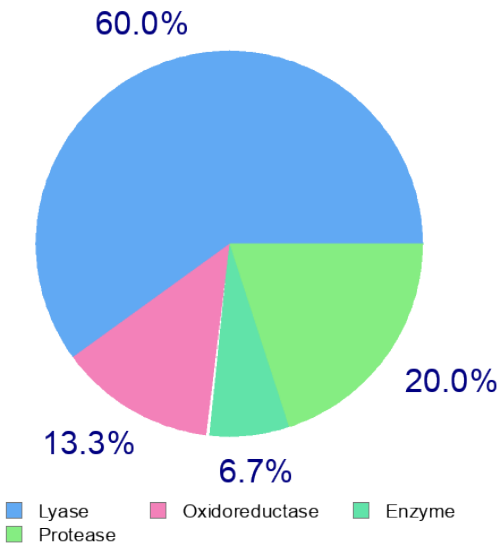

Figure 6-1 | Distribution of top 15 human targets of ferulic acid by enzyme classes as predicted by SwissTarget (Gfeller, Michielin, & Zoete, 2013)**.**
The result shows that the majority of predicted targets of ferulic acids are lyases.

Even without full knowledge about the activity of phenolic compounds, they already can be tested as natural antifungal compounds to inhibit the development of petal blight pathogen, especially during the early biotrophic phase of the infection. Two strategies of the delivery can be suggested for further testing. The first one is the formation of a layer of phenolic acids in terpene- or wax-based polymers on the surface of petals, to stop the attempted fungal entry. The alternative would be to use surfactants to facilitate deeper penetration of phenolic acids into petal tissues. Combination of various adjuvants and surfactants should be tested to ensure the safety of the treatment for *Camellia* petals.

Conclusion

- Phenylpropanoid pathway contributes to petal blight resistance via the rapid accumulation of phenolic acids with antifungal activity, such as ferulic and p-coumaric acids.

Future directions

- Observe the temporal dynamics of phenylpropanoid compounds concentration in *Camellia* 'Nicky Crisp' during the susceptible interaction with *C. camelliae*.
- Further verify the importance of the pathway for resistance by using various inhibitors of phenylpropanoid production, which may decrease the resistance in *C. lutchuensis*.
- Detect *C .camelliae* genes whose expression is affected by phenylpropanoid compounds.
- Perform *in silico* prediction of *C. camelliae* targets of phenolic acids.
- Check the toxicity of phenolic acids for various *S. cerevisiae* deletion mutant strains.
- Design and test antifungal treatments that use phenolic acids in combination with various delivery agents such as surfactants or terpene polymers.

Practical application: protecting the best flowers for *Camellia* shows

- Phenolic acids can be used as natural blight-protection agents to spray flowers before and during flower shows and contests.
- The efficiency of the treatment can be improved using various delivery methods which can enhance the penetration of compounds and make sprays rain-proof.

Unravelling the earliest steps of *Camellia* spp.-*C. camelliae* interaction.

Transcriptomic and proteomic databases of two *Camellia* plants and *C. camelliae* were generated and used in this study (the fungal proteome was predicted in the previous project (Denton-Giles, 2014)). Overall, the obtained results of qRT-PCR experiments and LC-MS/MS protein analyses verified the quality of assembled transcriptomes and predicted proteomes. These datasets can be used to pursue the studies on the earliest steps of *Camellia* spp.-*C. camelliae* interaction.

Multiple fungal CAZymes, detected in *C. camelliae* culture filtrate and apoplastic fluids of infected petals, are candidate factors that may cause necrosis in host and non-host plants. Further purification of these proteins using FPLC will make it possible to perform the functional tests on their activity, and also find the targets of these proteins in plant cells (Frías et al., 2014; L. Zhang et al., 2014). It has been shown for BcXYG1 xyloglucanase of *B. cinerea*, that this CAZyme promotes cell death, which is mediated by host-plant BAK1 and SOBIR1 receptor-like kinases. In this study, I demonstrated that both *BAK1* and *SOBIR1* are upregulated at 24 hpi during the susceptible interaction, which is very likely to facilitate the propagation of necrosis caused by fungal CAZymes in *Camellia* 'Nicky Crisp' petals. Remarkably, the resistant plant quickly downregulates the activity of *BAK1* and *SOBIR1* genes after an initial rapid response at 6 hpi, which possibly minimizes the necrogenic effect of secreted CAZymes in *C. lutchuensis* petals. The effect of *C. camelliae* culture filtrate injection on *BAK1* and *SOBIR1* gene expression should be tested in *Camellia* 'Nicky Crisp', *C. lutchuensis* and *N. benthamiana* to further our understanding of the role that these plant genes play in compatible and incompatible interactions.

According to the results of this study, I hypothesize that the early *C. camelliae* secretome might contain effectors suppressing immune responses in the susceptible plants. Thus, it can be recommended to continue study on fungal proteins, which are secreted within the first 12 hours after the germination of ascospores. The study can use the

comparative transcriptomic screening of fungal genes upregulated at the earliest steps during compatible and incompatible interactions (Bradshaw et al., 2016). The list of genes upregulated at 6 hpi during the incompatible interaction with *C. camelliae*, was obtained in this work and may be used for the future screening of effectors (e.g. polygalacturonases, SSPs) (Appendix C, Supplementary file 9). It also has been shown in the previous study that some tested *C. camelliae* SSPs have increased expression at 6 hpi (Denton-Giles, 2014). In contrast to the orthologous single-copy SSPs of *B. cinerea* and *S. sclerotiorum*, no necrogenic activity was shown for the tested SSPs of *C camelliae*, leaving the question about the functional activity of this protein family open. Thus, it may be hypothesised that they are the immune-suppressors, inhibiting early defence responses of the susceptible plants without causing any visible necrosis upon injection in petals.

The second approach to study the early fungal secretome would be to conduct a mass-spectrometric analysis of the proteins secreted by germinating ascospores. For example, previously, the early secretome of *B. cinerea* was extracted from liquid media with a high concentration of germinating fungal conidia (7×10^6 conidia/mL). The germination was induced with the addition of host-plant extracts enclosed in a dialysis bag (Espino et al., 2010). Although, when it comes to *C. camelliae*, this approach would require a high number of ascospores isolated in sterile conditions, which can be challenging to achieve using apothecia collected in nature.

Once proteins of interest are found, a fast and convenient system is required to test their activity. The seasonal character of *Camellia* flowering creates challenges for activity testing, so the establishment of a new testing system which uses model plants is necessary for the quick screening of multiple *C. camelliae* effector-candidates. For example, SsSSPs and CcSSPs were produced in *N. benthamiana* using *Agrobacterium* infiltration assay (McCarthy, 2019). The same technique can be used to test the activity of other proteins detected in the culture filtrate or in the early fungal secretome. Moreover, this approach

will allow us to detect not only necrogenic proteins but also *C. camelliae* immune suppressors. Coinfiltration of candidate immune suppressors with INF1 elicitin or Avr3a+R3a proteins from *Phytophthora infestans* – triggers of PTI or ETI respectively – will help to identify *C. camelliae* proteins inhibiting plant defence responses during the earliest steps of *Camellia* spp.-*C. camelliae* interaction (Q. Wang et al., 2011). Moreover, this approach can further allow us to detect *Camellia* targets of fungal necrotrophy effectors. For example, target proteins of *C. camelliae* effectors can be predicted from plant proteomes or an apoplastic subset detected in this study using *in silico* methods based on machine-learning or homology-based analysis of protein sequences (Basit, Abbasi, Asif, Gull, & Minhas, 2018; Eid, ElHefnawi, & Heath, 2016; Nourani, Khunjush, & Durmuş, 2015). A resulting list of probable plant targets can be used for coinfiltration tests with corresponding *C. camelliae* effectors. Hypothetically, coexpression of a *Camellia* susceptibility receptor and an interacting fungal effector will lead to necrosis in transformed *N. benthamiana* (Domazakis et al., 2017). A flowchart summarizing this suggested screening strategy is shown in Figure 6-2.

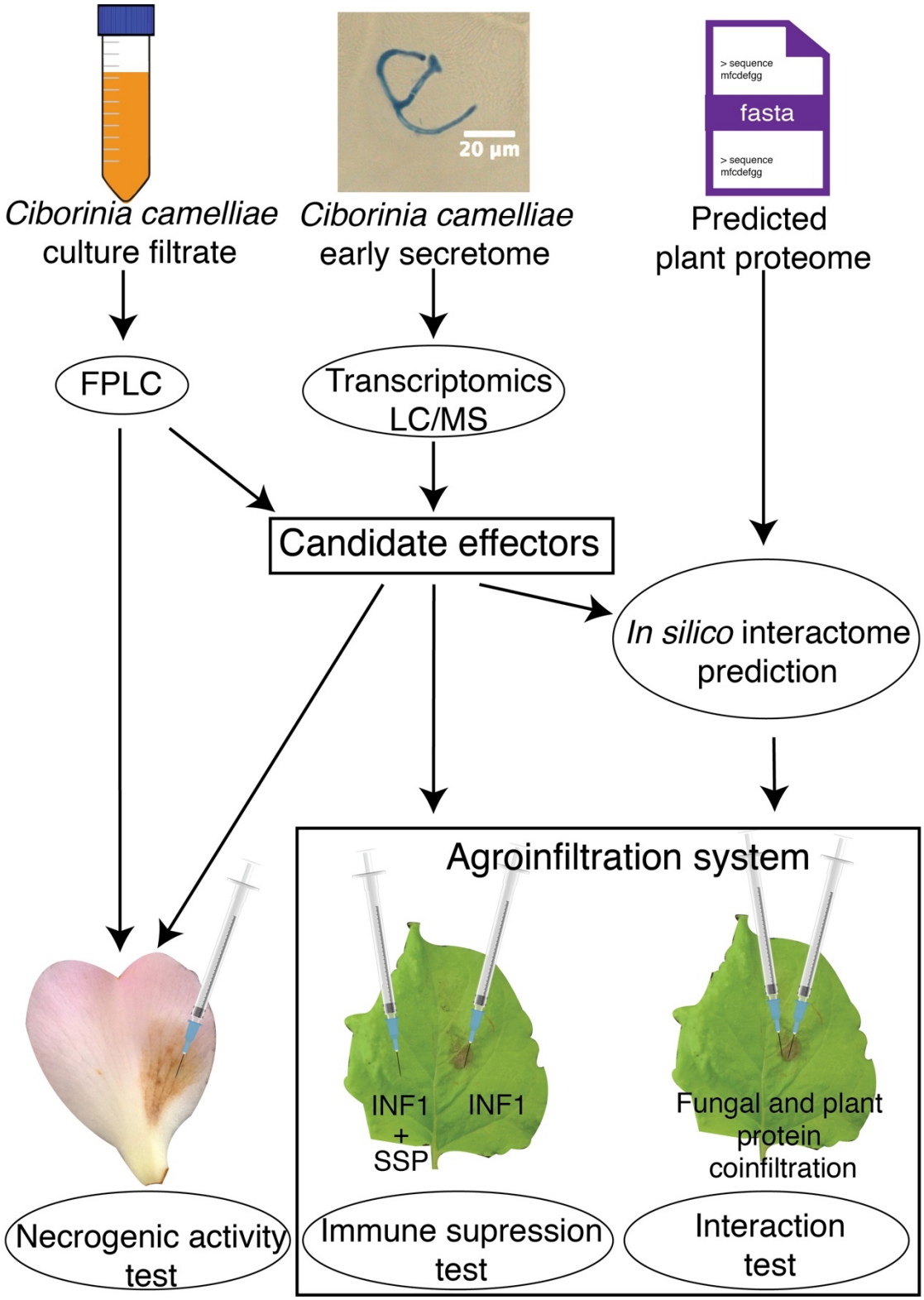

Figure 6-2 | Effector-screening strategy for *C. camelliae*.
The figure represents a possible plan for the detection of protein virulence factors of C. camelliae. *A list of candidate effector proteins can be generated using data from studies on the culture filtrate, and also analysis of the early secretome of* C. camelliae. *Candidate proteins from the list can be tested for the necrogenic activity in* Camellia *petals or immune suppression activity in* N. benthamiana *using agroinfiltration assays. Additionally, in silico analysis can predict plant proteins that are targets of* C. camelliae *secreted proteins, and the interaction can be verified using agroinfiltarion assays.*

Conclusion

- *In vivo* and *in vitro* secretomes of *C. camelliae*, studied in this work, included a *repertoire* of necrotrophic fungal secreted proteins and their necrogenic activity was demonstrated in plants which are susceptible and resistant to *Camellia* petal blight.

Future directions

- Find plant genes involved in responses to *C. camelliae* culture filtrate in resistant and susceptible *Camellia* petals (e.g. *BAK1*, *SOBIR1*).
- Study the early secretome of *C. camelliae* using transcriptomic or proteomic approaches.
- Screen the activity of candidate effectors and immune suppressors in *N. benthamiana* using agroinfiltration assays.

Practical application: susceptibility markers of *Camellia* cultivars

- Comparative analysis of responses, which are triggered in various *Camellia* cultivars by *C. camelliae* secreted proteins, may lead to the detection of petal blight resistance/susceptibility markers.

References

Abdollahi Mandoulakani, B., Eyvazpour, E., & Ghadimzadeh, M. (2017). The effect of drought stress on the expression of key genes involved in the biosynthesis of phenylpropanoids and essential oil components in basil (*Ocimum basilicum* L.). *Phytochemistry*, *139*, 1–7.

Ahn, E., Kumar, P., Mukha, D., Tzur, A., & Shlomi, T. (2017). Temporal fluxomics reveals oscillations in TCA cycle flux throughout the mammalian cell cycle. *Molecular Systems Biology*, *13*, 953.

Altschul, S. F., Gish, W., Miller, W., Myers, E. W., & Lipman, D. J. (1990). Basic local alignment search tool. *Journal of Molecular Biology*, *215*, 403–410.

Ashburner, M., Ball, C. A., Blake, J. A., Botstein, D., Butler, H., Cherry, M. J., … Sherlock, G. (2000). Gene Ontology: tool for the unification of biology. *Nature Genetics*, *25*, 25–29.

Asselbergh, B., Curvers, K., Franc, S. C., Audenaert, K., Vuylsteke, M., Van Bresegem, F., & Höfte, M. (2007). Resistance to *Botrytis cinerea* in *sitiens*, an abscisic acid-deficient tomato mutant, involves timely production of hydrogen peroxide and cell wall modifications in the epidermis. *Plant Physiology*, *144*, 1863–1877.

Badhan, A. (2016). Blue Native PAGE in combination with Mass Spectrometry as an effective tool to study multi-enzyme complex 's in secretome of aerobic fungus. *Annals of Chromatography and Separation Techniques*, *2*, 1019.

Bakker, E. G., Toomajian, C., Kreitman, M., & Bergelson, J. (2006). A genome-wide survey of R gene polymorphisms in Arabidopsis. *The Plant Cell*, *18*, 1803–1818.

Basit, A. H., Abbasi, W. A., Asif, A., Gull, S., & Minhas, F. U. A. A. (2018). Training host-pathogen protein-protein interaction predictors. *Journal of Bioinformatics and Computational Biology*, *16*, 1850014.

Beckers, G. J. M., Jaskiewicz, M., Liu, Y., Underwood, W. R., He, S. Y., Zhang, S., & Conrath, U. (2009). Mitogen-activated protein kinases 3 and 6 are required for full priming of stress responses in *Arabidopsis thaliana*. *The Plant Cell*, *21*, 944–953.

Bellincampi, D., Cervone, F., & Lionetti, V. (2014). Plant cell wall dynamics and wall-related susceptibility in plant-pathogen interactions. *Frontiers in Plant Science*, *5*, 228.

Ben M'Barek, S., Cordewener, J. H. G., Tabib Ghaffary, S. M., van der Lee, T. A. J., Liu, Z., Mirzadi Gohari, A., … Kema, G. H. J. (2015). FPLC and liquid-chromatography mass spectrometry identify candidate necrosis-inducing proteins from culture filtrates of the fungal wheat pathogen *Zymoseptoria tritici*. *Fungal Genetics and Biology*, *79*, 54–62.

Benedetti, M., Pontiggia, D., Raggi, S., Cheng, Z., Scaloni, F., Ferrari, S., … De Lorenzo, G. (2015). Plant immunity triggered by engineered in vivo release of

oligogalacturonides, damage-associated molecular patterns. *Proceedings of the National Academy of Sciences*, *112*, 5533–5538.

Berg, J. M., Tabb, D. L., Tymoczko, J. L., Vega-Montoto, L., Stryer, L., Rudnick, P. A., … Spiegelman, C. (2010). Repeatability and reproducibility in proteomic identifications by liquid chromatography−tandem mass spectrometry. *Journal of Proteome Research*, *9*, 761–776.

Betsuyaku, S., Katou, S., Takebayashi, Y., Sakakibara, H., Nomura, N., & Fukuda, H. (2018). Salicylic acid and jasmonic acid pathways are activated in spatially different domains around the infection site during effector-triggered immunity in *Arabidopsis thaliana*. *Plant & Cell Physiology*, *59*, 8–16.

Billon-Grand, G., Rascle, C., Droux, M., Rollins, J. A., & Poussereau, N. (2012). pH modulation differs during sunflower cotyledon colonization by the two closely related necrotrophic fungi *Botrytis cinerea* and *Sclerotinia sclerotiorum*. *Molecular Plant Pathology*, *13*, 568–578.

Biologie, D. De, Fribourg, U. De, & Gockel, R. a. (1998). Salicylic acid and systemic acquired resistance to pathogen attack. *Annals of Botany*, *82*, 535–540.

Birkenbihl, R. P., Diezel, C., & Somssich, I. E. (2012). Arabidopsis WRKY33 is a key transcriptional regulator of hormonal and metabolic responses toward *Botrytis cinerea* infection. *Plant Physiology*, *159*, 266–285.

Borges, A., Ferreira, C., Saavedra, M. J., & Simoes, M. (2013). Antibacterial activity and mode of action of ferulic and gallic acids against pathogenic bacteria. *Microbial Drug Resistance (Larchmont, N.Y.)*, *19*, 256–265.

Bradshaw, R. E., Guo, Y., Sim, A. D., Kabir, M. S., Chettri, P., Ozturk, I. K., … Cox, M. P. (2016). Genome-wide gene expression dynamics of the fungal pathogen *Dothistroma septosporum* throughout its infection cycle of the gymnosperm host *Pinus radiata*. *Molecular Plant Pathology*, *17*, 210–224.

Breen, S., Williams, S. J., Winterberg, B., Kobe, B., & Solomon, P. S. (2016). Wheat PR-1 proteins are targeted by necrotrophic pathogen effector proteins. *Plant Journal*, *88*, 13–25.

Byrne, R., & Schneider, G. (2019). *In silico* target prediction for small molecules. In S. Ziegler & H. Waldmann (Eds.), *Systems Chemical Biology: Methods and Protocols* (pp. 273–309). New York, NY: Springer New York.

Canturk, Z. (2018). Evaluation of synergistic anticandidal and apoptotic effects of ferulic acid and caspofungin against *Candida albicans*. *Journal of Food and Drug Analysis*, *26*, 439–443.

Celedon, J. M., Yuen, M. M. S., Chiang, A., Henderson, H., Reid, K. E., & Bohlmann, J. (2017). Cell-type- and tissue-specific transcriptomes of the white spruce (*Picea glauca*) bark unmask fine-scale spatial patterns of constitutive and induced conifer defense. *Plant Journal*, *92*, 710–726.

Cessna, S. G., Sears, V. E., Dickman, M. B., & Low, P. S. (2000). Oxalic acid, a pathogenicity factor for *Sclerotinia sclerotiorum*, suppresses the oxidative burst of the

host plant. *The Plant Cell*, *12*, 2191–2199.

Chanda, B., Xia, Y., Mandal, M. K., Yu, K., Sekine, K., Gao, Q., … Kachroo, P. (2011). Glycerol-3-phosphate is a critical mobile inducer of systemic immunity in plants. *Nature Genetics*, *43*, 421–427.

Chaudhari, P., Ahmed, B., Joly, D. L., & Germain, H. (2014). Effector biology during biotrophic invasion of plant cells. *Virulence*, *5*, 1–7.

Cheah, H.-L., Lim, V., & Sandai, D. (2014). Inhibitors of the glyoxylate cycle enzyme ICL1 in *Candida albicans* for potential use as antifungal agents. *PLOS ONE*, *9*, e95951.

Chezem, W. R., Memon, A., Li, F.-S., Weng, J.-K., & Clay, N. K. (2017). SG2-type R2R3-MYB transcription factor MYB15 controls defense-induced lignification and basal immunity in Arabidopsis. *The Plant Cell*, *29*, 1907–1926.

Choi, Y. E., Lee, C., & Goodwin, S. B. (2016). Generation of reactive oxygen species via NOXa is important for development and pathogenicity of *Mycosphaerella graminicola*. *Mycobiology*, *44*, 38–47.

Choquer, M., Fournier, E., Kunz, C., Levis, C., Pradier, J. M., Simon, A., & Viaud, M. (2007). *Botrytis cinerea* virulence factors: New insights into a necrotrophic and polyphageous pathogen. *FEMS Microbiology Letters*, *277*, 1–10.

Chowdhury, S., Basu, A., & Kundu, S. (2017). Biotrophy-necrotrophy switch in pathogen evoke differential response in resistant and susceptible sesame involving multiple signaling pathways at different phases. *Scientific Reports*, *7*, 17251.

Ciuffetti, L. M., Manning, V. A., Pandelova, I., Betts, M. F., & Martinez, J. P. (2010). Host-selective toxins, Ptr ToxA and Ptr ToxB, as necrotrophic effectors in the *Pyrenophora tritici-repentis*-wheat interaction. *New Phytologist*, *187*, 911–919.

Coll, N. S., Epple, P., & Dangl, J. L. (2011). Programmed cell death in the plant immune system. *Cell Death & Differentiation*, *18*, 1247–1256.

Conesa, A., Gotz, S., Garcia-Gomez, J. M., Terol, J., Talon, M., & Robles, M. (2005). Blast2GO: A universal tool for annotation, visualization and analysis in functional genomics research. *Bioinformatics*, *21*, 3674–3676.

Cook, D. E., Mesarich, C. H., & Thomma, B. P. H. J. (2015). Understanding plant immunity as a surveillance system to detect invasion. *Annual Review of Phytopathology*, *53*, 541–563.

Cox, M. P., Peterson, D. A., & Biggs, P. J. (2010). SolexaQA: At-a-glance quality assessment of Illumina second-generation sequencing data. *BMC Bioinformatics*, *11*, 485.

Csárdi, G., & Nepusz, T. (2006). The igraph software package for complex network research. *InterJournal Complex Systems*. https://doi.org/citeulike-article-id:3443126

Cui, H., Tsuda, K., & Parker, J. E. (2015). Effector-Triggered Immunity: from pathogen perception to robust defense. *Annu. Rev. Plant Biol*, *66*, 487–511.

Cuperlovic-Culf, M., Rajagopalan, N., Tulpan, D., & Loewen, M. C. (2016). Metabolomics and cheminformatics analysis of antifungal function of plant metabolites. *Metabolites*, *6*, e31.

Dangl, J., & Jones, J. (2001). Plant pathogens and integrated defence responses to infection. *Nature*, *411*, 826–833.

De Cremer, K., Mathys, J., Vos, C., Froenicke, L., Michelmore, R. W., Cammue, B. P. A., & De Coninck, B. (2013). RNAseq-based transcriptome analysis of *Lactuca sativa* infected by the fungal necrotroph *Botrytis cinerea*. *Plant, Cell and Environment*, *36*, 1992–2007.

Dean, R., Van Kan, J. a L., Pretorius, Z. a., Hammond-Kosack, K. E., Di Pietro, A., Spanu, P. D., … Foster, G. D. (2012). The Top 10 fungal pathogens in molecular plant pathology. *Molecular Plant Pathology*, *13*, 414–430.

Delaunois, B., Jeandet, P., Clement, C., Baillieul, F., Dorey, S., & Cordelier, S. (2014). Uncovering plant-pathogen crosstalk through apoplastic proteomic studies. *Frontiers in Plant Science*, *5*, 1–18.

Demkura, P. V., & Ballaré, C. L. (2012). UVR8 mediates UV-B-induced arabidopsis defense responses against *Botrytis cinerea* by controlling sinapate accumulation. *Molecular Plant*, *5*, 642–652.

Denoux, C., Galletti, R., Mammarella, N., Gopalan, S., Werck, D., De Lorenzo, G., … Dewdney, J. (2008). Activation of defense response pathways by OGs and Flg22 elicitors in Arabidopsis seedlings. *Molecular Plant*, *1*, 423–445.

Denton-Giles, M. (2014). *Characterization of incompatible and compatible Camellia - Ciborinia camelliae plant-pathogen interactions*. Massey University, Palmerston North, New Zealand.

Denton-Giles, M., Bradshaw, R. E., & Dijkwel, P. P. (2013). *Ciborinia camelliae* (Sclerotiniaceae) induces variable plant resistance responses in selected species of *Camellia*. *Phytopathology*, *103*, 725–732.

Dickman, M. B., & de Figueiredo, P. (2013). Death be not proud-cell death control in plant fungal interactions. *PLoS Pathogens*, *9*, 1–4.

Domazakis, E., Lin, X., Aguilera-Galvez, C., Wouters, D., Bijsterbosch, G., Wolters, P. J., & Vleeshouwers, V. G. A. A. (2017). Effectoromics-based identification of cell surface receptors in potato. In L. Shan & P. He (Eds.), *Plant Pattern Recognition Receptors* (Vol. 1578, pp. 337–353). New York, NY, United States: Humana Press.

Eid, F.-E., ElHefnawi, M., & Heath, L. S. (2016). DeNovo: virus-host sequence-based protein-protein interaction prediction. *Bioinformatics (Oxford, England)*, *32*, 1144–1150.

El Hadrami, A., Adam, L. R., El Hadrami, I., & Daayf, F. (2010). Chitosan in plant protection. *Marine Drugs*, *8*, 968–987.

Espino, J. J., Gutiérrez-Sánchez, G., Brito, N., Shah, P., Orlando, R., & González, C. (2010). The *Botrytis cinerea* early secretome. *Proteomics*, *10*, 3020–3034.

Fan, Z., Li, J., Li, X., Wu, B., Wang, J., Liu, Z., & Yin, H. (2015). Genome-wide

transcriptome profiling provides insights into floral bud development of summer-flowering *Camellia azalea*. *Scientific Reports*, *5*, 9729.

Ferrari, S., Plotnikova, J. M., De Lorenzo, G., & Ausubel, F. M. (2003). Arabidopsis local resistance to *Botrytis cinerea* involves salicylic acid and camalexin and requires EDS4 and PAD2, but not SID2, EDS5 or PAD4. *Plant Journal*, *35*, 193–205.

Flor, H. H. (1971). Current status of the Gene-For-Gene concept. *Annual Review of Phytopathology*, *9*, 275–296.

Fraser, C. M., & Chapple, C. (2012). The phenylpropanoid pathway in Arabidopsis. *The Arabidopsis Book*. https://doi.org/10.1199/tab.0152

Fraser, K., Lane, G. A., Otter, D. E., Hemar, Y., Quek, S. Y., Harrison, S. J., & Rasmussen, S. (2013). Analysis of metabolic markers of tea origin by UHPLC and high resolution mass spectrometry. *Food Research International*, *53*, 827–835.

Frías, M., Brito, N., González, M., & González, C. (2014). The phytotoxic activity of the cerato-platanin BcSpl1 resides in a two-peptide motif on the protein surface. *Molecular Plant Pathology*, *15*, 342–351.

Frías, M., González, C., & Brito, N. (2011). BcSpl1, a cerato-platanin family protein, contributes to *Botrytis cinerea* virulence and elicits the hypersensitive response in the host. *New Phytologist*, *192*, 483–495.

Friesen, T. L., Meinhardt, S. W., & Faris, J. D. (2007). The *Stagonospora nodorum*-wheat pathosystem involves multiple proteinaceous host-selective toxins and corresponding host sensitivity genes that interact in an inverse gene-for-gene manner. *Plant Journal*, *51*, 681–692.

Friesen, T. L., Stukenbrock, E. H., Liu, Z., Meinhardt, S., Ling, H., Faris, J. D., … Oliver, R. P. (2006). Emergence of a new disease as a result of interspecific virulence gene transfer. *Nature Genetics*, *38*, 953–956.

Fu, Z. Q., & Dong, X. (2013). Systemic acquired resistance: turning local infection into global defense. *Annual Review of Plant Biology*, *64*, 839–863.

Gfeller, D., Michielin, O., & Zoete, V. (2013). Shaping the interaction landscape of bioactive molecules. *Bioinformatics*, *29*, 3073–3079.

Gilbert, B. M., & Wolpert, T. J. (2013). Characterization of the LOV1-mediated, victorin-induced, cell-death response with virus-induced gene silencing. *Molecular Plant-Microbe Interactions : MPMI*, *26*, 903–917.

Glazebrook, J. (2005). Contrasting mechanisms of defense against biotrophic and necrotrophic pathogens. *Annual Review of Phytopathology*, *43*, 205–227.

Gori, A., Guidi, L., Fini, A., Brunetti, C., Ferrini, F., Loreto, F., … Tattini, M. (2015). Isoprenoids and phenylpropanoids are part of the antioxidant defense orchestrated daily by drought-stressed *Platanus* × *acerifolia* plants during Mediterranean summers. *New Phytologist*, *207*, 613–626.

Guo, L., Wang, P., Gu, Z., Jin, X., & Yang, R. (2017). Proteomic analysis of broccoli

sprouts by iTRAQ in response to jasmonic acid. *Journal of Plant Physiology*, *218*, 16–25.

Gururani, M. A., Venkatesh, J., Upadhyaya, C. P., Nookaraju, A., Pandey, S. K., & Park, S. W. (2012). Plant disease resistance genes: Current status and future directions. *Physiological and Molecular Plant Pathology*, *78*, 51–65.

Guyon, K., Balagué, C., Roby, D., & Raffaele, S. (2014). Secretome analysis reveals effector candidates associated with broad host range necrotrophy in the fungal plant pathogen *Sclerotinia sclerotiorum*. *BMC Genomics*, *15*, 336.

Haas, B. J., Papanicolaou, A., Yassour, M., Grabherr, M., Blood, P. D., Bowden, J., … Regev, A. (2013). *De novo* transcript sequence reconstruction from RNA-seq using the Trinity platform for reference generation and analysis. *Nature Protocols*, *8*, 1494–1512.

Han, G. Z. (2017). Evolution of jasmonate biosynthesis and signalling mechanisms. *Journal of Experimental Botany*, *68*, 1323–1331.

Hansen, H. N., & Thomas, H. E. (1940). Flower blight of camellias. *Phytopathology*, *30*, 166–170.

Hao, X., Horvath, D. P., Chao, W. S., Yang, Y., Wang, X., & Xiao, B. (2014). Identification and evaluation of reliable reference genes for quantitative real-time PCR analysis in tea plant (*Camellia sinensis* (L.) O. Kuntze). *International Journal of Molecular Sciences*, *15*, 22155–22172.

Hao, Y., Wang, T., Wang, K., Wang, X., Fu, Y., Huang, L., & Kang, Z. (2016). Transcriptome analysis provides insights into the mechanisms underlying wheat plant resistance to stripe rust at the adult plant stage. *PLoS ONE*, *11*, 1–21.

Hara, K. (1919). A sclerotial disease of camellia (*Camellia japonica*). *Dainippon Sanrin Kaiho*, *436*, 29–31.

Heise, A., Liedgens, H., Hahlbrock, K., Bednarek, P., Ciolkowski, I., Schmelzer, E., … Nu, T. (2003). Non-self recognition, transcriptional reprogramming, and secondary metabolite accumulation during plant/pathogen interactions. *Proceedings of the National Academy of Sciences of the United States of America*, *100*, 14569–14576.

Heller, A., & Witt-Geiges, T. (2013). Oxalic acid has an additional, detoxifying function in Sclerotinia sclerotiorum pathogenesis. *PLoS ONE*, *8*, e72292.

Hemaiswarya, S., & Doble, M. (2010). Synergistic interaction of phenylpropanoids with antibiotics against bacteria. *Journal of Medical Microbiology*, *59*, 1469–1476.

Ho, C.-L., Wu, Y., Shen, H., Provart, N. J., & Geisler, M. (2012). A predicted protein interactome for rice. *Rice*, *5*, 15.

Ho, C. H., Piotrowski, J., Dixon, S. J., Baryshnikova, A., Costanzo, M., & Boone, C. (2011). Combining functional genomics and chemical biology to identify targets of bioactive compounds. *Current Opinion in Chemical Biology*, *15*, 66–78.

Holl, J., Vannozzi, A., Czemmel, S., D'Onofrio, C., Walker, A. R., Rausch, T., … Bogs, J. (2013). The R2R3-MYB transcription factors MYB14 and MYB15 regulate stilbene biosynthesis in *Vitis vinifera*. *The Plant Cell*, *25*, 4135–4149.

Huang, H., Tong, Y., Zhang, Q. J., & Gao, L. Z. (2013). Genome size variation among and within *Camellia* species by using flow cytometric analysis. *PLoS ONE*, *8*, e64981.

Huang, H., Yao, Q., Xia, E., & Gao, L. (2018). Metabolomics and transcriptomics analyses reveal nitrogen influences on the accumulation of flavonoids and amino acids in young shoots of tea plant (*Camellia sinensis* L.) associated with tea flavor. *Journal of Agricultural and Food Chemistry*, *66*, 9828–9838.

Hunter, J. D. (2007). Matplotlib: A 2D graphics environment. *Computing In Science & Engineering*, *9*, 90–95.

Huot, B., Yao, J., Montgomery, B. L., & He, S. Y. (2014). Growth-defense tradeoffs in plants: A balancing act to optimize fitness. *Molecular Plant*, *7*, 1267–1287.

Jashni, M. K., Mehrabi, R., Collemare, J., Mesarich, C. H., & de Wit, P. J. G. M. (2015). The battle in the apoplast: further insights into the roles of proteases and their inhibitors in plant–pathogen interactions. *Frontiers in Plant Science*, *6*, 1–7.

Jaskiewicz, M., Conrath, U., & Peterhänsel, C. (2011). Chromatin modification acts as a memory for systemic acquired resistance in the plant stress response. *EMBO Reports*, *12*, 50–55.

Jayaswall, K., Mahajan, P., Singh, G., Parmar, R., Seth, R., Raina, A., … Sharma, R. K. (2016). Transcriptome analysis reveals candidate genes involved in blister blight defense in tea (*Camellia sinensis* (L) Kuntze). *Scientific Reports*, *6*, 30412.

Ji, H.-G., Lee, Y.-R., Lee, M.-S., Hwang, K. H., Park, C. Y., Kim, E.-H., … Hong, Y.-S. (2018). Diverse metabolite variations in tea (*Camellia sinensis* L.) leaves grown under various shade conditions revisited: a metabolomics study. *Journal of Agricultural and Food Chemistry*, *66*, 1889–1897.

Jia, Y., McAdams, S. A., Bryan, G. T., Hershey, H. P., & Valent, B. (2000). Direct interaction of resistance gene and avirulence gene products confers rice blast resistance. *The EMBO Journal*, *19*, 4004–4014.

Jones, A. M. P., Chattopadhyay, A., Shukla, M., Zoń, J., & Saxena, P. K. (2012). Inhibition of phenylpropanoid biosynthesis increases cell wall digestibility, protoplast isolation, and facilitates sustained cell division in American elm (*Ulmus americana*). *BMC Plant Biology*, *12*, 75.

Jones, J. D. G., & Dangl, J. L. (2006). The plant immune system. *Nature*, *444*, 323–329.

Juge, N. (2006). Plant protein inhibitors of cell wall degrading enzymes. *Trends in Plant Science*, *11*, 359–367.

Kabbage, M., Yarden, O., & Dickman, M. B. (2015). Pathogenic attributes of *Sclerotinia sclerotiorum*: Switching from a biotrophic to necrotrophic lifestyle. *Plant Science*, *233*, 53–60.

Kars, I., Krooshof, G. H., Wagemakers, L., Joosten, R., Benen, J. A. E., & Van Kan, J. A. L. (2005). Necrotizing activity of five *Botrytis cinerea* endopolygalacturonases produced in *Pichia pastoris*. *Plant Journal*, *43*, 213–225.

Katagiri, F., & Tsuda, K. (2010). Understanding the plant immune system. *Molecular Plant-Microbe Interactions*, *23*, 1531–1536.

Kim, H., Chen, C., Kabbage, M., & Dickman, M. B. (2011). Identification and characterization of *Sclerotinia sclerotiorum* NADPH oxidases. *Applied and Environmental Microbiology*, *77*, 7721–7729.

Kim, K. S., Min, J.-Y., & Dickman, M. B. (2008). Oxalic acid is an elicitor of plant programmed cell death during *Sclerotinia sclerotiorum* disease development. *Molecular Plant-Microbe Interactions : MPMI*, *21*, 605–612.

Kim, M. G., Da Cunha, L., McFall, A. J., Belkhadir, Y., DebRoy, S., Dangl, J. L., & Mackey, D. (2005). Two *Pseudomonas syringae* type III effectors inhibit RIN4-regulated basal defense in *Arabidopsis*. *Cell*, *121*, 749–759.

Koeck, M., Hardham, A. R., & Dodds, P. N. (2011). The role of effectors of biotrophic and hemibiotrophic fungi in infection. *Cellular Microbiology*, Vol. 13, pp. 1849–1857.

Kohn, L. M., & Nagasawa, E. (1984). A taxonomic reassessment of *Sclerotinia camelliae* Hara (=*Ciborinia camelliae* Kohn), with observations on flower blight in Japan. *Transactions of the Mycological Society of Japan*, *25*, 149–161.

König, S., Feussner, K., Kaever, A., Landesfeind, M., Thurow, C., Karlovsky, P., … Feussner, I. (2014). Soluble phenylpropanoids are involved in the defense response of Arabidopsis against *Verticillium longisporum*. *New Phytologist*, *202*, 823–837.

Kubicek, C. P., Starr, T. L., & Glass, N. L. (2014). Plant cell wall–degrading enzymes and their secretion in plant-pathogenic fungi. *Annual Review of Phytopathology*, *52*, 427–451.

Kumar, M., Brar, A., Yadav, M., Chawade, A., Vivekanand, V., & Pareek, N. (2018). Chitinases—potential candidates for enhanced plant resistance towards fungal pathogens. *Agriculture*, *8*, 88.

Langmead, B., & Salzberg, S. L. (2012). Fast gapped-read alignment with Bowtie 2. *Nat Methods*, *9*, 357–359.

Leaf, D. E., Siew, E. D., Eisenga, M. F., Singh, K., Mc Causland, F. R., Srivastava, A., … Waikar, S. S. (2018). Fibroblast growth factor 23 associates with death in critically ill patients. *Clinical Journal of the American Society of Nephrology*, *13*, 531–541.

Lee, J.-E., Lee, B.-J., Chung, J.-O., Hwang, J.-A., Lee, S.-J., Lee, C.-H., & Hong, Y.-S. (2010). Geographical and climatic dependencies of green tea (*Camellia sinensis*) metabolites: A ^{1}H NMR-based metabolomics study. *Journal of Agricultural and Food Chemistry*, *58*, 10582–10589.

Lee, J.-E., Lee, B.-J., Chung, J.-O., Kim, H.-N., Kim, E.-H., Jung, S., … Hong, Y.-S. (2015). Metabolomic unveiling of a diverse range of green tea (*Camellia sinensis*) metabolites dependent on geography. *Food Chemistry*, *174*, 452–459.

Lehmann, S., Serrano, M., L'Haridon, F., Tjamos, S. E., & Metraux, J. P. (2015). Reactive oxygen species and plant resistance to fungal pathogens. *Phytochemistry*, *112*, 54–62.

Leupold, S., Hubmann, G., Litsios, A., Meinema, A. C., Takhaveev, V., Papagiannakis,

A., … Heinemann, M. (2018). *Saccharomyces cerevisiae* goes through distinct metabolic phases during its replicative lifespan. *ELife*, *8*, e41046.

Li, S., & Liu, X. (2011). Cold-pressed oil extraction of camellia seeds. *ICAE 2011 Proceedings: 2011 International Conference on New Technology of Agricultural Engineering*, 135–138.

Li, W., & Godzik, A. (2006). Cd-hit: A fast program for clustering and comparing large sets of protein or nucleotide sequences. *Bioinformatics*, *22*, 1658–1659.

Li, X., Zhang, Y., Huang, L., Ouyang, Z., Hong, Y., Zhang, H., … Song, F. (2014). Tomato SlMKK2 and SlMKK4 contribute to disease resistance against *Botrytis cinerea*. *BMC Plant Biology*, *14*, 1–17.

Liang, X., Liberti, D., Li, M., Kim, Y. T., Hutchens, A., Wilson, R., & Rollins, J. A. (2015). Oxaloacetate acetylhydrolase gene mutants of *Sclerotinia sclerotiorum* do not accumulate oxalic acid, but do produce limited lesions on host plants. *Molecular Plant Pathology*, *16*, 559–571.

Liebrand, T. W. H., van den Burg, H. A., & Joosten, M. H. A. J. (2014). Two for all: Receptor-associated kinases SOBIR1 and BAK1. *Trends in Plant Science*, *19*, 123–132.

Liu, Z. H., Faris, J. D., Meinhardt, S. W., Ali, S., Rasmussen, J. B., & Friesen, T. L. (2004). Genetic and physical mapping of a gene conditioning sensitivity in wheat to a partially purified host-selective toxin produced by *Stagonospora nodorum*. *Phytopathology*, *94*, 1056–1060.

Liu, Z., Zhang, Z., Faris, J. D., Oliver, R. P., Syme, R., McDonald, M. C., … Friesen, T. L. (2012). The cysteine rich necrotrophic effector SnTox1 produced by *Stagonospora nodorum* triggers susceptibility of wheat lines harboring Snn1. *PLoS Pathogens*, *8*, e1002467.

Lo Presti, L., Lanver, D., Schweizer, G., Tanaka, S., Liang, L., Tollot, M., … Kahmann, R. (2015). Fungal effectors and plant susceptibility. *Annual Review of Plant Biology*, *66*, 513–545.

Lorang, J. M., Carkaci-Salli, N., & Wolpert, T. J. (2004). Identification and characterization of victorin sensitivity in *Arabidopsis thaliana*. *Molecular Plant-Microbe Interactions : MPMI*, *17*, 577–582.

Love, M. I., Anders, S., & Huber, W. (2014). Differential analysis of count data - the DESeq2 package. In *Genome Biology*. https://doi.org/110.1186/s13059-014-0550-8

Lu, H., Zhang, J., Yang, Y., Yang, X., Xu, B., Yang, W., … Wu, N. (2016). Earliest tea as evidence for one branch of the Silk Road across the Tibetan Plateau. *Scientific Reports*, *6*, 18955.

Lu, S., Faris, J. D., Sherwood, R., Friesen, T. L., & Edwards, M. C. (2014). A dimeric PR-1-type pathogenesis-related protein interacts with ToxA and potentially mediates ToxA-induced necrosis in sensitive wheat. *Molecular Plant Pathology*, *15*, 650–663.

Luengo Escobar, A., Magnum de Oliveira Silva, F., Acevedo, P., Nunes-Nesi, A., Alberdi, M., & Reyes-Díaz, M. (2017). Different levels of UV-B resistance in *Vaccinium*

corymbosum cultivars reveal distinct backgrounds of phenylpropanoid metabolites. *Plant Physiology and Biochemistry*, *118*, 541–550.

Ma, L., He, J., Liu, H., & Zhou, H. (2018). The phenylpropanoid pathway affects apple fruit resistance to *Botrytis cinerea*. *Journal of Phytopathology*, *166*, 206–215.

Maere, S., Heymans, K., & Kuiper, M. (2005). BiNGO: A Cytoscape plugin to assess overrepresentation of Gene Ontology categories in Biological Networks. *Bioinformatics*, *21*, 3448–3449.

Malinovsky, F. G., Fangel, J. U., & Willats, W. G. T. (2014). The role of the cell wall in plant immunity. *Frontiers in Plant Science*, Vol. 5, p. 178.

Manela, N., Oliva, M., Ovadia, R., Sikron-Persi, N., Ayenew, B., Fait, A., … Oren-Shamir, M. (2015). Phenylalanine and tyrosine levels are rate-limiting factors in production of health promoting metabolites in *Vitis vinifera* cv. *Gamay Red* cell suspension. *Frontiers in Plant Science*, *6*, 1–13.

Mao, G., Meng, X., Liu, Y., Zheng, Z., Chen, Z., & Zhang, S. (2011). Phosphorylation of a WRKY transcription factor by two pathogen-responsive MAPKs drives phytoalexin biosynthesis in Arabidopsis. *The Plant Cell*, *23*, 1639–1653.

Martin, M. (2011). Cutadapt removes adapter sequences from high-throughput sequencing reads. *EMBnet.Journal*, *17*, 10–12.

Mbengue, M., Navaud, O., Peyraud, R., Barascud, M., Badet, T., Vincent, R., … Raffaele, S. (2016). Emerging trends in molecular interactions between plants and the broad host range fungal pathogens *Botrytis cinerea* and *Sclerotinia sclerotiorum*. *Frontiers in Plant Science*, *7*, 422.

McCarthy, H. M. (2019). *Characterisation of the cell death-inducing activity of the conserved family of Ciborinia camelliae-like small secreted proteins (CCL-SSPs) of C. camelliae, Botrytis cinerea and Sclerotinia sclerotiorum*. Massey University, Palmerston North, New Zealand.

Mendgen, K., & Hahn, M. (2002). Plant infection and the establishment of fungal biotrophy. *Trends in Plant Science*, Vol. 7, pp. 352–356.

Mendiburu, F., & Simon, R. (2015). Agricolae -Ten years of an open source statistical tool for experiments in breeding, agriculture and biology. *PeerJ PrePrints*. https://doi.org/10.7287/peerj.preprints.1404v1

Mengiste, T. (2012). Plant immunity to necrotrophs. *Annual Review of Phytopathology*, *50*, 267–294.

Miedes, E., Vanholme, R., Boerjan, W., & Molina, A. (2014). The role of the secondary cell wall in plant resistance to pathogens. *Frontiers in Plant Science*, *5*, 1–13.

Minz-Dub, A., Bowler, K., Savidor, A., Zhu, W., Gur, Y., Braus, G. H., … Sharon, A. (2017). BcXYG1, a secreted xyloglucanase from *Botrytis cinerea*, triggers both cell death and plant immune responses. *Plant Physiology*, *175*, 438–456.

Mondal, T. K. (2011). Camellia. In C. Kole (Ed.), Wild Crop Relatives: Genomic and Breeding Resources (pp. 15–39). Berlin, Germany: Springer.

Münch, S., Lingner, U., Floss, D. S., Ludwig, N., Sauer, N., & Deising, H. B. (2008). The hemibiotrophic lifestyle of *Colletotrichum species*. *Journal of Plant Physiology*, *165*, 41–51.

Musungu, B., Bhatnagar, D., Brown, R. L., Fakhoury, A. M., & Geisler, M. (2015). A predicted protein interactome identifies conserved global networks and disease resistance subnetworks in maize. *Frontiers in Genetics*, *6*, 201.

Noda, J., Brito, N., & González, C. (2010). The *Botrytis cinerea* xylanase Xyn11A contributes to virulence with its necrotizing activity, not with its catalytic activity. *BMC Plant Biology*, *10*, 38.

Nourani, E., Khunjush, F., & Durmuş, S. (2015). Computational approaches for prediction of pathogen-host protein-protein interactions. *Frontiers in Microbiology*, *6*, 94.

Oliver, R. P., Friesen, T. L., Faris, J. D., & Solomon, P. S. (2012). *Stagonospora nodorum*: from pathology to genomics and host resistance. *Annual Review of Phytopathology*, *50*, 23–43.

Palanga, K. K., Jamshed, M., Rashid, M. H. or, Gong, J., Li, J., Iqbal, M. S., … Yuan, Y. (2017). Quantitative trait locus mapping for *Verticillium* wilt resistance in an upland cotton recombinant inbred line using SNP-Based high density genetic map. *Frontiers in Plant Science*, *8*, 1–13.

Park, S.-W., Kaimoyo, E., Kumar, D., Mosher, S., & Klessig, D. F. (2007). Methyl salicylate is a critical mobile signal for plant systemic acquired resistance. *Science (New York, N.Y.)*, *318*, 113–116.

Paul, A., Jha, A., Bhardwaj, S., Singh, S., Shankar, R., & Kumar, S. (2014). RNA-seq-mediated transcriptome analysis of actively growing and winter dormant shoots identifies non-deciduous habit of evergreen tree tea during winters. *Scientific Reports*, *4*, 5932.

Peltier, A. J., Bradley, C. a., Chilvers, M. I., Malvick, D. K., Mueller, D. S., Wise, K. a., & Esker, P. D. (2012). Biology, yield loss and control of *Sclerotinia* stem rot of soybean. *Journal of Integrated Pest Management*, *3*, 1–7.

Peterlunger, E., Mattivi, F., Wong, D. C. J., Bucchetti, B., Fait, A., Arapitsas, P., … Castellarin, S. D. (2016). Transcriptome and metabolite profiling reveals that prolonged drought modulates the phenylpropanoid and terpenoid pathway in white grapes (*Vitis vinifera* L.). *BMC Plant Biology*, *16*, 1–17.

Piasecka, A., Jedrzejczak-Rey, N., & Bednarek, P. (2015). Secondary metabolites in plant innate immunity: Conserved function of divergent chemicals. *New Phytologist*, *206*, 948–964.

Piotrowski, J. S., Okada, H., Lu, F., Li, S. C., Hinchman, L., Ranjan, A., … Ohya, Y. (2015). Plant-derived antifungal agent poacic acid targets β-1,3-glucan. *Proceedings of the National Academy of Sciences*, 201410400.

Pusztahelyi, T., Holb, I. J., & Pócsi, I. (2015). Secondary metabolites in fungus-plant interactions. *Frontiers in Plant Science*, *6*, 1–23.

R Development Core Team. (2017). *R: A language and environment for statistical computing*. https://doi.org/10.1016/j.jssas.2015.06.002

Raut, J. S., Shinde, R. B., Chauhan, N. M., & Karuppayil, S. M. (2014). Phenylpropanoids of plant origin as inhibitors of biofilm formation by *Candida albicans*. *Journal of Microbiology and Biotechnology*, *24*, 1216–1225.

Ren, H., Jian, S., Chen, Y., Liu, H., Zhang, Q., Liu, N., … Luo, J. (2014). Distribution, status, and conservation of *Camellia changii* Ye (Theaceae), a Critically Endangered plant endemic to southern China. *Oryx*, *48*, 358–360.

Ren, H., Wang, J., Liu, H., Yuan, L., Xu, Y., Zhang, Q., … Luo, J. (2016). Conservation introduction resulted in similar reproductive success of *Camellia changii* compared with augmentation. *Plant Ecology*, *217*, 219–228.

Ross, A. F. (1961). Systemic acquired resistance induced by localized virus infections in plants. *Virology*, *14*, 340–358.

Rossum, G. van. (1995). Python tutorial, Technical Report CS-R9526. *Python*. Amsterdam: Centrum voor Wiskunde en Informatica (CWI).

Roux, F., Voisin, D., Badet, T., Balagué, C., Barlet, X., Huard-Chauveau, C., … Raffaele, S. (2014). Resistance to phytopathogens *e tutti quanti*: Placing plant quantitative disease resistance on the map. *Molecular Plant Pathology*, *15*, 427–432.

Ruijter, J. M., Ramakers, C., Hoogaars, W. M. H., Karlen, Y., Bakker, O., van den hoff, M. J. B., & Moorman, A. F. M. (2009). Amplification efficiency: linking baseline and bias in the analysis of quantitative PCR data. *Nucleic Acids Research*, *37*, e45.

Saavedra, G. M., Sanfuentes, E., Figueroa, P. M., & Figueroa, C. R. (2017). Independent preharvest applications of methyl jasmonate and chitosan elicit differential upregulation of defense-related genes with reduced incidence of gray mold decay during postharvest storage of *Fragaria chiloensis* fruit. *International Journal of Molecular Sciences*, *18*, 1420.

Saracchi, M., Locati, D., Colombo, E. M., & Pasquali, M. (2018). Updates on *Ciborinia camelliae*, the causal agent of camellia flower blight. *Journal of Plant Pathology*, *101*, 215–223.

Schalk, M., Cabello-Hurtado, F., Pierrel, M. A., Atanossova, R., Saindrenan, P., & Werck-Reichhart, D. (1998). Piperonylic acid, a selective, mechanism-based inactivator of the trans-cinnamate 4-hydroxylase: A new tool to control the flux of metabolites in the phenylpropanoid pathway. *Plant Physiology*, *118*, 209–218.

Schindelin, J., Arganda-Carreras, I., Frise, E., Kaynig, V., Longair, M., Pietzsch, T., … Cardona, A. (2012). Fiji: An open-source platform for biological-image analysis. *Nature Methods*, *9*, 676–682.

Schouten, A., Van Baarlen, P., & Van Kan, J. a L. (2008). Phytotoxic Nep1-like proteins from the necrotrophic fungus *Botrytis cinerea* associate with membranes and the nucleus of plant cells. *New Phytologist*, *177*, 493–505.

Sels, J., Mathys, J., De Coninck, B. M. A., Cammue, B. P. A., & De Bolle, M. F. C. (2008). Plant pathogenesis-related (PR) proteins: A focus on PR peptides. *Plant Physiology and Biochemistry*, Vol. 46, pp. 941–950.

Semba, R. D., Shardell, M., Trehan, I., Moaddel, R., Maleta, K. M., Ordiz, M. I., … Manary, M. J. (2016). Metabolic alterations in children with environmental enteric dysfunction. *Scientific Reports*, *6*, 1–9.

Shah, J., & Zeier, J. (2013). Long-distance communication and signal amplification in systemic acquired resistance. *Frontiers in Plant Science*, *4*, 1–16.

Shannon, P., Markiel, A., Ozier, O., Baliga, N. S., Wang, J. T., Ramage, D., … Ideker, T. (2003). Cytoscape: a software environment for integrated models of biomolecular interaction networks. *Genome Research*, *13*, 2498–2504.

Shi, C.-Y., Yang, H., Wei, C.-L., Yu, O., Zhang, Z.-Z., Jiang, C.-J., … Wan, X.-C. (2011). Deep sequencing of the *Camellia sinensis* transcriptome revealed candidate genes for major metabolic pathways of tea-specific compounds. *BMC Genomics*, *12*, 131.

Simão, F. A., Waterhouse, R. M., Ioannidis, P., Kriventseva, E. V., & Zdobnov, E. M. (2015). BUSCO: Assessing genome assembly and annotation completeness with single-copy orthologs. *Bioinformatics*, *31*, 3210–3212.

Sivasithamparam, K., Barbetti, M. J., & Li, H. (2005). Recurring challenges from a necrotrophic fungal plant pathogen: A case study with *Leptosphaeria maculans* (causal agent of blackleg disease in Brassicas) in Western Australia. *Annals of Botany*, Vol. 96, pp. 363–377.

Smith, J. E., Mengesha, B., Tang, H., Mengiste, T., & Bluhm, B. H. (2014). Resistance to *Botrytis cinerea* in *Solanum lycopersicoides* involves widespread transcriptional reprogramming. *BMC Genomics*, *15*, 334.

Sperschneider, J., Gardiner, D. M., Dodds, P. N., Tini, F., Covarelli, L., Singh, K. B., … Taylor, J. M. (2016). EffectorP : predicting fungal effector proteins from secretomes using machine learning. *New Phytologist*, *210*, 743–761.

Spoel, S. H., & Dong, X. (2012). How do plants achieve immunity ? Defence without specialized immune cells. *Nature Reviews Immunology*, *12*, 89–100.

Staal, J., Kaliff, M., Bohman, S., & Dixelius, C. (2006). Transgressive segregation reveals two Arabidopsis TIR-NB-LRR resistance genes effective against *Leptosphaeria maculans*, causal agent of blackleg disease. *Plant Journal*, *46*, 218–230.

Staal, J., Kaliff, M., Dewaele, E., Persson, M., & Dixelius, C. (2008). RLM3, a TIR domain encoding gene involved in broad-range immunity of Arabidopsis to necrotrophic fungal pathogens. *Plant Journal*, *55*, 188–200.

Stewart, T. M., & Neilson, H. (1993). Flower blight, a new disease of camellias in New Zealand. *New Zealand Camellia Bulletin*, *116*, 29–33.

Szklarczyk, D., Morris, J. H., Cook, H., Kuhn, M., Wyder, S., Simonovic, M., … Von Mering, C. (2017). The STRING database in 2017: Quality-controlled protein-protein association networks, made broadly accessible. *Nucleic Acids Research*, *45*, 362–368.

Tai, Y., Liu, C., Yu, S., Yang, H., Sun, J., Guo, C., … Wan, X. (2018). Gene co-expression network analysis reveals coordinated regulation of three characteristic secondary biosynthetic pathways in tea plant (*Camellia sinensis*). *BMC Genomics*, *19*, 1–13.

Tanaka, S., Brefort, T., Neidig, N., Djamei, A., Kahnt, J., Vermerris, W., … Kahmann, R. (2014). A secreted *Ustilago maydis* effector promotes virulence by targeting anthocyanin biosynthesis in maize. *ELife*, *3*, e01355.

Taylor, C. H. (2004). *Studies of camellia flower blight (Ciborinia camelliae Kohn)*. Massey University, Palmerston North, New Zealand.

Taylor, C. H., & Long, P. G. (2000). Review of literature on camellia flower blight caused by *Ciborinia camelliae*. *New Zealand Journal of Crop and Horticultural Science*, *28*, 123–138.

Teodoro, G. R., Ellepola, K., Seneviratne, C. J., & Koga-Ito, C. Y. (2015). Potential use of phenolic acids as anti-Candida agents: A review. *Frontiers in Microbiology*, *6*, 1–11.

The Arabidopsis Genome Initiative. (2000). Analysis of the genome sequence of the flowering plant *Arabidopsis thaliana*. *Nature*, *408*, 796–815.

Tintor, N., Ross, A., Kanehara, K., Yamada, K., Fan, L., Kemmerling, B., … Saijo, Y. (2013). Layered pattern receptor signaling via ethylene and endogenous elicitor peptides during Arabidopsis immunity to bacterial infection. *Proceedings of the National Academy of Sciences of the United States of America*, *110*, 6211–6216.

Toruño, T. Y., Shen, M., Coaker, G., & Mackey, D. (2018). Regulated disorder: posttranslational modifications control the RIN4 plant immune signaling hub. *Molecular Plant-Microbe Interactions*, *32*, 56–64.

Trapnell, C., Roberts, A., Goff, L., Pertea, G., Kim, D., Kelley, D. R., … Pachter, L. (2012). Differential gene and transcript expression analysis of RNA-seq experiments with TopHat and Cufflinks. *Nature Protocols*, *7*, 562–578.

van de Wouw, A. P., Cozijnsen, A. J., Hane, J. K., Brunner, P. C., McDonald, B. A., Oliver, R. P., & Howlett, B. J. (2010). Evolution of linked avirulence effectors in Leptosphaeria maculans is affected by genomic environment and exposure to resistance genes in host plants. *PLoS Pathogens*, *6*, e1001180.

van Esse, H. P., Bolton, M. D., Stergiopoulos, I., Wit, P. J. G. M. De, Thomma, B. P. H. J., van Esse, H. P., … Thomma, B. P. H. J. (2007). The chitin-binding *Cladosporium fulvum* effector protein Avr4 is a virulence factor. *Molecular Plant-Microbe Interactions : MPMI*, *20*, 1092–1101.

van Esse, H. P., Van't Klooster, J. W., Bolton, M. D., Yadeta, K. A., van Baarlen, P., Boeren, S., … Thomma, B. P. (2008). The *Cladosporium fulvum* virulence protein Avr2 inhibits host proteases required for basal defense. *Plant Cell*, *20*, 1948–1963.

van Toor, R. F. (2002). *Development of biocontrol methods for camellia flower blight caused by Ciborinia camelliae Kohn*. Lincoln University, Canterbury, New Zealand.

Veloso, J., & van Kan, J. A. L. (2018). Many shades of grey in Botrytis–host plant interactions. *Trends in Plant Science*, *23*, 613–622.

Vingana-Singam, V., Long, P., & Rowland, R. (2000). Infection processes of *Ciborinia camelliae* on camellia flower tissue. *New Zealand Plant Protection*, *53*, 151–156.

Vogt, T. (2010). Phenylpropanoid biosynthesis. *Molecular Plant*, *3*, 2–20.

Wan, J., Zhang, X.-C., Neece, D., Ramonell, K. M., Clough, S., Kim, S.-Y., … Stacey, G. (2008). A LysM receptor-like kinase plays a critical role in chitin signaling and fungal resistance in Arabidopsis. *The Plant Cell*, *20*, 471–481.

Wang, K., Liao, Y., Kan, J., Han, L., & Zheng, Y. (2015). Response of direct or priming defense against *Botrytis cinerea* to methyl jasmonate treatment at different concentrations in grape berries. *International Journal of Food Microbiology*, *194*, 32–39.

Wang, Q., Han, C., Ferreira, A. O., Yu, X., Ye, W., Tripathy, S., … Wang, Y. (2011). Transcriptional programming and functional interactions within the *Phytophthora sojae* RXLR effector repertoire. *The Plant Cell*, *23*, 2064–2086.

Wang, X.-C., Zhao, Q.-Y., Ma, C.-L., Zhang, Z.-H., Cao, H.-L., Kong, Y.-M., … Yang, Y.-J. (2013). Global transcriptome profiles of *Camellia sinensis* during cold acclimation. *BMC Genomics*, *14*, 415.

Wang, X., Jiang, N., Liu, J., Liu, W., & Wang, G.-L. (2014). The role of effectors and host immunity in plant-necrotrophic fungal interactions. *Virulence*, *5*, 722–732.

Wang, Y.-C., Qian, W.-J., Li, N.-N., Hao, X.-Y., Wang, L., Xiao, B., … Yang, Y.-J. (2016). Metabolic changes of caffeine in tea plant (*Camellia sinensis* (L.) O. Kuntze) as defense response to *Colletotrichum fructicola*. *Journal of Agricultural and Food Chemistry*, *64*, 6685–6693.

Wang, Y. S., Gao, L. P., Wang, Z. R., Liu, Y. J., Sun, M. L., Yang, D. Q., … Xia, T. (2012). Light-induced expression of genes involved in phenylpropanoid biosynthetic pathways in callus of tea (*Camellia sinensis* (L.) O. Kuntze). *Scientia Horticulturae*, *133*, 72–83.

Wang, Yiming, Gupta, R., Song, W., Huh, H. H., Lee, S. E., Wu, J., … Kim, S. T. (2017). Label-free quantitative secretome analysis of *Xanthomonas oryzae* pv. *oryzae* highlights the involvement of a novel cysteine protease in its pathogenicity. *Journal of Proteomics*, *169*, 202–214.

Wang, Yiming, Schuck, S., Wu, J., Yang, P., Doering, A.-C., Zeier, J., & Tsuda, K. (2018). A MPK3/6-WRKY33-ALD1-pipecolic acid regulatory loop contributes to systemic acquired resistance. *The Plant Cell*, *30*, 2480–2494.

Wang, Yin, Chantreau, M., Sibout, R., Hawkins, S., Loqué, D., Berkeley, L., … State, M. (2013). Plant cell wall lignification and monolignol metabolism. *Frontiers in Plant Science*, *4*, 1–14.

Wang, Yuchun, Hao, X., Lu, Q., Wang, L., Qian, W., Li, N., … Yang, Y. (2018). Transcriptional analysis and histochemistry reveal that hypersensitive cell death and H_2O_2 have crucial roles in the resistance of tea plant (*Camellia sinensis* (L.) O. Kuntze) to anthracnose. *Horticulture Research*, *5*, 18.

Wang, Z., Jiang, C., Wen, Q., Wang, N., Tao, Y. yuan, & Xu, L. an. (2014). Deep sequencing of the *Camellia chekiangoleosa* transcriptome revealed candidate genes for anthocyanin biosynthesis. *Gene*, *538*, 1–7.

Warnes, G. R., Bolker, B., Bonebakker, L., Gentleman, R., Liaw, W. H. A., Lumley, T., … Venables, B. (2019). *gplots: Various R Programming Tools for Plotting Data*. Retrieved from

https://cran.r-project.org/package=gplots

Wei, C., Yang, H., Wang, S., Zhao, J., Liu, C., Gao, L., … Wan, X. (2018). Draft genome sequence of *Camellia sinensis* var. *sinensis* provides insights into the evolution of the tea genome and tea quality. *Proceedings of the National Academy of Sciences*, *115*, E4151–E4158.

Weiberg, A., Wang, M., Lin, F.-M., Zhao, H., Zhang, Z., Kaloshian, I., … Peer, Y. Van de. (2013). Fungal small RNAs suppress plant immunity by hijacking host RNA interference pathways. *Science (New York, N.Y.)*, *342*, 118–123.

Wickham, H. (2017). Tidyverse. *CRAN*.

Williams, B., Kabbage, M., Kim, H. J., Britt, R., & Dickman, M. B. (2011). Tipping the balance: *Sclerotinia sclerotiorum* secreted oxalic acid suppresses host defenses by manipulating the host redox environment. *PLoS Pathogens*, *7*, e1002107.

Wood, S. N. (2017). Generalized additive models: An introduction with R, second edition. In *Generalized Additive Models: An Introduction with R, Second Edition*. https://doi.org/10.1201/9781315370279

Wu, J., Zhao, Q., Yang, Q., Liu, H., Li, Q., Yi, X., … Zhou, Y. (2016). Comparative transcriptomic analysis uncovers the complex genetic network for resistance to *Sclerotinia sclerotiorum* in *Brassica napus*. *Scientific Reports*, *6*, 19007.

Xia, E. H., Jiang, J. J., Huang, H., Zhang, L. P., Zhang, H. Bin, & Gao, L. Z. (2014). Transcriptome analysis of the oil-rich tea plant, *Camellia oleifera*, reveals candidate genes related to lipid metabolism. *PLoS ONE*, *9*, e104150.

Xia, E. H., Zhang, H. Bin, Sheng, J., Li, K., Zhang, Q. J., Kim, C., … Gao, L. Z. (2017). The tea tree genome provides insights into tea flavor and independent evolution of caffeine biosynthesis. *Molecular Plant*, *10*, 866–877.

Xiao, X., Xie, J., Cheng, J., Li, G., Yi, X., Jiang, D., & Fu, Y. (2014). Novel secretory protein Ss-Caf1 of the plant-pathogenic fungus *Sclerotinia sclerotiorum* is required for host penetration and normal sclerotial development. *Molecular Plant-Microbe Interactions : MPMI*, *27*, 40–55.

Xin, T., de Riek, J., Guo, H., Jarvis, D., Ma, L., & Long, C. (2015). Impact of traditional culture on *Camellia reticulata* in Yunnan, China. *Journal of Ethnobiology and Ethnomedicine*, *11*, 74.

Xu, L., Zhu, L., Tu, L., Liu, L., Yuan, D., Jin, L., … Zhang, X. (2011). Lignin metabolism has a central role in the resistance of cotton to the wilt fungus *Verticillium dahliae* as revealed by RNA-Seq-dependent transcriptional analysis and histochemistry. *Journal of Experimental Botany*, *62*, 5607–5621.

Xu, Q., He, Y., Yan, X., Zhao, S., Zhu, J., & Wei, C. (2018). Unraveling a crosstalk regulatory network of temporal aroma accumulation in tea plant (*Camellia sinensis*) leaves by integration of metabolomics and transcriptomics. *Environmental and Experimental Botany*, *149*, 81–94.

Yang, X., Islam, M. S., Sood, S., Maya, S., Hanson, E. A., Comstock, J., & Wang, J. (2018).

Identifying quantitative trait loci (QTLs) and developing diagnostic markers linked to orange rust resistance in sugarcane (*Saccharum* spp.). *Frontiers in Plant Science*, *9*, 1–10.

Yang, X., Sood, S., Luo, Z., Todd, J., & Wang, J. (2018). Genome-wide association studies identified resistance loci to orange rust and yellow leaf virus diseases in sugarcane (*Saccharum* spp.). *Phytopathology*, *109*, 623–631.

Yao, Q.-Y., Huang, H., Tong, Y., Xia, E.-H., & Gao, L.-Z. (2016). Transcriptome analysis identifies candidate genes related to triacylglycerol and pigment biosynthesis and photoperiodic flowering in the ornamental and oil-producing plant, *Camellia reticulata* (Theaceae). *Frontiers in Plant Science*, *7*, 163.

Zeng, W., Sun, Z., Cai, Z., Chen, H., Lai, Z., Yang, S., & Tang, X. (2017). Proteomic analysis by iTRAQ-MRM of soybean resistance to *Lamprosema indicate*. *BMC Genomics*, *18*, 1–22.

Zhang, H.-B., Xia, E.-H., Huang, H., Jiang, J.-J., Liu, B.-Y., & Gao, L.-Z. (2015). *De novo* transcriptome assembly of the wild relative of tea tree (*Camellia taliensis*) and comparative analysis with tea transcriptome identified putative genes associated with tea quality and stress response. *BMC Genomics*, *16*, 298.

Zhang, L., Kars, I., Essenstam, B., Liebrand, T. W. H., Wagemakers, L., Elberse, J., … van Kan, J. A. L. (2014). Fungal endopolygalacturonases are recognized as microbe-associated molecular patterns by the arabidopsis receptor-like protein RESPONSIVENESS TO BOTRYTIS POLYGALACTURONASES1. *Plant Physiology*, *164*, 352–364.

Zhang, Y. Y., Zhang, Y. Y., Qiu, D., Zeng, H., Guo, L., & Yang, X. (2015). BcGs1, a glycoprotein from *Botrytis cinerea*, elicits defence response and improves disease resistance in host plants. *Biochemical and Biophysical Research Communications*, *457*, 627–634.

Zhao, Z., Liu, H., Wang, C., & Xu, J. R. (2014). Correction to Comparative analysis of fungal genomes reveals different plant cell wall degrading capacity in fungi [BMC Genomics 14(2013) 274]. *BMC Genomics*, *15*. https://doi.org/10.1186/1471-2164-15-6

Zhou, J., Fu, Y., Xie, J., Li, B., Jiang, D., Li, G., & Cheng, J. (2012). Identification of microRNA-like RNAs in a plant pathogenic fungus *Sclerotinia sclerotiorum* by high-throughput sequencing. *Molecular Genetics and Genomics*, *287*, 275–282.

Zhu, W., Ronen, M., Gur, Y., Minz-Dub, A., Masrati, G., Ben-Tal, N., … Sharon, A. (2017). BcXYG1, a secreted xyloglucanase from *Botrytis cinerea* induces cell death and triggers plant defense. *Plant Physiology*, *175*, 438–456.

Zhu, W., Wei, W., Fu, Y., Cheng, J., Xie, J., Li, G., … Jiang, D. (2013). A secretory protein of necrotrophic fungus *Sclerotinia sclerotiorum* that suppresses host resistance. *PLoS ONE*, *8*, e53901.

Zhu, Z., & Tian, S. (2012). Resistant responses of tomato fruit treated with exogenous methyl jasmonate to *Botrytis cinerea* infection. *Scientia Horticulturae*, *142*, 38–43.

Zipfel, C., & Robatzek, S. (2010). Pathogen-associated molecular pattern-triggered

immunity: Veni, Vidi...? *Plant Physiology*, *154*, 551–554.

Appendix A. Supplementary Tables and Figures

Table A-1 | Primer sequences used in the research.

Transcript ID	Annotation	Forward primer	Reverse primer	Product size
Camellia lutchuensis				
TRINITY_DN1789_c0_g1_i1_u	*MYB15*	TCGGTCACAGACTTAACTGGC	GTAACTCCTCGGCGAAACCA	166
TRINITY_DN24648_c0_g1_i1_u	*WRKY33*	GGAAACAGCAACGTGCCAAT	AGTTTCCGAACCCTGCGAAT	175
TRINITY_DN23937_c0_g1_i2	*MPK3*	CCACATGTCAATCCGTTGGC	ACCGGTTCGTCAGCTATGTC	134
TRINITY_DN23551_c1_g2_i3	*RIN4*	AAGGCACGGAAGGGTAGAAC	CCTTACTGCTCCCCGTCTTG	156
TRINITY_DN25310_c0_g1_i6	*BAK1*	CGCTGTTCTCACTGTTGCAC	TCGGTTATTTCGGGCCTCTG	155
TRINITY_DN22734_c0_g1_i2	*SOBIR1*	ACAAGCCATTCTCCGCGTAT	TTCCCGCAACATTGGAGGTT	151
TRINITY_DN24082_c0_g1_i1	*LOX*	ATCAGTGTGATTGCCCCTGG	GAAGAGCAATGAAGCCGTGC	126
TRINITY_DN23984_c0_g1_i1	*AOS*	GGCCAAGGACCATCAAAGGA	TACCAAACTCGGACACGACG	80
TRINITY_DN15095_c0_g2_i1	*OPCL*	CGATGCGAGGACACTACTCC	TCCAACCTCCCGATCGTACT	197
TRINITY_DN28026_c0_g1_i1_u	*OPR*	GGTGGGAGCTTAGAGAACCG	TGCATCAGGGTTCGAGTCAC	141
TRINITY_DN24077_c0_g4_i3	*PTB1* (housekeeping)	ACGCTGTCACAGTGGATGTC	GCTTGGGTTCCCCCATTCTT	94
TRINITY_DN23201_c0_g1_i1_u	*EF1-alpha* (housekeeping)	ATCCTGAAGTGGGAGACGGA	ACCTCGACTGGTACAAGGGT	101

Table A-1 (continued)

Transcript ID	Annotation	Forward primer	Reverse primer	Product size
Camellia 'Nicky Crisp'				
TRINITY_DN26107_c0_g1_i3	*MYB15*	ATGTCCAAACCCAGTTGTCCA	GGCCCTTCAACTCACCACTC	128
TRINITY_DN25612_c3_g2_i1	*WRKY33*	TCGCGAACGGTTCTATTCCC	ATGGATTCTGTGGCAACCCC	179
TRINITY_DN26639_c1_g1_i1	*MPK3*	CCACATGTCAATCCGTTGGC	ACCGGTTCGTCAGCTATGTC	134
TRINITY_DN20453_c0_g1_i1	*RIN4*	TGCCGCTGTTCCAAAATTCG	TGTTTTGCCTCCGTGCATTG	164
TRINITY_DN44570_c3_g3_i6_u	*BAK1*	ACGTGGATTTTGCATGACGC	TATCGGCCAATCAAGTGGGG	121
TRINITY_DN26091_c0_g1_i1	*SOBIR1*	GGCTTCTGGGCTGGAGTATC	TTTGCGAGCCCAAAATCTGC	126
TRINITY_DN24521_c0_g1_i1	*4CL*	AGTGTAGAACGGGTTGGCTG	CCTACACCTACGCCGATGTC	182
TRINITY_DN24692_c0_g1_i3	*C4H*	ATCCAGAAAAAGCTCCGGCA	AGCTTGGAGGTAGGGGAGTT	96
TRINITY_DN24627_c0_g1_i1	*F5H*	CCAGCCGAGCCAAGGAATAA	TGGTGTTCGAACTCACTCGG	152
TRINITY_DN43745_c0_g1_i1_u	*LOX*	CACCCCTGATGCGTCGATTA	ACCAAATCGATGGCTGGTGT	198
TRINITY_DN28477_c0_g1_i1	*AOS*	TGGGAAACAAGCAATGTGCG	CCAACCTCCGTCTCAAACGA	103
TRINITY_DN24810_c0_g1_i1	*OPCL*	CGATGCGAGGACACTACTCC	TCCAACCTCCCGATCGTACT	197
TRINITY_DN30127_c0_g2_i2	*OPR*	ATTTGAAAGCCCCAACACGC	TCCGGATTCGCCAGAAACAA	156
TRINITY_DN42484_c1_g1_i2_u	*PTB1* (housekeeping)	ACTGAGATCAGTGTGGCGTG	ACGGAGGAGTTCAGGCTTTG	140
TRINITY_DN26973_c0_g1_i3	*Tubulin* (housekeeping)	CCTGACCTCGTCGATAACGG	TCAGCCCGATGGTATGATGC	148

Table A-2 | Details of *A. thaliana* STRING interaction networks.

Cluster	Number of transcript sequences	Number of nodes in STRING	Average node degree	Maximal node degree	Expected number of edges	Observed number of edges	PPI enrichment *P* value
1	200	118	0.576	6	15	34	3.15×10^{-5}
2	196	109	1.82	6	26	49	2.54×10^{-5}
3	4109	1662	9.56	126	4571	7942	$< 1\times10^{-16}$
4	288	163	3.09	25	36	252	$< 1\times10^{-16}$
5	2209	1042	6.26	67	1665	3263	$< 1\times10^{-16}$
6	1747	1132	7.01	89	1690	3969	$< 1\times10^{-16}$
7	2498	1647	21.8	188	10320	17972	$< 1\times10^{-16}$
8	531	346	2.27	21	211	392	$< 1\times10^{-16}$
9	1380	874	4.35	52	1204	1901	$< 1\times10^{-16}$
10	440	299	2.02	14	302	122	$< 1\times10^{-16}$
RN* 1	NA	1700	5.29	63	4500	4496	0.528
RN 2	NA	1700	5.51	73	4729	4686	0.734
RN 3	NA	346	1.06	12	184	183	0.528

The table shows mapping and network statistics of Camellia lutchuensis *transcripts onto* Arabidopsis thaliana *STRING interactome. Cluster numbering corresponds to the expression clusters from Figure 3-3. Protein-protein interaction (PPI) enrichment P values show the probability to observe the same number of interactions (graph edges) in a randomly generated* A. thaliana *PPI-network. Random networks (RN) were generated from randomly sampled proteins of* A. thaliana.

Table A-3 | RNA-seq results and mapping rates of *C. lutchuensis* samples at different stages of petal blight infection.

Sample	Number of raw reads	Number of high-quality reads	Mapping rate (%)
0 hours, infected	11,298,970	10,655,035	96.0
0 hours, infected	11,523,835	10,865,911	96.1
0 hours, infected	11,663,519	11,029,131	96.2
6 hours, infected	11,388,445	10,791,462	94.8
6 hours, infected	12,814,399	12,063,582	95.3
6 hours, infected	11,821,505	11,221,873	95.1
12 hours, infected	12,007,525	11,352,725	95.7
12 hours, infected	12,001,101	11,385,065	95.1
12 hours, infected	12,030,319	11,406,584	95.5
12 hours, mock	12,180,983	11,524,519	96.1
12 hours, mock	12,738,975	12,115,172	96.3
12 hours, mock	12,238,793	11,596,329	96.6
24 hours, infected	9,942,425	9,412,198	95.7
24 hours, infected	12,634,585	12,003,473	95.9
24 hours, infected	11,644,992	11,072,541	95.9
24 hours, mock	12,637,201	11,965,284	96.1
24 hours, mock	12,071,541	11,458,831	95.9
24 hours, mock	13,522,380	12,780,002	96.2

Table A-4 | Contingency table of upregulated plant transcripts.

	Transcription Factors	Kinases	Ubiquitin ligases	Others
Cluster 3	133	115	25	1139
Cluster 5	57	42	12	729
Cluster 8	22	6	2	237

Table A-5 | Contingency table of plant apoplastic proteins.

	Cell wall	Oxidoreductases	Proteases	Pathogen-resistance	Stress	Signalling	Lipid-related	Cytosolic	Unassigned
Mock-treated	49	12	11	18	12	3	11	0	28
Infected	12	11	2	13	6	5	6	2	15

Table A-6 | Contingency table of secreted fungal proteins.

	CAZymes	Oxidoreductases	Proteases	HR-elicitors	Unassigned
In vitro	37	15	15	3	24
In planta	20	6	6	0	10

Figure A-1 | Functional distribution of mock-treated *Camellia* 'Nicky Crisp' proteins.

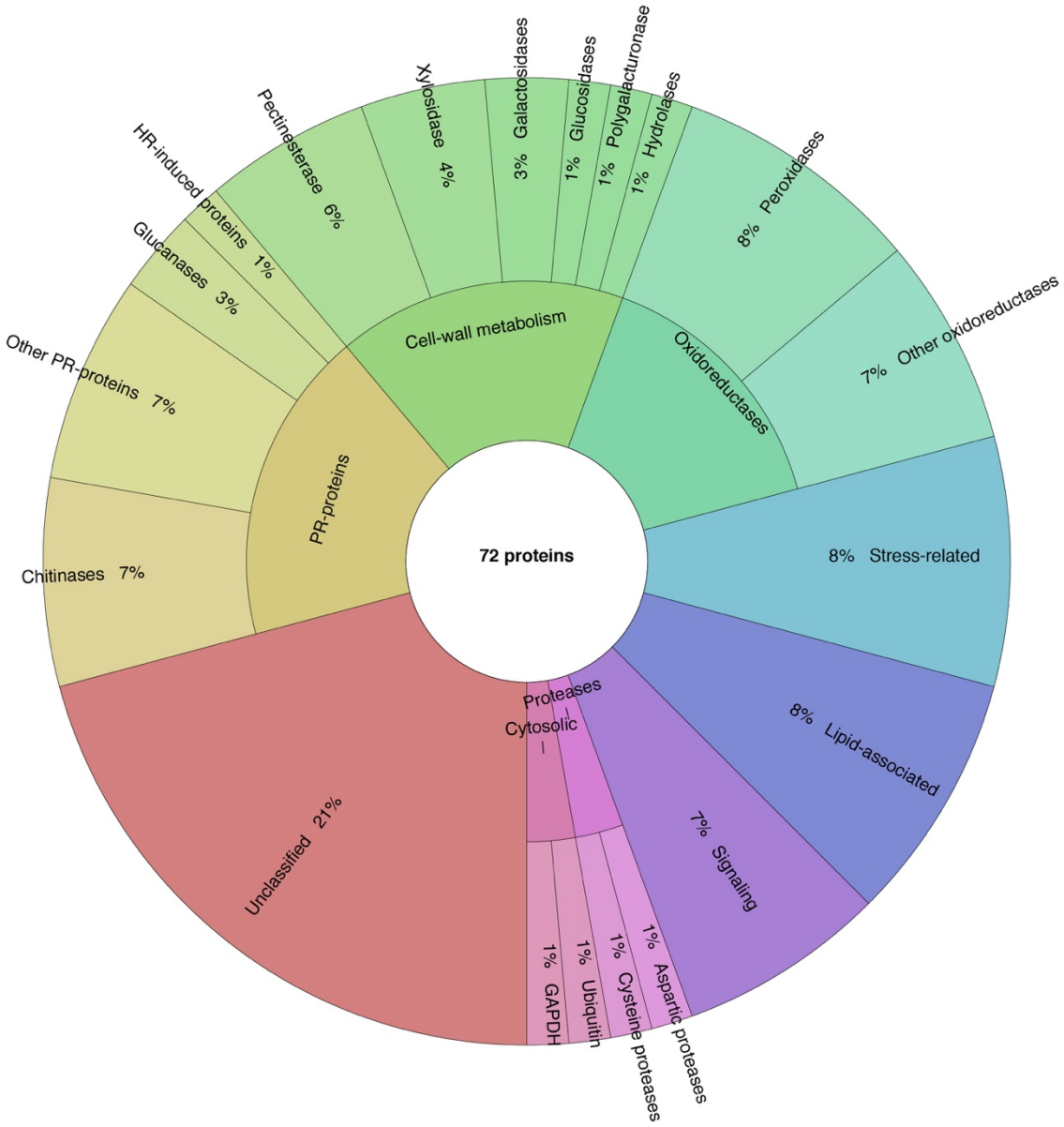

Figure A-2 | Functional distribution of infected *Camellia* 'Nicky Crisp' proteins.

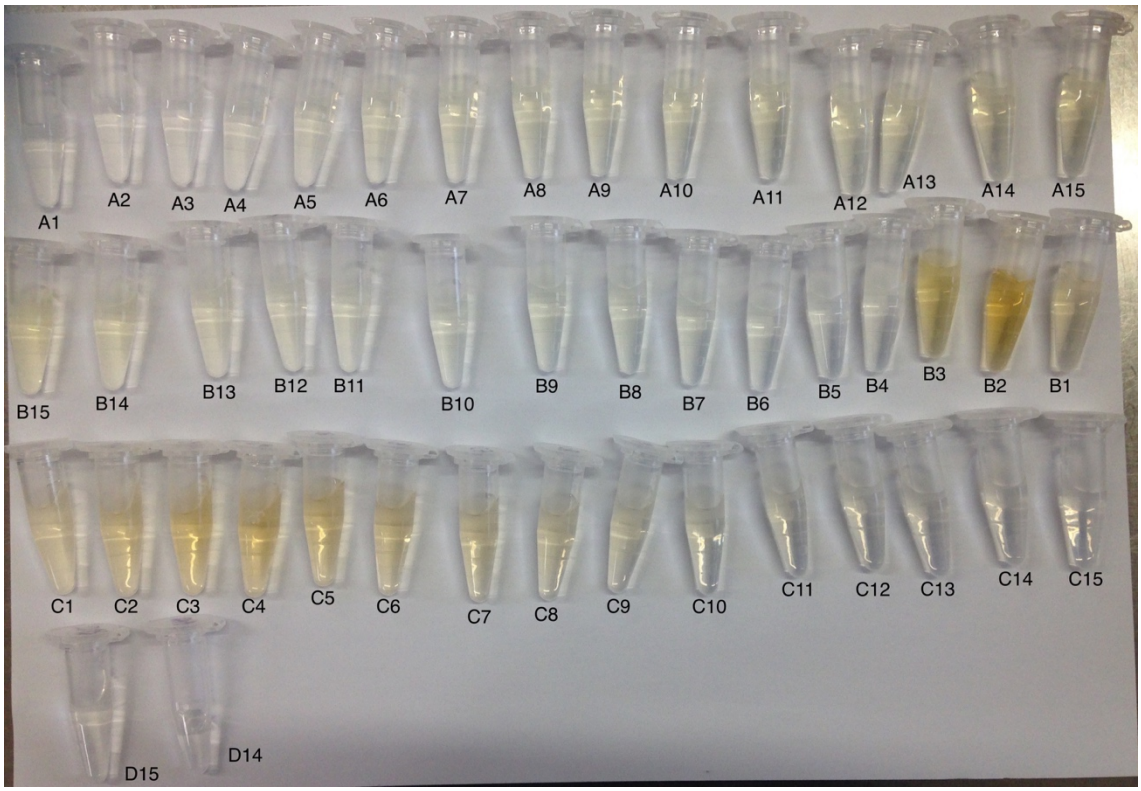

Figure A-3 | Fractions obtained from the anion-exchange FPLC of 100 mL of two-weeks-old *C. camelliae* culture filtrate.

Table A-7 | Estimation of *C. lutchuensis* apoplastic protein concentration.

	Standard curve							Apoplastic wash	
Sample		**1**	**2**	**3**	**4**	**5**	**6**		**7**
Assay preparation (10 min incubation)	Volume of milliQ water added, µL	80	75	70	60	40	20	Volume of milliQ water added, µL	30
	Volume of 0.1 µg/mL BSA solution added, µL	0	5	10	20	40	60		
	Bio-Rad dye added, µL	20	20	20	20	20	20	Bio-Rad dye added, µL	20
	Final amount of BSA, µg	0	0,5	1	2	4	6	Volume of apoplastic wash, µL	50
Absorbance, 595 nm	**Replicate 1**	0.16	0.241	0.3	0.393	0.595	0.615	**Replicate 1**	0.413
	Replicate 2	0.176	0.235	0.273	0.378	0.611	0.649	**Replicate 2**	0.416
	Replicate 3	0.172	0.229	0.262	0.375	0.612	0.068	**Replicate 3**	0.393
	Mean	0.169	0.235	0.278	0.382	0.606	0.632 (excluded)	**Mean**	0.407
Conclusion: 100 µL of *C. lutchuensis* apoplastic wash (extracted from 15 petals) contains 4.34 µg of protein.									

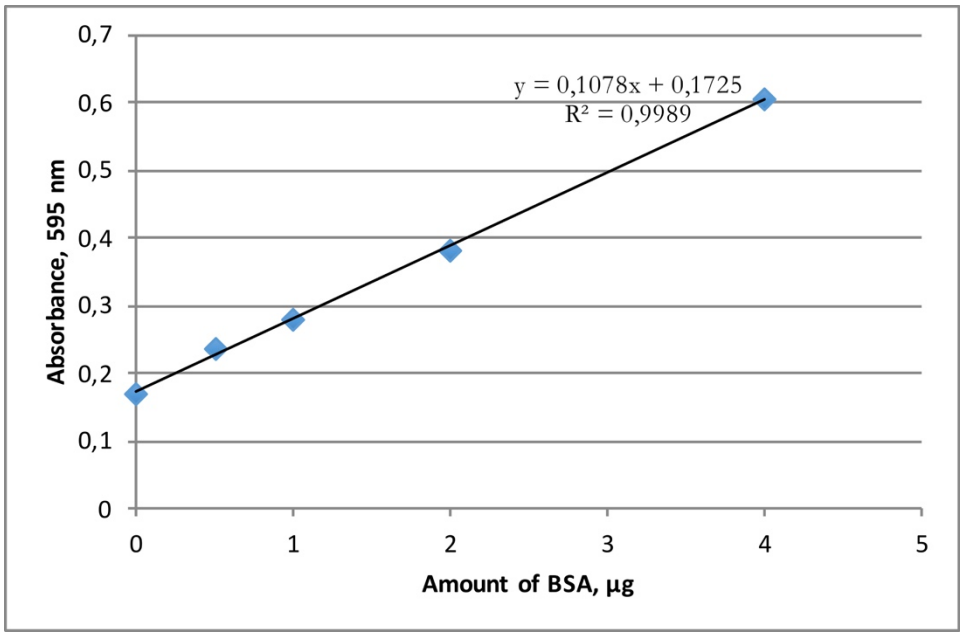

Figure A-4 | BSA standard curve used for *C. lutchuensis* apoplastic protein quantification.
The curve is based on data from Table A-7.

Appendix B. Code

B.1. Assembly and annotation of plant and fungal transcriptomes

Fungal transcriptome assembly

```
# 1. building reference genome indexes with Bowtie 2
bowtie2-build GENOME_FILE.fasta GENOME_INDEX

# 2. infected "Nicky Crisp" read mapping with TopHat
tophat -p 8 -o susceptible GENOME_INDEX PAIRED_READS_1.fq PAIRED
_READS_2.fq

# 3. infected C. lutchuensis read mapping with TopHat
tophat -p 8 -o resistant GENOME_INDEX PAIRED_READS_1.fq PAIRED_R
EADS_2.fq

# 4. fungal transcriptome assembly with Cufflinks
cufflinks -p 8 -o susceptible_transcripts susceptible/accepted_h
its.bam
cufflinks -p 8 -o resistant_transcripts resistant/accepted_hits.
bam
```

***De novo* plant transcriptome assembly**

```
# 5. de novo assembly of uninfected plant transcriptomes with Tr
inity
Trinity --seqType fq --left Reads1.cut.trimmed.paired
--right Reads2.cut.trimmed.paired --CPU 16 --max_memory 70G

# 6. de novo assembly of infected plant transcriptomes with Trin
ity
Trinity --seqType fq --single tophat_out/unmapped.bam
--run_as_paired --CPU 16 --max_memory 70G
```

Search for additional fungal transcripts in *de novo* infected plant transcriptomes

```
# 7. creating blast databases with fungal genomes
makeblastdb -in sclirotinia_botrytis_genome –dbtype nucl –out sc
```

```
lerotinia_botrytis_db

# 8. fungal transcript detection from infected plant #transcript
ome using blastn
blastn -query trinity_assembly.fasta –db sclerotinia_botrytis_db
–outfmt 6 –evalue 1e-30
–out fungal_transcripts
```

Joining infected and uninfected plant transcriptomes, and removing the redundancy

```
# 9. concatenation of mock-inoculated and infected transcriptome
s
cat trinity_mock.fasta trinity_infected.fasta > total_transcript
s.fasta

# 10. removing redundancy
cd-hitest -i total_transcripts.fasta –c 0.9 –n 8 –o nr_transcrip
ts.fasta
```

Prediction of plant proteomes

```
# 11. predict lomgest ORF
~/TransDecoder-3.0.1/TransDecoder.LongOrfs -t nr_transcripts.fas
ta

# 12. search ORFs against Swiss-Prot
blastp -query nr_transcripts.fasta.transdecoder_dir/longest_orfs
.pep -db /databases/blast_db/swissprot -outfmt 6 -out nr_transcr
ipts-swiss.outfmt6 -max_target_seqs 1  -evalue 1e-5 -num_threads
15

# 13. predict proteome from lom longest ORFs with Swiss-Prot hit
s
~/TransDecoder-3.0.1/TransDecoder.Predict -t nr_transcripts.fast
a --retain_blastp_hits nr_transcripts-swiss.outfmt6
```

Prediction of orthology groups for *C. lutchuensis*, *Camellia* 'Nicky Crisp', and *A. thaliana*

```
# 14. use two predicted proteomes, and one reference proteome as
an input for the program
proteinortho5.pl -project=plant_orthologs CL_proteome.fasta CN_p
roteome.fasta AT_reference_proteome.fasta
```

B.2. Quantitative RNA-seq analysis of the resistance response

Datasets obtained from quantitative RNA-seq analysis

Sample	hpi	Treatment	File
I0-4	0	infected	CBKM2ANXX-2679-01-1-2_S7_L004_R1_001.fastq.gz
			CBKM2ANXX-2679-01-1-2_S7_L004_R2_001.fastq.gz
I0-5	0	infected	CBKM2ANXX-2679-02-1-2_S8_L004_R1_001.fastq.gz
			CBKM2ANXX-2679-02-1-2_S8_L004_R2_001.fastq.gz
I0-6	0	infected	CBKM2ANXX-2679-03-1-2_S9_L004_R1_001.fastq.gz
			CBKM2ANXX-2679-03-1-2_S9_L004_R2_001.fastq.gz
I6-4	6	infected	CBKM2ANXX-2679-04-1-2_S10_L004_R1_001.fastq.gz
			CBKM2ANXX-2679-04-1-2_S10_L004_R2_001.fastq.gz
I6-5	6	infected	CBKM2ANXX-2679-05-1-2_S11_L004_R1_001.fastq.gz
			CBKM2ANXX-2679-05-1-2_S11_L004_R2_001.fastq.gz
I6-6	6	infected	CBKM2ANXX-2679-06-1-2_S12_L004_R1_001.fastq.gz
			CBKM2ANXX-2679-06-1-2_S12_L004_R2_001.fastq.gz
I12-4	12	infected	CBKM2ANXX-2679-07-1-2_S13_L004_R1_001.fastq.gz
			CBKM2ANXX-2679-07-1-2_S13_L004_R2_001.fastq.gz
I12-5	12	infected	CBKM2ANXX-2679-08-1-2_S14_L004_R1_001.fastq.gz
			CBKM2ANXX-2679-08-1-2_S14_L004_R2_001.fastq.gz
I12-6	12	infected	CBKM2ANXX-2679-09-1-2_S15_L004_R1_001.fastq.gz
			CBKM2ANXX-2679-09-1-2_S15_L004_R2_001.fastq.gz
m12-1	12	mock	CBKM2ANXX-2679-10-1-2_S16_L004_R1_001.fastq.gz
			CBKM2ANXX-2679-10-1-2_S16_L004_R2_001.fastq.gz
m12-4	12	mock	CBKM2ANXX-2679-11-1-2_S17_L004_R1_001.fastq.gz
			CBKM2ANXX-2679-11-1-2_S17_L004_R2_001.fastq.gz
m12-6	12	mock	CBKM2ANXX-2679-12-1-2_S18_L004_R1_001.fastq.gz
			CBKM2ANXX-2679-12-1-2_S18_L004_R2_001.fastq.gz
I24-4	24	infected	CBKM2ANXX-2679-13-1-2_S19_L004_R1_001.fastq.gz
			CBKM2ANXX-2679-13-1-2_S19_L004_R2_001.fastq.gz
I24-5	24	infected	CBKM2ANXX-2679-14-1-2_S20_L004_R1_001.fastq.gz
			CBKM2ANXX-2679-14-1-2_S20_L004_R2_001.fastq.gz
I24-6	24	infected	CBKM2ANXX-2679-15-1-2_S21_L004_R1_001.fastq.gz
			CBKM2ANXX-2679-15-1-2_S21_L004_R2_001.fastq.gz
m24-4	24	mock	CBKM2ANXX-2679-16-1-2_S22_L004_R1_001.fastq.gz
			CBKM2ANXX-2679-16-1-2_S22_L004_R2_001.fastq.gz
m24-5	24	mock	CBKM2ANXX-2679-17-1-2_S23_L004_R1_001.fastq.gz
			CBKM2ANXX-2679-17-1-2_S23_L004_R2_001.fastq.gz
m24-6	24	mock	CBKM2ANXX-2679-18-1-2_S24_L004_R1_001.fastq.gz
			CBKM2ANXX-2679-18-1-2_S24_L004_R2_001.fastq.gz

Unzip

File copying:

```
#Copy files to my working directory
cp /home/nkondratev/project/nzgl02679/archive/NZGL02679/NZGL0267
9_fastq/* .
```

Unzipping using the 'loop.sh' script:

```
#!/bin/bash
for i in $(ls *.gz); do
    gzip -d $i
done
```

and bash command

```
bash loop.sh
```

Cut adaptor sequences

```
cutadapt -a AGATCGGAAGAGCACACGTCTGAACTCCAGTCA \
-A AGATCGGAAGAGCGTCGTGTAGGGAAAGAGTGT \
-o read_1.fastq.cut -p read_2.fastq.cut \
../Unzipped/read_1.fastq ../Unzipped/read_2.fastq
```

Check quality

```
#!/bin/bash
for i in $(ls ../Adaptors/*.cut); do
    SolexaQA++ analysis $i -h 20 -d .
done
```

Trimming

```
#!/bin/bash
for i in $(ls ../Adaptors/*.cut); do
    SolexaQA++ dynamictrim $i -h 20 -d . >> trimming.txt
done
```

Length Sort

```
SolexaQA++ lengthsort CBKM2ANXX-2679-01-1-2_S7_L004_R1_001.fastq
.cut.trimmed \
CBKM2ANXX-2679-01-1-2_S7_L004_R2_001.fastq.cut.trimmed
```

Bowtie and read counting

```
bowtie2 -x reference -p 16 \
```

```
-1 ../SolexaQA/CBKM2ANXX-2679-04-1-2_S10_L004_R1_001.fastq.cut.t
rimmed.paired \
-2 ../SolexaQA/CBKM2ANXX-2679-04-1-2_S10_L004_R2_001.fastq.cut.t
rimmed.paired \
-S $TMPFILE/i6-1.sam

perl map_count3.pl -f Lu_nr_new.fasta -s i6-1.sam -p -o i6-1-cou
nt
```

Exporting count data into R

```
library(tidyverse)

i0_1 = read_tsv("DEG/i0-1-count")
i0_2 = read_tsv("DEG/i0-2-count")
i0_3 = read_tsv("DEG/i0-3-count")
i6_1 = read_tsv("DEG/i6-1-count")
i6_2 = read_tsv("DEG/i6-2-count")
i6_3 = read_tsv("DEG/i6-3-count")
m12_1 = read_tsv("DEG/m12-1-count")
m12_2 = read_tsv("DEG/m12-2-count")
m12_3 = read_tsv("DEG/m12-3-count")
i12_1 = read_tsv("DEG/i12-1-count")
i12_2 = read_tsv("DEG/i12-2-count")
i12_3 = read_tsv("DEG/i12-3-count")
m24_1 = read_tsv("DEG/m24-1-count-ref")
m24_2 = read_tsv("DEG/m24-2-count-ref")
m24_3 = read_tsv("DEG/m24-3-count-ref")
i24_1 = read_tsv("DEG/i24-1-count-ref")
i24_2 = read_tsv("DEG/i24-2-count-ref")
i24_3 = read_tsv("DEG/i24-3-count-ref")

save(i0_1,i0_2,i0_3,
     i6_1,i6_2,i6_3,
     m12_1,m12_2,m12_3,
     i12_1,i12_2,i12_3,
     m24_1,m24_2,m24_3,
     i24_1,i24_2,i24_3, file = "countData.rda")
```

Creating separate count table datasets for the fungus and plant

```
library(tidyverse)
library(pander)

load("countData.rda")

#Count read number
count_data = bind_cols(i0_1,i0_2[,2],i0_3[,2],
```

```
                        i6_1[,2],i6_2[,2],i6_3[,2],
                        m12_1[,2],m12_2[,2],m12_3[,2],
                        i12_1[,2],i12_2[,2],i12_3[,2],
                        m24_1[,2],m24_2[,2],m24_3[,2],
                        i24_1[,2],i24_2[,2],i24_3[,2])

rm(i0_1,i0_2,i0_3,
   i6_1,i6_2,i6_3,
   m12_1,m12_2,m12_3,
   i12_1,i12_2,i12_3,
   m24_1,m24_2,m24_3,
   i24_1,i24_2,i24_3)

count_data_p = count_data[8423:117713,]
count_data_f = count_data [1:8422,]
count_data_f = column_to_rownames(count_data_f,"id")
count_data_p = column_to_rownames(count_data_p,"id")
colnames(count_data_f) = c("i0.1","i0.2","i0.3",
                           "i6.1","i6.2","i6.3",
                           "m12.1","m12.2","m12.3",
                           "i12.1","i12.2","i12.3",
                           "m24.1","m24.2","m24.3",
                           "i24.1","i24.2","i24.3")
colnames(count_data_p) = colnames(count_data_f)
fungal_readnum = summarise_all(count_data_f,funs(sum))
plant_readnum = summarise_all(count_data_p,funs(sum))
df = bind_rows(fungal_readnum,plant_readnum)
rownames(df) = c("fungus","plant")
```

Fungal read percentage

```
library(tidyverse)
data = data_frame(c("i0","i0","i0",
                    "i6","i6","i6",
                    "m12","m12","m12",
                    "i12","i12","i12",
                    "m24","m24","m24",
                    "i24","i24","i24"))
percent_fungal_reads = fungal_readnum/(plant_readnum+fungal_read
num)*100
names(percent_fungal_reads)  = c()
data = cbind(data, unlist(percent_fungal_reads))
colnames(data) = c("condition","percent")
data$condition <- factor(data$condition,
                         levels=c("i0","i6","i12","i24","m12","m
24"))
fun_pic = ggplot(data, aes(condition,percent)) +
  stat_summary(fun.y = mean, geom = "bar", fill = "grey75") +
  stat_summary(fun.data = mean_se, geom = "errorbar",
```

```
                colour = "grey50", width = 0.1) +
  geom_point() +
  scale_x_discrete(labels = c("0 hpi","6 hpi","12 hpi",
                              "24 hpi","control 12 hpi",
                              "control 24 hpi")) +
  xlab ("Treatment") + ylab ("Percent of fungal read pairs") +
  theme_bw() +
  theme(panel.grid.major = element_blank())
```

PCA analysis of the data

Make plant DESeq2 datasets

```
library(DESeq2)

resistanceDesign = data.frame(row.names = colnames(count_data_p)
,
                      treatment=c(rep("infected",6),rep("mock",3
),
                                  rep("infected",3),rep("mock",3
),
                                  rep("infected",3)),
                      time = c(rep("0",3),rep("6",3),rep("12",6)
,
                               rep("24",6)))
pds = DESeqDataSetFromMatrix(countData = count_data_p,
                             colData = resistanceDesign,
                             design = ~treatment+time)
pds = DESeq(pds)
rld <- rlog(pds, blind=FALSE)
save(file = "plant_DE_sets.rda", pds,rld)
```

Make PCA graphs

```
library(DESeq2)
library(tidyverse)
load("plant_DE_sets.rda")
p <- plotPCA(rld, intgroup=c("treatment", "time")) +
  theme_bw() +
  theme(panel.grid.major = element_blank(),
        panel.grid.minor = element_blank())

plot(p)
ggsave(plot=p, filename="PCA.pdf", useDingbats=FALSE)
```

Pairwise differential expression analysis

```
library(DESeq2)
library(tidyverse)

#Function to create DESeq datasets
DESeq_make <- function(count_matrix, reference_cols, treatment_c
ols){
  ## Create a smaller matrix with columns being compared
  count_data <- count_matrix[,c(reference_cols,treatment_cols)]
  rownames(count_data) = rownames(count_matrix)
  design = data.frame(row.names = colnames(count_data),
                      conditions=c("control","control","control"
,
                                   "infection","infection","infe
ction"))
  print(design)

  ## DESeq2 step
  dds <- DESeqDataSetFromMatrix(
    countData=count_data, colData=design, design=~conditions)
  dds <- DESeq(dds)

  ## Saving results into a new object
  res <- results(dds)

  ## Order by adjusted p-value
  res <- res[order(res$padj), ]

  ## Merge with normalized count data
  resdata <- merge(as.data.frame(res), as.data.frame(counts(dds,
normalized=TRUE)), by="row.names", sort=FALSE)
  names(resdata)[1] <- "Transcript"
  head(resdata)

  ## Find significant, up- and down-regulated transcripts

  resdata_sign = filter(resdata, padj < 0.01)
  resdata_up = filter(resdata, padj < 0.01 & log2FoldChange > 1)
  resdata_down = filter(resdata, padj < 0.01 & log2FoldChange <
-1)

  ## Create list object with results

  output = list()

  output$DESeqOutput <- dds
  output$DESeqResult <- res
  output$resultTable <- resdata
  output$significant <- resdata_sign
```

```
  output$upRegulated <- resdata_up
  output$downRegulated <- resdata_down

  return(output)
}

#Here I predict differentially expressed transcripts between 0 h
pi samples and infected 6 hpi samples using my function
comparison_i0_m12 = DESeq_make(count_data_p, c(1,2,3), c(4,5,6))
```

B.3. Cluster analysis of differentially expressed genes

```
library (tidyverse)
library (RColorBrewer)
library (gplots)
library(dendextend)

#Hierarchical clustering of expression profiles which generates
a tree
hcluster = hclust(as.dist(1-cor(t(fold_change_matrix), method="p
earson")))

#Cut tree into 10 clusters and color them
dend1 <- as.dendrogram(hcluster)
dend1 <- color_branches(dend1, k = 10, col = brewer.pal(10, "Set
3"))
source("https://raw.githubusercontent.com/talgalili/dendextend/m
aster/R/attr_access.R")
col_labels <- get_leaves_branches_col(dend1)
col_labels <- col_labels[order(order.dendrogram(dend1))]

#Generate a heatmap using initial fold-chage data and dendrogram
with colored branches
heatmap.2(as.matrix(fold_chage_matrix),
          trace = "none", density.info=c("none"),
          col = rev(brewer.pal(11, "PiYG")),
          labRow = F,
          Colv = c("m12","m24","6","12","24"),
          dendrogram = "none",
          Rowv = dend1,
          margins = c(1,30),
          RowSideColors = col_labels, scale = "row")
```

B.4. Export and analysis of protein networks

```
library (igraph)
```

```
#Import STRING network into R
graph_tsv = read_tsv ("EXPORTED_STRING_NETWORK.tsv")

graph = graph_from_dataframe (graph_tsv)

#Count number of interactors for each protein

table_interactions = degree (graph)
```

B.5. Statistical analysis

```
library (tidyverse)
library (agricolae)

#T-test
t.test (observations_1, observations_2)

#ANOVA
model_anova = aov (data = Data_table, Column_observations ~ Colu
mn_treatment)
summary (model_anova)

#Tukey's HSD
model_HSD_test = HSD.test (model_anova, trt = Column_treatment)

#Fisher's LSD
model_LSD_test = LSD.test (model_anova, trt = Column_treatment)

#Chi-squared independence test
chisq.test (contingency_table)

#Correlation test
cor.test (array1, array2)

#Regression analysis with cubic splines

library (mgcv)

Line_chart = ggplot (data = concentration_data, aes (x = Time, y
= Metabolite_concentration, col = Infection))

+ geom_point()

+ geom_smooth(method = "gam", level = 0.95, formula = y ~ s(x, b
s = "cr", k = 5), alpha = 0.25, aes(fill = Infection))

+ theme_classic()

+ theme(axis.title.x=element_blank(), axis.title.y=element_blank
(), legend.position = "none")

+ ggtitle("Metabolite X")
```

```
+ scale_x_discrete(limits = c(0,6,12,24,48))
+ scale_y_continuous(breaks = scales::pretty_breaks(n = 3))
```

Appendix C. Supplementary Files

The following supplementary files are available for downloading from fig**share**:

Kondratev, Nikolai (2019): Identification of mechanisms defining resistance and susceptibility of Camellia plants to necrotrophic petal blight disease. figshare. Dataset.

https://doi.org/10.6084/m9.figshare.8273864.v1

Supplementary File 1 | Assembled *Camellia lutchuensis* transcriptome

Supplementary File 2 | Assembled *Camellia* 'Nicky Crisp' transcriptome

Supplementary File 3 | Assembled *Ciborinia camelliae* transcriptome

Supplementary File 4 | Annotation and cluster analysis results of *C. lutchuensis* differentially expressed transcripts

Supplementary File 5 | Results of GO enrichment analysis of *C. lutchuensis* expression clusters

Supplementary File 6 | STRING mapping results of *C. lutchuensis* upregulated transcript clusters

Supplementary File 7 | Differentially-expressed phenylpropanoid genes of *C. lutchuensis*

Supplementary File 8 | Secreted proteins of *C. camelliae* and *Camellia* 'Nicky Crisp'

Supplementary File 9 | List of *C. camelliae* transcripts upregulated at 6 hpi of incompatible interaction with *C. lutchuensis*

Appendix D. Publications and Presentations

Publications

Kondratev N, Denton-Giles M, Bradshaw RE, Cox MP, Dijkwel PP. 2019. *Camellia* plant resistance and susceptibility to petal blight disease are defined by the timing of defense responses. *Submitted to Molecular Plant-Microbe Interactions*

Other publications

Kondratev N, Denton-Giles M, Fulton CD, Dijkwel PP. 2017. A transcriptomic database of petal blight-resistant *Camellia lutchuensis*. *International Camellia Journal* **49**, 47-55

Kondratev N, Saracchi M, Couselo JL, Dijkwel PP. 2019. Combating camellia petal blight: can modern biology help our camellias. In *Rhododendrons with Camellias and Magnolias 2019, UK Royal Horticultural Society Group Yearbook*

Conference presentations

Kondratev N, Bradshaw RE, Cox MP, Dijkwel PP. 2017. Proteomic analysis of *Ciborinia camelliae* necrosis-inducing culture filtrate revealed potential pathogenicity factors. Queenstown Research Week, Queenstown, New Zealand [Poster presentation]

Kondratev N, Dijkwel PP. 2018. Camellia petal blight resistance: uncovering the veil. International Camellia Congress, Nantes, France [Oral presentation]

Kondratev N, Denton-Giles M, Bradshaw RE, Cox MP, Dijkwel PP. 2019. Resistance and susceptibility of *Camellia* plants to petal blight disease are defined by the timing of defence responses. Plant Science Central Conference, Palmerston North, New Zealand [Oral presentation]